Mechanics Analysis of Coupled Large Deformation and Diffusion in Gels

by

Jiaping Zhang

A Dissertation Presented in Partial Fulfillment
of the Requirements for the Degree
Doctor of Philosophy

Approved May 2012 by the
Graduate Supervisory Committee:

Hanqing Jiang, Chair
Pedro Peralta
Lenore Dai
Subramaniam Rajan
Nikhilesh Chawla

ARIZONA STATE UNIVERSITY

August 2012

ABSTRACT

Gels are three-dimensional polymer networks with entrapped solvent (water etc.). They bear amazing features such as stimuli-responsive (temperature, PH, electric field etc.), high water content and biocompatibility and thus find a lot of applications. To understand the complex physics behind gel's swelling phenomenon, it is important to build up fundamental mechanical model and extend to complicated cases. In this dissertation, a coupled large deformation and diffusion model regarding gel's swelling behavior is presented. In this model, free-energy of the total gel is constituted by polymer stretching energy and polymer-solvent mixing energy. In-house nonlinear finite element code is implemented with fast computational capability. Complex phenomenon such as buckling and healing of cracked gel by swelling are studied. Due to the wide coverage of polymeric materials and solvents, solvent diffusion in gels not only follows Fickian diffusion law where concentration map is continuous but also follows non-Fickian diffusion law where concentration map shows high gradient. Phenomenological model with viscoelastic polymer constitutive and concentration dependent diffusivity is created. The model well captures this special diffusion phenomenon such as sharp diffusion front and distinctive swollen and unswollen region.

ACKNOWLEDGMENTS

During the course of my graduate study, I would like to first express my sincerest gratitude to my advisor and chair, Professor Hanqing Jiang. His guidance and support have helped me to overcome numerous obstacles that I would not be able to defeat on my own. He guides me from a college graduates step by step to be a professional researcher. I have benefited from his daily dedicated cultivation and instruction. He paid extensive patience in the past five years to guide me to fulfill my research. His diligence, dedication and courage have shaped and will continue to shape my future career. I attribute the level of my PhD degree to his encouragement and effort.

Gratitude also goes to my committee professors and collaborators. Professor Subramanian Rajan, who is always willing to offer good advice and perspective, enlightens me by his deep understanding of mechanics and his professional attitude toward research. I'd like to express my gratitude to Prof. Lenore Dai, Prof. Nikhilesh Chawla and Prof. Pedro Peralta, who offered their precious advice to polish my work. Credits should also go to Dr. Howon Lee and Prof. Nicholas Fang, who used to work at University of Illinois at Urbana-Champaign and now work at Massachusetts Institute of Technology. They provide me most of the experimental results to support my modeling and simulation. We had gone through a lot of discussions which is invaluable to the final completion of my work.

I’d like to express my thanks to my colleagues in Prof. Jiang’s lab, Dr. Huiyang Fei, Dr. Cunjiang Yu, Amit Abraham, Swathisri Kondagari, Dr. Lan He, Yonghao An, Teng Ma, Yuping Pan , Dr. Zheng Duan, Joseph Shaffer and and so on. They not only helped me on my research but also my personal life.

Finally, I should express my gratitude to financial support from the National Science Foundation and special thanks to Fulton High Performance Computing Initiative at Arizona State University and Dr. Gil Speyer and Dr. Scott Menor who work there. Without their support, the work would not be completed in the current pace.

TABLE OF CONTENTS

Page

CHAPTER Page

CHAPTER Page

CHAPTER Page

LIST OF FIGURES

Figure Page

Figure Page

Figure Page

Figure Page

1 INTRODUCTION TO GELS

1.1. GELS FUNDAMENTALS AND THEIR APPLICATIONS

Hydrogel is three dimensional polymer networks that are capable to absorb solvents and swells to a certain limit without dissolving (Figure 1.1). There are several ways of classification of gels. Among them there are two common classifications. One is based on the type of crosslinking that creates the 3D network, it could be classified as physical gels and chemical gels. The other one is based on the way it is generated; it is classified as natural gel and synthetic gel.

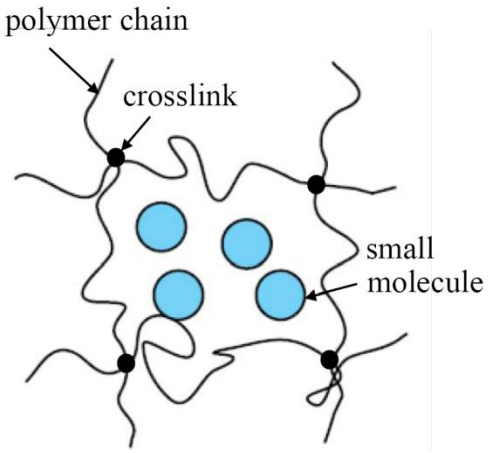

Figure 1.1. Structure representation of a gel

Physical gels have weak bonding cross-linked structure. Upon the change of the environment, the bonding could be reversible. This type of bonding includes hydrogen bonding, van de Waals bonding, ionic bonding. One example of this bonding is hydrogen bonding. Gels formed by hydrogen bonding are vulnerable to environment, such as subjected to elevated temperature. In this case, the physical gel behavior like a liquid when dissolve. Another weak bonding

example is coordination bonding. Common class of physical gels are block copolymers(Kissel, Li, and Unger 2002, ; Jeong et al. 1997, ; Li et al. 2006). The good feature of physical gel is that most of them are thermally reversible.

Chemical gels are created by chemical reaction. And it could not be dissolve again which become irreversible. The bond formed is mechanically strong and stable. They are made by cross-link individual polymer chains. The chemical reaction could be initiated by heat, pressure, change in pH, or UV radiation, and usually accompany cross-linking agents. As one example, the fabrication of a common gel Poly(N-isopropylacrylamide)(PNIPAM) involve the following process (Figure 1.2):(Zhao et al. 2008)

(1) Monomer(N-isopropylacrylamide), cross-linker (N,N_-methylenebisacrylamide) and initiator (azobis-isobutyronitrile) is mixed at a certain ratio and dissolve in solvent(acetone).

(2) The mixed solution is then put into reactors where gelation is completed by heating or radiation

(3) After a long time of reaction, the PNIPAAm hydrogel is immersed in pure water to remove non-reactive materials and dries under vacuum environment.

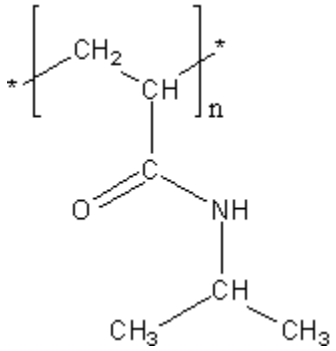

Figure 1.2. Chemical structure of PNIPAM gel

Chemical gels typically have strong bonding structure. Common types of bonding include covalent bonding and coulomb bonding. Chemical gels are polymerized by adding crosslinking agent when the polymer monomers are synthesized. Usual examples of chemical gels formed by covalent bonding include acrylamide gel, poly(ethylene glycol)gel, poly(vinyl alcohol) gel.

Another classification is based on the way the polymer is made, it could be categorized as natural gel or synthetic gel (Lee and Mooney 2001, ; Slaughter et al. 2009). Common natural gels include collagen and gelatin, chitosan, alginate, fibrin, agarose and many others. Collagen is tissue-derived natural polymer and is the main components of human tissue such as skin and cartilage. Alginate is a well-known biomaterial obtained from blown algae and is widely used in drug delivery and tissue engineering.

Synthetic gels include poly(ethylene glycol) (PEG) and its derivatives, poly(vinyl alcohol) (PVA) , polyacrylates, Poly(ethylene oxide) (PEO) and its copolymers. For example, PEG-based gels are used extensively in tissue scaffold because its biocompatibility and degradation ability. Cell is capable to adhere to the 3D gel network and proliferate.

Common applications of gel could be summarized as:

(1) Tissue engineering, where gel is used as tissue scaffold;

(2) Sustained-release drug delivery systems;

(3) Sensors, due to their responsiveness to temperature, PH, solvent concentration and biological constitute;

(4) Disposable diapers where they could be used to absorb urine;

(5) Contact lenses, made by silicone hydrogels;

(6) Swellable oil packers. It has rising interests in oil industry that gels, or more commonly called swellable elastomers, is used for zonal isolation and to enhance oil productivity.

1.2. MOTIVATION OF STUDY

Though the gel has been used for many years, it is surprising to find out that the modeling work is still in its preliminary stage, especially from the mechanics community. This certainly will pose limits on its applications.

The demand to modeling gel swelling/deswelling not only relies on the fact that modeling is an important complementary to experiment, as it saves time and reduces cost, but also relies on the situation that the underlying physics behind swelling need to be understood, from the most fundamental level, to help us explain more complicated phenomenon. Taking as gel swelling for example, interesting complex swelling patterns are observed, such as buckling(Sultan and Boudaoud 2008), creasing(Jin, Cai, and Suo 2011, ; Cai et al. 2010) and snapping(Forterre et al. 2005). Without a quantitative characterizing and without modeling, we would not be able to see through these phenomena.

Another aspect is that the quantitative prediction really matters in a lot of applications. For example, in drug delivery systems, George and Abraham(2007) have designed a pH-sensitive alginate–guar gum hydrogel crosslinked with glutaraldehyde for the controlled delivery of protein drugs, where the release of protein drugs from the tested hydrogels was at minimal at pH 1.2 (about 20%) and

reaches maximum higher at pH 7.4 (about 90%), precise controlled is required and this should be accomplished with the aid of modeling.

1.3. RESEARCH OBJECTIVE

The main objective of the dissertation is to build a "framework" and corresponding numerical methods to study gel swelling, and applying this tool to study several interesting pattern phenomena with comparison of experiment. This framework should consider both the mechanical deformation of the gel polymeric network and the diffusion of solvent. And it should couple the deformation with the deformation. And due to the fact that the swelling ratio of gel could be very large, large deformation analysis is required. Because the various combinations of polymer-solvent system exist, the model should be extendable to many different scenarios. Those phenomena include, but not limited to:

(1) Simple swelling. This is the fundamental of gel swelling. However, finite element analysis (FEA) would be able to verify our perception about swelling in mind and create a clearer picture. Simple swelling like cubic free swelling and creep of swollen gel are starting points for complex swelling. More specifically, the study would help to visualize the stress inside the gel body, would help to build a time scale associated with diffusion and geometry, would tell us that inhomogeneous swelling is common during transient swelling process.

(2) Buckling phenomenon of thin-structure gel swelling under constraint. Buckling exists commonly in biological systems, for example, tissue growth under constraint(Li et al. 2011). The thin gel ring which is confined in the bottom

surface and allowed to swelling, produced fascinating buckling patterns after swelling. A simple model based on energy method is created and well characterize the wave numbers which changes with the geometry. Those studies certainly will expand our understanding of buckling phenomena.

(3) An interesting phenomena that solvent swelling in gels could “heal” the original cracked notch. Through FEA and experimental validation, this process could be seen clearly. The crack tip field showed a transition from a tensional high stress zone to a compressive zone which indicates that the crack has been closed. Potential benefits are obvious, we could wisely choose the amount of solvent to repair a damaged structure and improve structure integrity.

The present study would be able to build a foundation to study more complicated and diverse gel deformation when gel is integrated with other functional materials and help to realize more functionality. The present study also sheds light on coupled deformation and diffusion modeling, as well as how to develop nonlinear numerical solutions to simulate such behavior. The numerical package is expected to be applied in more practical industry application.

2 THEORIES ABOUT GEL SWELLING

2.1. INTRODUCTION TO GEL SWELLING AND MECHANICAL MODELING

Gel swelling is an interest process which involves deformation and solvent transport. Biot's(1941) consolidation model is one of the earliest piece of work in study this fluid diffusion in solids. Due to its simplicity, it is still used a lot in soil mechanics and various engineering practices. And it applies to gel swelling if consider the polymer networks as a solid. Specifically consider the properties of the polymer networks, Flory(1953) did a lot of work using thermodynamics principles. Flory's theory starts from the free energy of the polymer solutions which is derived from the random walk of the polymer chains. Later, Tanaka et al.(1973, ; 1979, ; 1978) did a lot of experiments and theoretical studies on gel swelling kinetics.

2.2. REPRESENTATIVE THEORIES ABOUT GEL SWELLING

2.2.1 Biot Theory

The Biot consolidation theory(1941) is a notorious theory in soil mechanics and still used a lot in many engineering disciplines. Because swelling in gels shares similar features as fluid transport in soils. The theory could be applied into gel swelling modeling as well. The basic assumptions behind Biot's theory contain:

(1) The solid skeleton deformation is linear elastic;

(2) The deformation is small;

(3) The fluid flow follows Darcy's law;

(4) The fluid is incompressible.

For a saturated elastic gel, the stress follows

$$\sigma_{ij} = 2G\varepsilon_{ij} + \lambda\varepsilon_{kk}\delta_{ij} + p\delta_{ij} \tag{2.1}$$

Where G and ν are shear modulus and Poisson's ratio of polymer network, $\lambda = \frac{2G\nu}{1-2\nu}$ is lame's constant. p is pore pressure. The stress satisfy the equilibrium equation

$$\sigma_{ij,j} = 0 \tag{2.2}$$

and strain relates to displacement via

$$\varepsilon_{ij} = \frac{1}{2}\left(u_{i,j} + u_{j,i}\right) \tag{2.3}$$

The above three equations simplifies to

$$G\nabla^2 u + \frac{G}{1-2\nu}\frac{\partial}{\partial x}\left(\frac{\partial u}{\partial x} + \frac{\partial v}{\partial y} + \frac{\partial w}{\partial z}\right) - \frac{\partial p}{\partial x} = 0 \tag{2.4}$$

$$G\nabla^2 v + \frac{G}{1-2\nu}\frac{\partial}{\partial y}\left(\frac{\partial u}{\partial x}+\frac{\partial v}{\partial y}+\frac{\partial w}{\partial z}\right)-\frac{\partial p}{\partial y}=0 \tag{2.5}$$

$$G\nabla^2 w + \frac{G}{1-2\nu}\frac{\partial}{\partial z}\left(\frac{\partial u}{\partial x}+\frac{\partial v}{\partial y}+\frac{\partial w}{\partial z}\right)-\frac{\partial p}{\partial z}=0 \tag{2.6}$$

The fluid flow follows Darcy's law, which states that the flux is proportional to the gradient of pore pressure, i.e.,

$$j_i = kp_{,i}/\gamma \tag{2.7}$$

, where k is coefficient of permeability and γ is specific weight of water.

The incompressibility condition for the pore fluid is

$$\frac{\partial \varepsilon_{kk}}{\partial t}+\nabla \bullet j = 0 \tag{2.8}$$

Equations (2.7) and (2.8) together generate:

$$\frac{\partial}{\partial t}\left(\frac{\partial u}{\partial x}+\frac{\partial v}{\partial y}+\frac{\partial w}{\partial z}\right)-\frac{k}{\gamma}\nabla^2 p = 0 \tag{2.9}$$

Equations (2.4), (2.5), (2.6) and (2.9) are a set of equations regarding displacements u, v, w and pore pressure p, which could be solved given appropriate boundary conditions.

2.2.2 THB Theory

Tanaka is one of the noted researchers who contributed a lot in the development of kinetic of gel swelling. Tanaka, Hocker and Benedek(1973) developed a theory about gel swelling known as THB theory. In the THB theory, the fluid flow is not considered explicitly. And a frictional coefficient f is introduced to characterize the drag force caused by the relative motion of the polymer network through the pore fluid. Equilibrium equation becomes:

$$f\frac{\partial u_i}{\partial t} - \sigma_{ij,j} = 0 \tag{2.10}$$

And

$$\sigma_{ij} = 2G\varepsilon_{ij} + \lambda\varepsilon_{kk}\delta_{ij} \tag{2.11}$$

Under this theory, they derived that the diffusion coefficient is linearly proportional to inverse of friction coefficient

$$D = \left(K + 4\mu/3\right)/\ f \tag{2.12}$$

, which implicate that the swelling time is limited by the friction between the friction of the polymer network and fluid.

Biot's theory and THB theory are two simple theories with clear physics that could study the fluid flow inside solid such as gel swelling. However, the underlying small strain and linear elastic assumption limits their applications,

considering that a lot of gels are made of polymers, which undergo large strain following hyperelastic or viscoelastic behavior. A more realistic theory is developed by Flory from a statistical mechanics perspective.

2.2.3 Flory Theory

Flory(1953) did extensive work in polymer swelling behavior using thermodynamic concepts. In his theory, gel is considered as a polymer solution which contains solvent molecules and polymer molecules. The Gibbs free energy that accompany the deformation of the gel is written as

$$\Delta G = \Delta G_m + \Delta G_e \tag{2.13}$$

, where ΔG_m comes from the mixing of solvent and polymer and ΔG_e is from the elastic deformation.

The mixing energy is derived as

$$\Delta G_m = kT\left[n_1 \ln(1-\phi) + n_2 \ln\phi + \chi n_1 \phi \right] \tag{2.14}$$

Where k is Boltzmann constant and ϕ is volume fraction of polymer and n_1 is number of solvent molecules and n_2 is number of polymer chains. χ is a dimensionless parameter called polymer-solvent interaction parameter. The elastic deformation energy is derived on 3D lattice model taking into account to the end-to-end distance change of each polymer chain. And the elastic energy is written as

$$\Delta G_e = \frac{3}{2} NkT\left(\alpha^2 - 1 - \ln\alpha\right) \tag{2.15}$$

,where α is elongation of the polymer network and N is number of polymer segments per volume. The osmotic pressure is obtained from the free energy as

$$\pi_{mixing} = -\frac{N_A}{v_1}\frac{\partial \Delta G_m}{\partial n_1} \tag{2.16}$$

Where

$$\pi_{elastic} = -\frac{N_A}{v_1}\frac{\partial \Delta G_e}{\partial n_1} \tag{2.17}$$

, π_{mixing} and $\pi_{elastic}$ are osmotic pressure from mixing energy and elastic energy, respectively. Equilibrium is reached when

$$\pi_{mixing} + \pi_{elastic} = 0 \tag{2.18}$$

Flory's theory is one of the very successful theories and is extended later to a coupled theory stated in the next section.

2.2.4 Wallmersperger Theory

Wallmersperger and coworkers(2004) formulated a theory which takes into account the coupling of mechanical, chemical, and electrical effect for ionic gels. The basic equations in the theory include Nernst-Planck equation which

governs the concentration of ionic species, Poisson equation which governs the electrical field and mechanical equilibrium equations.

The Nernst-Planck equation is given by

$$D_k \frac{\partial^2 c_k}{\partial x^2} + \mu_k z_k \frac{\partial c_k}{\partial x}\frac{\partial \psi}{\partial x} + \mu_k z_k c_k \frac{\partial^2 \psi}{\partial x^2} = 0 \tag{2.19}$$

Where D_k and μ_k are diffusivity and mobility of the *k*th ionic species, c_k and z_k are the concentration and valence of *k*th ionic species. ψ is electrical potential, which is governed by Poisson's equation

$$\frac{\partial^2 \psi}{\partial x^2} = -\frac{F}{\varepsilon \varepsilon_0}\left(\sum_{k=1}^{N} z_k c_k + z_f c_f\right) \tag{2.20}$$

, where F is Farady constant, ε_0 is dielectric constant of vacuum and ε is relative dielectric constant, z_f and c_f are the valence and concentration of the fixed charged group attached to the gel network. c_f relates to the state of the hydrogel by

$$c_f = \frac{1}{H}\frac{c_f^0 K}{\left(K + c_H\right)} \tag{2.21}$$

Where H is the local degree of hydration of the hydrogel, c_f^0 is the total concentration of the ionizable groups before swelling, K is dissociation constant, c_H is concentration of hydrogen ions in the gel.

The gel should also follow the mechanical equilibrium law

$$\sigma_{ij,j} = 0 \tag{2.22}$$

, where stress σ_{ij} here also depends on the osmotic pressure

$$\pi = RT\sum_{k=1}^{N}\left(c_k^h - c_k^s\right) \tag{2.23}$$

, where c_k^h is concentration of gel and c_k^s is concentration of bulk solution.

This model is based on fundamental physics laws and provides a convenient approach to simulation the ionic gels deformation. However, the formulation neglects the interaction between polymer and solvents, which could be significant when the osmotic pressure caused by the solvent is large.

It should be noted that the above listed model is just a few representative models. A lot more theories(Dolbow, Fried, and Jia 2004, ; Durning and Morman 1993, ; Baek and Srinivasa 2004, ; Ji et al. 2006, ; Doi 2009, ; Lai, Hou, and Mow 1991) which have important contribution are omitted here.

2.3. A COUPLED THEORY ABOUT GEL SWELLING

Based on the pioneering work of Biot and Flory, Hong et al.(2008) came up with a coupled field theory that couples the gel deformation and solvent diffusion. In the theory, the polymeric natural of the network is taken into account through thermodynamics and large deformation swelling is considered.

2.3.1 Kinematics of the Network

In this theory, continuum mechanics is used to describe the kinematics of the network. The gel moves in a three-dimensional space. Imagine that each differential element of the network is attached with a marker. Any configuration of the gel can serve as a reference configuration (Figure 2.1). When the gel is in the reference configuration, the marker occupies in the space a place with coordinates $\mathbf{X}$, which will be used to label the marker. In the reference configuration, let $dV(\mathbf{X})$ be an element of volume, $dA(\mathbf{X})$ be an element of area, and $N_K(\mathbf{X})$ be the unit vector normal to the element of area.

At time t, the gel is in the current configuration, and the marker X moves in the space to a new place with coordinates $\mathbf{x}$. The functions $x_i(\mathbf{X},t)$ specify the kinematics of the network. As usual, the deformation gradient of the network is defined as

$$F_{iK}(\mathbf{X},t)=\frac{\partial x_i(\mathbf{X},t)}{\partial X_K} \tag{2.24}$$

Deformation gradient $\mathbf{F}$ will be used to characterize the state of deformation of an element of the gel.

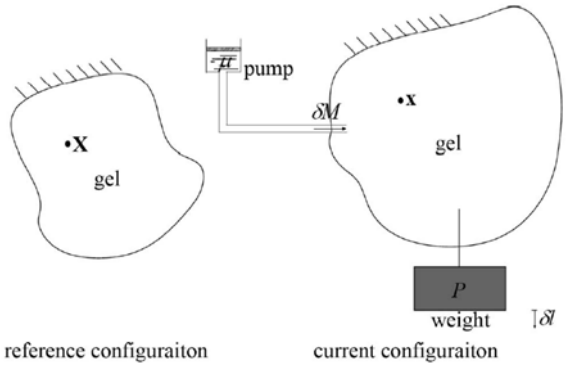

Figure 2.1. The reference and current configuration with an illustration of two ways doing work on a gel

2.3.2 Conservation of Solvent Molecules

Nominal quantities will be used to describe the conservation of the solvent molecules. Let $C(\mathbf{X},t)$ be the nominal concentration of the solvent in the gel in the current configuration, namely, $C(\mathbf{X},t)dV(\mathbf{X})$ is the number of solvent molecules in the element of volume. Let $J_K(\mathbf{X},t)$ be the nominal flux of the solvent in the gel, namely, $J_K(\mathbf{X},t)N_K(\mathbf{X})A(\mathbf{X})$ is the number of the solvent molecules per unit time migrating across the element of area. Imagine that the network is attached with a field of pumps, which inject the solvent into the gel. In the current configuration, the pumps inject $r(\mathbf{X},t)dV(\mathbf{X})$ number of the solvent molecules into the element of volume per unit time, and $i(\mathbf{X},t)dA(\mathbf{X})$ number of

the solvent molecules into the element of area per unit time. We assume that no chemical reaction occurs, so that the number of the solvent molecules is conserved, namely,

$$\frac{\partial C(\mathbf{X},t)}{\partial t}+\frac{\partial J_K(\mathbf{X},t)}{\partial X_K}=r(\mathbf{X},t) \tag{2.25}$$

in the volume of the gel, and

$$J_K(\mathbf{X},t)N_K(\mathbf{X})=-i(\mathbf{X},t) \tag{2.26}$$

on the part of the surface of the gel where the pumps inject solvent molecules.

2.3.3 Conditions of Local Equilibrium

Let us examine the conditions of local equilibrium. Elements of the gel in different locations may not be in equilibrium with each other, and this disequilibrium motivates the solvent to migrate. Each differential element of the gel, however, is taken to be locally in a state of equilibrium. That is, the migration of the solvent is such a slow process that the effect of inertia is negligible, the viscoelastic process in the element has enough time to relax, and the solvent in the element has enough time to equilibrate with the solvent in the pump attached to the element. Furthermore, the gel is assumed to be held at a constant temperature. We characterize the thermodynamic state of the differential element of the gel by the deformation gradient of the network, $\mathbf{F}(\mathbf{X},t)$, and the chemical potential of

the solvent, $\mu(\mathbf{X},t)$. Let $\hat{W}(\mathbf{F},\mu)$ be the free-energy density function of the gel, namely, $\hat{W}(\mathbf{F},\mu)dV(\mathbf{X})$ is the free energy associated with the element of the gel. The conditions of local equilibrium requite that the nominal concentration be given by

$$C = -\frac{\partial \hat{W}(\mathbf{F},\mu)}{\partial \mu} \tag{2.27}$$

and the nominal stress be given by

$$s_{iK} = \frac{\partial \hat{W}(\mathbf{F},\mu)}{\partial F_{iK}} \tag{2.28}$$

, where the free-energy density function $\hat{W}(\mathbf{F},\mu)$ is prescribed for a gel and equation (2.27) and (2.28) constitute the equations of state.

Imagine that the network is attached with a field of weights, which apply forces to the gel. In the current configuration, the weights apply a force $B_i(\mathbf{X},t)dV(\mathbf{X})$ to the element of volume, namely, $B_i(\mathbf{X},t)$ is the applied forces in the current configuration per unit volume of the reference configuration. Similarly, the weights apply a force $T_i(\mathbf{X},t)dA(\mathbf{X})$ to the element of area, namely, $T_i(\mathbf{X},t)$ is the applied forces in the current configuration per unit area of the reference configuration. The conditions of local equilibrium require that the

inertia effect be negligible and that the viscoelastic process in the element be fully relaxed, so that

$$\frac{\partial s_{iK}\left(\mathbf{X},t\right)}{\partial X_K}+B_i\left(\mathbf{X},t\right)=0 \tag{2.29}$$

in the volume of the gel, and

$$s_{iK}\left(\mathbf{X},t\right)N_K\left(\mathbf{X}\right)=T_i\left(\mathbf{X},t\right) \tag{2.30}$$

on the part of the surface of the gel where forces are applied.

2.3.4 Kinetics of Migration

Nominal quantities are used describe the kinetics of migration. The flux of the solvent is taken to be linear in the gradient of the chemical potential of the solvent:

$$J_K=-M_{KL}\left(\mathbf{F},\mu\right)\frac{\partial\mu\left(\mathbf{X},t\right)}{\partial X_L} \tag{2.31}$$

where M_{KL} is the mobility tensor. The mobility tensor is symmetric and positive-definite, and in general depends on the thermodynamic state of the element, namely, on local values of the deformation gradient and the chemical potential.

The above theory evolves the configuration of the gel, namely, evolves concurrently the two fields $\mathbf{x}(\mathbf{X},t)$ and $\mu(\mathbf{X},t)$, once the following items are prescribed:

(1) The initial conditions $\mathbf{x}(\mathbf{X},t_0)$ and $\mu(\mathbf{X},t_0)$ at a particular time t_0;

(2) The applied force $B_i(\mathbf{X},t)$ and the rate of injection $r(\mathbf{X},t)$ inside the gel;

(3) Either $i(\mathbf{X},t)$ or $\mu(\mathbf{X},t)$ on the surface of the gel either $T_i(\mathbf{X},t)$ or $\mathbf{x}(\mathbf{X},t)$ on the surface of the gel.

(4) The free-energy function $\hat{W}(\mathbf{F},\mu)$ and the mobility tensor $M_{KL}(\mathbf{F},\mu)$.

, the theory is able to solve the problem given specific material models stated in the following paragraph.

2.3.5 Specific Material Model

Within the theory presented in the previous section, a material model is specified by the functions $\hat{W}(\mathbf{F},\mu)$ and the mobility tensor. The free energy of Flory and Rehner (1943) is rewritten in the form

$$\begin{aligned}\hat{W}(\mathbf{F},\mu) = {} & \frac{1}{2}NkT\left[F_{iK}F_{iK}-3-2\log(\det\mathbf{F})\right] \\ & -\frac{kT}{v}\left[(\det\mathbf{F}-1)\log\left(\frac{\det\mathbf{F}}{\det\mathbf{F}-1}\right)+\frac{\chi}{\det\mathbf{F}}\right]-\frac{\mu}{v}(\det\mathbf{F}-1)\end{aligned} \tag{2.32}$$

where N is the number of polymer chains in the gel divided by the volume of the gel in the reference state, kT is the temperature in the unit of energy, v is the volume per solvent molecule, and χ is a dimensionless parameter characterizing the enthalpy of mixing. In writing equation (2.32), the reference configuration is taken to be the dry network, and $\mu = 0$ when the solvent is in the pure liquid state in equilibrium with its own vapor.

Assuming that the small molecules diffuse in the gel and that the coefficient of diffusion of the solvent molecules, D is isotropic and independent of deformation gradient and concentration, Hong et al.(2008) expressed the mobility tensor as

$$M_{KL} = \frac{D}{vkT}\left(\det \mathbf{F} - 1\right) H_{iK} H_{iL} \tag{2.33}$$

, where H_{iK} is the transpose of the inverse of the deformation gradient, namely, $H_{iK} F_{iL} = \delta_{KL}$. In writing (2.33) the reference state is taken to be the dry network.

2.4. DISCUSSIONS ABOUT THE THEORY

The theory considers the large swelling of polymer network caused by solvent absorption, and has received a lot of attentions(Liu et al. 2011, ; Hong, Zhao, and Suo 2010, ; Gernandt et al. 2011, ; Li and Mulay 2011, ; Wong et al. 2010). Both mechanical equilibrium equation and solvent transport are standard equations but extended to large deformation regime. Deformation and diffusion

are coupled smartly through the molecular incompressible condition. And the free energy of the polymer network comes from thermodynamics. Taking into these facts into consideration, the theory is still very neat and allows for numerical implementation with limited restrictions. This theory is considered to build a framework to study various coupled phenomenon in solvent diffusion in polymers, as long as the mechanism is driven by diffusion and the free energy of polymer is give. However, it has been noted that this model fits well for small and moderate stretching of polymer networks, where the polymer chains follows Gaussian statistics (Treloar 2005) .For very large deformation, non-Gaussian polymer chain statistics should be used(Chester and Anand 2011, ; Arruda and Boyce 1993). In this case, the free energy should be written as:

$$W = -N_A k_B T \lambda_L^2 \left[\left(\frac{\lambda}{\lambda_L} \right) \beta + \ln \frac{\beta}{\sinh \beta} - \frac{1}{\lambda_L} \beta_0 - \ln \frac{\beta_0}{\sinh \beta_0} \right] + N_A k_B T \left(\frac{\lambda_L}{3} \beta_0 \right) \ln J \tag{2.34}$$

Where $\beta_0 = L^{-1}\left(\frac{1}{\lambda_L} \right)$ and $L^{-1}(x)$ is the inverse of Langevin function $L^{-1}(x) = \coth(x) - x^{-1}$. These considerations help complete the theory instead of diminish it. As a direct numerical implementation of the theory, not only in equilibrium swelling, but also transient swelling, the numerical method described in the next chapter enable the theory to be applied to practical applications.

3 NUMERICAL SIMULATION OF GEL SWELLING

3.1. INTRODUCTION TO GEL SWELLING NUMERICAL METHODS

There have been several previous efforts to develop finite element methods for gels. For example, Westbrook and Qi (2008) and Hong et al.(2009) have developed finite element methods for gels in a state of equilibrium. Suematsu (1990) conducted the three-dimensional explicit finite element analysis to study the pattern formation of swelling gels by introducing a friction constant between the polymeric chains and solvents (Tanaka and Fillmore 1979). As pointed out by Suematsu et al (1990), this method is not suited for larger systems over longer time intervals. Dolbow et al. (2004) used a hybrid eXtended-Finite-Element/Level-Set Method to study the swelling of gels. Li et al. (2007) used an explicit method to alternately solve the coupled problems for gels, namely, the deformation of gels is solved after the convergent results for mass transport is obtained. Birgersson et al. (2008) conducted transient analysis of temperature-sensitive two-dimensional gels by using finite element software COMSOL Multiphysics.

Given various theories and numerical methods, as well as a large number of phenomena and applications, ample room exists for more computational work to connect principles of mechanics, thermodynamics and kinetics to experiments and to molecular models. In particular, a finite element method is developed using the free-energy function of Flory (1943) and the kinetic model proposed by Hong et al. (2008). Using this model, solvent transport and polymer deformation are

solved concurrently. The method will be implemented in an in-house coded FORTRAN program and a user material subroutine UMAT in commercial FEA software ABAQUS.

3.2. NUMERICAL IMPLEMENTATION OF COUPLED GEL THEORY

In this section, the theory described in chapter 2 is used to develop a numerical method. First, the stress and tangential stiffness is presented, and the formulation for equilibrium swelling is described, the equilibrium swelling could either be implemented in UMAT or the in-house FORTRAN code. Second, the transient swelling is realized by adding the diffusion equations, together they formed a coupled system of equations regarding the displacement field and chemical potential field. The numerical scheme has been tested for different cases and showed to be robust.

3.2.1 Numerical Derivation of Equilibrium Swelling

To start, let's go back to the previous definition of strain energy density. Normalize free energy density $\hat{W}$ defined in equation (2.32) by kT/v, i.e.,

$$U = \hat{W}/\left(kT/v\right) \tag{3.1}$$

And use the notation $J = \det\left(\mathbf{F}\right)$, the normalized free energy density is

$$U = \frac{1}{2}Nv\left(I_1 - 3 - 2\ln J\right) - \left[\left(J-1\right)\ln\frac{J}{J-1} + \frac{\chi}{J}\right] - \mu\left(J-1\right) \tag{3.2}$$

Where

$$I_1 = \lambda_1^2 + \lambda_2^2 + \lambda_3^2 \tag{3.3}$$

Is the first strain invariance and

$$I_3 = J^2 = \lambda_1^2 \lambda_2^2 \lambda_3^2 \tag{3.4}$$

is the third strain invariance.

For hyperelastic materials, the deviatoric and volumetric part of the deformation could be splitted(Bonet and Wood 1997) by introducing $\bar{I}_1$, where

$$\bar{I}_1 = \bar{\lambda}_1^2 + \bar{\lambda}_2^2 + \bar{\lambda}_3^2 = J^{-\frac{2}{3}} I_1 \tag{3.5}$$

In the above formulation, $\bar{\lambda}_i = J^{-\frac{1}{3}} \lambda_i \ (i = 1, 2, 3)$. So the expression for free energy density could be transformed

$$U = \frac{1}{2} Nv \left(J^{\frac{2}{3}} \bar{I}_1 - 3 - 2 \ln J \right) - \left[(J-1) \ln \frac{J}{J-1} + \frac{\chi}{J} \right] - \mu (J-1) \tag{3.6}$$

To avoid the numerical singularities at $J = 1$, which is unphysical since the gel could not be perfectly dry, an small initial swelling configuration is introduced by assuming an initial homogeneous swelling $\lambda_1 = \lambda_2 = \lambda_3 = \lambda_0$, in this case,

$I_1 \to \lambda_0^2 I_1,\ J \to \lambda_0^3 J\ , I_3 \to \lambda_0^6 I_3$.

And the strain energy density also changed to

$$U=\frac{1}{2}Nv\left[I_1\lambda_0^2-3-2\ln\left(J\lambda_0^3\right)\right]-\left[\left(J\lambda_0^3-1\right)\ln\frac{J\lambda_0^3}{J\lambda_0^3-1}+\frac{\chi}{J\lambda_0^3}\right]-\mu\left(J\lambda_0^3-1\right) \quad (3.7)$$

The nominal stress **s** depends on the free energy and could be derived from equation (2.28):

$$s_{iK}=\frac{\partial U}{\partial F_{iK}}=\frac{\partial U}{\partial I_1}\frac{\partial I_1}{\partial F_{iK}}+\frac{\partial U}{\partial J}\frac{\partial J}{\partial F_{iK}} \quad (3.8)$$

Using the following relations:

$$\frac{\partial I_1}{\partial F_{iK}}=2F_{iK},\ J=\frac{1}{6}e_{ijk}e_{KQR}F_{iK}F_{mQ}F_{kR},\ \frac{\partial J}{\partial F_{iK}}=\frac{1}{2}e_{ijk}e_{KQR}F_{jQ}F_{kR},\ \sigma_{ij}=\frac{1}{J}s_{iK}F_{jK} \quad (3.9)$$

It is not difficult to obtain that:

$$\sigma_{ij}=Nv\lambda_0^2J^{-\frac{1}{3}}\bar{B}_{ij}+\delta_{ij}\left(-\frac{1}{J}Nv-\lambda_0^3\ln\frac{J\lambda_0^3}{J\lambda_0^3-1}+\frac{1}{J}+\frac{\chi}{J^2\lambda_0^3}-\mu\lambda_0^3\right) \quad (3.10)$$

Where $\bar{B}_{ij}=J^{-\frac{2}{3}}F_{iK}F_{jK}$ is the left Cauchy-Green tensor. For convenience of later study, we could split equation (3.10) by defining a reference chemical potential μ^0 .and increment of chemical potential $\Delta\mu$.

$$\sigma_{ij}=\sigma_{ij}^0-\Delta\mu\delta_{ij} \quad (3.11)$$

Where:

$$\sigma_{ij}^{0} = Nv\lambda_0^2 J^{-\frac{1}{3}}\bar{B}_{ij} + \delta_{ij}\left(-\frac{1}{J}Nv - \lambda_0^3 \ln\frac{J\lambda_0^3}{J\lambda_0^3 - 1} + \frac{1}{J} + \frac{\chi}{J^2\lambda_0^3} - \mu^0\lambda_0^3\right) \tag{3.12}$$

Through the definition of velocity gradient $\delta\mathbf{L}$ and rate of deformation $\delta\mathbf{D}$,

$$\delta\mathbf{L} = \frac{\partial(\delta\mathbf{u})}{\partial\mathbf{x}},\ \delta\mathbf{D} = \frac{1}{2}\left(\delta\mathbf{L} + \delta\mathbf{L}^T\right) \tag{3.13}$$

Variation of σ_{ij} would be derived as:

$$\begin{aligned}\delta\sigma_{ij} = {} & Nv\lambda_0^2 J^{-\frac{1}{3}}\left[H_{ijkl}\left(\delta D_{kl} - \frac{\delta_{kl}}{3}\delta D_{mm}\right) + \bar{B}_{kj}\delta W_{ik} - \bar{B}_{iK}\delta W_{kj}\right] - \frac{1}{3}Nv\lambda_0^2\bar{B}_{ij}J^{-\frac{1}{3}}\delta D_{kk} \\ & + \delta_{ij}\frac{1}{J^3\lambda_0^3\left(J^3\lambda_0^3 - 1\right)}\left(2\chi + J\lambda_0^3 - 2J\chi\lambda_0^3\right)J\delta D_{kk} + \frac{1}{J}Nv\delta D_{kk}\delta_{ij}\end{aligned} \tag{3.14}$$

Where:

$$H_{ijkl} = \frac{1}{2}\left(\delta_{ik}\bar{B}_{jl} + \delta_{il}\bar{B}_{jk} + \delta_{jk}\bar{B}_{il} + \delta_{jl}\bar{B}_{ik}\right) \tag{3.15}$$

The virtue rate of Kirchhoff stress $\boldsymbol{\tau}$ is $\delta\boldsymbol{\tau} = \delta\left(J\boldsymbol{\sigma}\right)$ and could be decomposed as

$$\delta\left(J\sigma_{ij}\right) = J\delta\sigma_{ij} + \sigma_{ij}\delta J \tag{3.16}$$

After some calculations, it is not difficult to find that

$$\delta\left(J\sigma_{ij}\right)=Nv\lambda_0^2J^{\frac{2}{3}}H_{ijkl}\left(\delta D_{kl}-\frac{\delta_{kl}}{3}\delta D_{mm}\right)-\frac{1}{3}Nv\lambda_0^2\bar{B}_{ij}J^{\frac{2}{3}}\delta D_{kk}$$
$$+\delta_{ij}\frac{1}{J\lambda_0^3\left(J\lambda_0^3-1\right)}\left(2\chi+J\lambda_0^3-2J\chi\lambda_0^3\right)\delta D_{kk}+Nv\lambda_0^3J^{\frac{2}{3}}\bar{B}_{ij}\delta D_{kk}$$
$$+\delta_{ij}\left(-\lambda_0^3\ln\frac{J\lambda_0^3}{J\lambda_0^3-1}+\frac{1}{J}+\frac{\chi}{J^2\lambda_0^3}-\mu\lambda_0^3\right)J\delta D_{kk}+Nv\lambda_0^2J^{\frac{2}{3}}\left(\bar{B}_{kj}\delta W_{ik}-\bar{B}_{ik}\delta W_{kj}\right) \tag{3.17}$$

In the above formulation, virtual rate of spin $\delta\mathbf{W}$ relates to velocity gradient via

$$\delta W_{ij}=\frac{1}{2}\left(\delta L_{ij}-\delta L_{ji}\right) \tag{3.18}$$

Actually, because

$$\begin{cases}\boldsymbol{\sigma}\bullet\delta\mathbf{W}=\sigma_{ik}\delta W_{kj}=Nv\lambda_0^2J^{-\frac{1}{3}}\bar{B}_{ik}\delta W_{kj}+\left(-\dfrac{1}{J}Nv-\lambda_0^3\ln\dfrac{J\lambda_0^3}{J\lambda_0^3-1}+\dfrac{1}{J}+\dfrac{\chi}{J^2\lambda_0^3}-\mu\lambda_0^3\right)\delta W_{ij},\\ \delta\mathbf{W}\bullet\boldsymbol{\sigma}=\delta W_{ik}\sigma_{kj}=Nv\lambda_0^2J^{-\frac{1}{3}}\bar{B}_{kj}\delta W_{ik}+\left(-\dfrac{1}{J}Nv-\lambda_0^3\ln\dfrac{J\lambda_0^3}{J\lambda_0^3-1}+\dfrac{1}{J}+\dfrac{\chi}{J^2\lambda_0^3}-\mu\lambda_0^3\right)\delta W_{ij}\end{cases} \tag{3.19}$$

It is not difficult to find that:

$$Nv\lambda_0^2J^{\frac{2}{3}}\left(\bar{B}_{kj}\delta W_{ik}-\bar{B}_{ik}\delta W_{kj}\right)=J\left(\delta\mathbf{W}\bullet\boldsymbol{\sigma}-\boldsymbol{\sigma}\bullet\delta\mathbf{W}\right) \tag{3.20}$$

If define tangential modulus C_{ijkl} as:

$$C_{ijkl}=Nv\lambda_0^2J^{-\frac{1}{3}}H_{ijkl}+\left(-\frac{\chi}{J^2\lambda_0^3}+\frac{\lambda_0^3}{J\lambda_0^3-1}-\lambda_0^3\ln\frac{J\lambda_0^3}{J\lambda_0^3-1}-\mu\lambda_0^3\right)\delta_{ij}\delta_{kl} \tag{3.21}$$

Then equation (3.17) could be simplified to a more simple expression

$$\delta\left(J\sigma_{ij}\right) = JC_{ijkl}\delta D_{kl} + J\left(\sigma_{kj}\delta W_{ik} - \sigma_{ik}\delta W_{kj}\right) \tag{3.22}$$

In the above expression, $\delta\left(J\sigma_{ij}\right) = \delta\tau_{ij}$ is the Kirchhoff stress rate, on the right hand side, the first term represents the stress change due to stretching, and the second term represents the stress change due to rotation.

It should be noted that the expression of σ_{ij} in equation (3.10) and tangential modulus C_{ijkl} in equation (3.21) are two key components to write an ABAQUS user material subroutine named UMAT. Rui and coworkers(Kang and Huang 2010) have also done similar work to develop a UMAT. However, with the capabilities in the UMAT, only equilibrium swelling with constant chemical potential is able to be studied. In UMAT, chemical potential serves as a state variable and only the displacement variables changes. To study the transient swelling, chemical potential change should be addressed.

3.2.2 Numerical Simulation of Transient Swelling

First let's simplify the deformation terms. To study the transient gel swelling, we first review some of the fundamental principles in continuum mechanics. Define virtual strain as

$$\delta\boldsymbol{\varepsilon} = \frac{1}{2}\left(\frac{\partial\delta\mathbf{u}}{\partial\mathbf{x}} + \frac{\partial\delta\mathbf{u}^{T}}{\partial\mathbf{x}}\right) \tag{3.23}$$

As stated in virtual work principle, the internal energy variation is caused by external work done by body force $\mathbf{Q}$ and surface traction $\mathbf{t}$,

$$\int_V \boldsymbol{\sigma} : \delta\boldsymbol{\varepsilon} dV = \int_S \mathbf{t} \bullet \delta\mathbf{u} dS + \int_V \mathbf{Q} \bullet \delta\mathbf{u} dV \tag{3.24}$$

The above equation could be reduced to a set of equation regarding $\delta\mathbf{u}$, by moving the right terms to the left, i.e., and the difference produces the residual force vector $\mathbf{R}$, i.e.,

$$\mathbf{R}_u(\delta\mathbf{u}) = \int_V \boldsymbol{\sigma} : \delta\boldsymbol{\varepsilon} dV - \int_S \mathbf{t} \bullet \delta\mathbf{u} dS - \int_V \mathbf{Q} \bullet \delta\mathbf{u} dV \tag{3.25}$$

Linearize residual force $\mathbf{R}$ with respect to displacement gives Jacobian matrix $\mathbf{K}_{uu}$, i.e.,

$$\mathbf{K}_{uu} = \frac{d\mathbf{R}}{d\mathbf{u}} = \frac{d\left(\int_V \boldsymbol{\sigma} : \delta\boldsymbol{\varepsilon} dV - \int_S \mathbf{t} \bullet \delta\mathbf{u} dS - \int_V \mathbf{Q} \bullet \delta\mathbf{u} dV\right)}{d\mathbf{u}} \tag{3.26}$$

, where subscript "*uu*" is used to represent that it is the stiffness for the displacement variables.

Let's take a look at the body force and surface traction terms in equation (3.26). First look at body force term $d\left(\int_V \mathbf{Q} \bullet \delta\mathbf{u} dV\right) / d\mathbf{u}$. Take a common type of body force self-weight as an example. $\mathbf{Q} = \rho\mathbf{g}$, where ρ is current density and $\mathbf{g}$ is acceleration due to gravity, in this case,

$$\int_V \mathbf{Q}\bullet\delta\mathbf{u}dV = \int_V \rho\mathbf{g}\bullet\delta\mathbf{u}dV = \int_V \frac{\rho_0}{J}\mathbf{g}\bullet\delta\mathbf{u}dV = \int_{V_0} \rho_0\mathbf{g}\bullet\delta\mathbf{u}dV_0 \tag{3.27}$$

Since $\mathbf{g}$ remains constant, the linearization of the above formulation equals zero. Then look at the surface traction term $d\left(\int_S \mathbf{t}\bullet\delta\mathbf{u}dS\right)/d\mathbf{u}$. Surface traction $\mathbf{t}$ could be decomposed as $\mathbf{t} = \mathbf{t}_N + \mathbf{t}_x + \mathbf{t}_y$, where $\mathbf{t}_N$ is normal component and $\mathbf{t}_x$, $\mathbf{t}_y$ are two in-plane components. In a simple case where a normal pressure is applied, i.e., $\mathbf{t} = p\mathbf{n}$, where $\mathbf{n}$ is current surface normal. Because variation of surface normal is nonzero, i.e., $d\mathbf{n} \neq 0$. $d\left(\int_S \mathbf{t}\bullet\delta\mathbf{u}dS\right)/d\mathbf{u}$ is nonzero and contributes to a term known as pressure stiffness(Bonet and Wood 1997).

However, for most of the applications in the current study, load is applied directly on finite element nodes and neither body force loading nor surface traction is necessary. Under this circumstance, complex mathematical derivation about any term related to body force or surface traction is omitted here.

The first term on the right hand side of equation (3.26) could be simplified as

$$d\left(\int_V \boldsymbol{\sigma} : \delta\boldsymbol{\varepsilon}dV\right) = \int_V d\boldsymbol{\sigma} : \delta\boldsymbol{\varepsilon}dV + \int_V \boldsymbol{\sigma} : d\delta\boldsymbol{\varepsilon}dV \tag{3.28}$$

And after some derivation, it could be simplified as

$$d\left(\int_V \boldsymbol{\sigma} : \delta\boldsymbol{\varepsilon}dV\right) = \int_V \left[\delta\boldsymbol{\varepsilon} : \mathbf{C} : d\boldsymbol{\varepsilon} - \boldsymbol{\sigma} : \left(2\delta\boldsymbol{\varepsilon}\bullet d\boldsymbol{\varepsilon} - \frac{\partial\delta\mathbf{u}^T}{\partial\mathbf{x}} \bullet \frac{\partial d\mathbf{u}}{\partial\mathbf{x}}\right)\right]dV \tag{3.29}$$

, where $\boldsymbol{\sigma}$ and $\mathbf{C}$ has already been defined in equation (3.10) and (3.21), respectively.

The form of equation (3.29) was first used by Nagtegaal et al.(1974) and now finds its application in major commercial finite element software for their continuum elements formulation since they have been proved to yield fast rate of convergence. The difference for the gel is that the Cauchy stress $\boldsymbol{\sigma}$ also depends on chemical potential. To summarize the discussions above, the Jacobian of the displacement field is obtained as

$$\mathbf{K}_{uu} = \int_V \left[\delta\boldsymbol{\varepsilon} : \mathbf{C} : d\boldsymbol{\varepsilon} - \boldsymbol{\sigma} : \left(2\delta\boldsymbol{\varepsilon} \bullet d\boldsymbol{\varepsilon} - \frac{\partial \delta \mathbf{u}^T}{\partial \mathbf{x}} \bullet \frac{\partial d\mathbf{u}}{\partial \mathbf{x}} \right) \right] dV \tag{3.30}$$

For real numerical situations, the choice of rate of deformation $\delta\boldsymbol{\varepsilon}$ is stringent. Standard formulation, which is defined directly from strain-displacement formulation as in equation (3.23), is not sufficient to deal with complex situations. Shear locking and volumetric locking(Bonet and Wood 1997) behavior could happen when the material is approaching incompressible limit. The elements show unphysical stiffness when get “locked”. In the simulation for gel, when it is near dry, it is close to incompressible and subject to the same problem. In order to overcome this problem and to develop more general finite element formulations, a lot of element technology are available and among them B-bar element technology(Hughes 1980) is employed. The B-bar method works by treating the volumetric part and deviatoric part of the strain-displacement

matrix differently, and is similar to selectively reduced integration method by simply modifying the definition of strain. The volumetric strain is averaged over all the elements in order to eliminate volumetric locking.

To better clarify the idea of B-bar technique. Use 3D brick element as an example, the B-Bar formulation would be:

$$\begin{bmatrix} \delta\varepsilon_{11} \\ \delta\varepsilon_{22} \\ \delta\varepsilon_{33} \\ 2\delta\varepsilon_{23} \\ 2\delta\varepsilon_{13} \\ 2\delta\varepsilon_{12} \end{bmatrix} = \begin{bmatrix} B_1^1 + \frac{\hat{B}_1^1 - B_1^1}{3} & \frac{\hat{B}_2^1 - B_2^1}{3} & \frac{\hat{B}_3^1 - B_3^1}{3} & \cdots & \cdots & \cdots & \frac{\hat{B}_3^8 - B_3^8}{3} \\ \frac{\hat{B}_1^1 - B_1^1}{3} & B_2^1 + \frac{\hat{B}_2^1 - B_2^1}{3} & \frac{\hat{B}_3^1 - B_3^1}{3} & \cdots & \cdots & \cdots & \frac{\hat{B}_3^8 - B_3^8}{3} \\ \frac{\hat{B}_1^1 - B_1^1}{3} & \frac{\hat{B}_2^1 - B_2^1}{3} & B_3^1 + \frac{\hat{B}_3^1 - B_3^1}{3} & \cdots & \cdots & \cdots & B_3^8 + \frac{\hat{B}_3^8 - B_3^8}{3} \\ 0 & B_3^1 & B_2^1 & \cdots & \cdots & \cdots & B_2^8 \\ B_3^1 & 0 & B_1^1 & \cdots & \cdots & \cdots & B_1^8 \\ B_2^1 & B_1^1 & 0 & \cdots & \cdots & \cdots & 0 \end{bmatrix} \begin{bmatrix} \delta u_1^1 \\ \delta u_2^1 \\ \delta u_3^1 \\ \cdots \\ \delta u_1^8 \\ \delta u_2^8 \\ \delta u_2^8 \end{bmatrix}$$

, (3.31)

where $B_i^\alpha = \frac{\partial N_\alpha}{\partial X_i}$ is standard shape function derivative and

$\hat{B}_i^\alpha = \int_{V^e} \frac{\partial N_\alpha}{\partial X_i} dV^e / \int_{V^e} dV^e$ is averaged shape function derivative. Write equation (3.31) in symbolic form, we have:

$$\delta\boldsymbol{\varepsilon} = \bar{\mathbf{B}} \bullet \delta\mathbf{u} \tag{3.32}$$

Where $\bar{\mathbf{B}}$ is the coefficient matrix in equation (3.31).

Linearize R_u^P with respect to chemical potential increment $\Delta\bar{\mu}$, the off-diagonal coupling stiffness $K_{u\mu}^{PQ}$ could be obtained as:

$$K_{u\mu}^{PQ} = \frac{\partial R_u^P}{\partial \Delta\bar{\mu}^Q} = -\delta u_k^P \int \left[\bar{B}_{ii}\right]_k^P N^Q dV d\Delta\bar{\mu}^Q \tag{3.33}$$

In the above discussions, the stiffness matrix relates to the deformation part has been derived. In the following discussion, the stiffness matrix for the diffusion part will be investigated.

The diffusion equation in reference configuration has been defined previously in equation (2.25), and if there is no source contribution, it could be simplified as

$$\frac{\partial C}{\partial t} + \frac{\partial j_i}{\partial x_i}\det(\mathbf{F}) = 0 \tag{3.34}$$

, where $j_i = \dfrac{F_{iK} J_K}{\det(\mathbf{F})}$ is the flux defined in the current configuration and $x_i\,(i = 1,2,3)$ are coordinates in the current configuration. At the same time, j_i relates to chemical potential by

$$j_i = -\frac{cD}{kT}\frac{\partial \mu}{\partial x_i} \tag{3.35}$$

Applying molecular incompressibility condition $1 + vC = \det(\mathbf{F})$ and define normalized variable $\bar{j}_i = v j_i$ and $\bar{\mu} = \mu / kT$, we have

$$\bar{j}_i = -\frac{\left(\det \mathbf{F} - 1\right) D}{\det \mathbf{F}} \frac{\partial \bar{\mu}}{\partial x_i} \tag{3.36}$$

Then equation (3.34) could be simplified as

$$\frac{1}{\det \mathbf{F}} \frac{\partial \left(\det \mathbf{F} - 1\right)}{\partial t} + \frac{\partial \bar{j}_i}{\partial x_i} = 0 \tag{3.37}$$

On the surface, the flux should satisfy

$$\bar{j}_i n_i = \bar{q} \left(\text{on } S_j\right) \tag{3.38}$$

Introduce arbitrary test function $\delta\bar{\mu}$, multiply equation (3.37) by $\delta\bar{\mu}$, integrate in the volume dV and apply divergence theorem, we have

$$\int_V \delta\bar{\mu} \frac{1}{\det\left(\mathbf{F}\right)} \frac{\partial \left(\det\left(\mathbf{F}\right) - 1\right)}{\partial t} dV - \int_V \delta \left(\frac{\partial \bar{\mu}}{\partial \mathbf{x}}\right) \bullet \mathbf{f} dV - \int_{S_j} \delta\bar{\mu}\bar{q} dS = 0 \tag{3.39}$$

Residual force vector for chemical potential is:

$$R_\mu = -\int_V \delta\bar{\mu} \frac{1}{\det\left(\mathbf{F}\right)} \frac{\partial \left(\det\left(\mathbf{F}\right) - 1\right)}{\partial t} dV + \int_V \delta \left(\frac{\partial \bar{\mu}}{\partial \mathbf{x}}\right) \bullet \mathbf{f} dV + \int_{S_j} \delta\bar{\mu}\bar{q} dS \tag{3.40}$$

Discretize element chemical potential using shape function N^P and nodal chemical potential value $\bar{\mu}^P$, i.e., $\bar{\mu} = N^P \bar{\mu}^P$. Then the residual force vector R_μ could be simplified as

$$R_{\mu}^{P} = -\delta\bar{\mu}^{P}\int_{V} N^{P}\,\frac{1}{\det\mathbf{F}}\,\frac{\det\mathbf{F}-\det\mathbf{F}^{0}}{\Delta t}\,dV + \delta\bar{\mu}^{P}\int_{V}\frac{\partial N^{P}}{\partial\mathbf{x}}\bullet\mathbf{f}dV + \delta\bar{\mu}^{P}\int_{S_j} N^{P}\bar{q}dS \quad (3.41)$$

Obviously, the residual force vector for chemical potential depends on the deformation via location $\mathbf{x}$ and deformation gradient $\det\mathbf{F}$.

The corresponding Jacobian matrix for chemical potential term $K_{\mu\mu}^{PQ}$ could be obtained via linearization of R_{μ}^{P}, i.e.,

$$K_{\mu\mu}^{PQ} = \frac{dR_{\mu}^{P}}{d\,\bar{\mu}^{Q}} + \frac{dR_{\mu}^{P}}{d\left(\partial\bar{\mu}/\partial x\right)^{Q}} \quad (3.42)$$

Since flux $\mathbf{f}$ depends on chemical potential gradient, we have $dR_{\mu}^{P}/d\,\bar{\mu}^{Q} = 0$ and

$$\frac{dR_{\mu}^{P}}{d\left(\partial\bar{\mu}/\partial x\right)^{Q}} = -\delta\bar{\mu}^{P}\int\frac{\partial N^{P}}{\partial\mathbf{x}}\bullet\frac{\partial N^{Q}}{\partial\mathbf{x}}\left[-\frac{\left(\det\mathbf{F}-1\right)D}{\det\mathbf{F}}\right]dVd\,\bar{\mu}^{P} \quad (3.43)$$

So equation (3.42) simplifies to

$$K_{\mu\mu}^{PQ} = -\delta\bar{\mu}^{P}\int\frac{\partial N^{P}}{\partial\mathbf{x}}\bullet\frac{\partial N^{Q}}{\partial\mathbf{x}}\left[-\frac{\left(\det\mathbf{F}-1\right)D}{\det\mathbf{F}}\right]dVd\,\bar{\mu}^{P} \quad (3.44)$$

At the same time, coupling terms between chemical potential $\bar{\mu}$ and displacement $\mathbf{u}$ could be derived:

$$K_{\mu u}^{PQ} = \frac{\partial R_{\mu}^{P}}{\partial u_k^Q} = \delta\bar{\mu}^P \frac{1}{\Delta t}\int N^P \frac{\partial}{\partial u_k^Q}\left[\frac{\det \mathbf{F} - \det \mathbf{F}^0}{\det \mathbf{F}}\right] dV du_k^Q - \delta\bar{\mu}^P \int \frac{\partial N^P}{\partial \mathbf{x}} \bullet \frac{\partial \mathbf{f}}{\partial u_k^Q} dV du_k^Q \tag{3.45}$$

Where

$$\frac{\partial \mathbf{f}}{\partial u_k^Q} = -D\frac{\partial \bar{\mu}}{\partial \mathbf{x}}\frac{1}{\det \mathbf{F}} H_{kK}\frac{\partial N^Q}{\partial X_K} \tag{3.46}$$

And finally, $K_{\mu u}^{PQ}$ could be finally simplified to

$$\begin{aligned} K_{\mu u}^{PQ} &= \delta\bar{\mu}^P \frac{1}{\Delta t}\int_V N^P \left[\frac{1}{\det \mathbf{F}} H_{kK}\frac{\partial N^Q}{\partial X_K}\right] dV du_k^Q \\ &+ \delta\bar{\mu}^P \int_V \frac{\partial N^P}{\partial \mathbf{x}} \bullet \left[D\frac{\partial \bar{\mu}}{\partial \mathbf{x}}\frac{1}{\det \mathbf{F}} H_{kK}\frac{\partial N^Q}{\partial X_K}\right] dV du_k^Q \end{aligned} \tag{3.47}$$

To summarize the above derivation, equations (3.30), (3.42), (3.33) and (3.47) defines the Jacobian matrices and equations (3.25) and (3.41) defines the residual force vector , they together forms the coupled equations to solve for displacement and chemical potential increment, i.e.,

$$\begin{bmatrix} \mathbf{K}_{\mathbf{u}u} & \mathbf{K}_{\mathbf{u}\mu} \\ \mathbf{K}_{\mu\mathbf{u}} & \mathbf{K}_{\mu\mu} \end{bmatrix} \begin{bmatrix} \Delta\mathbf{u} \\ \Delta\bar{\mu} \end{bmatrix} = \begin{bmatrix} \mathbf{R}_{\mathbf{u}} \\ \mathbf{R}_{\mu} \end{bmatrix} \tag{3.48}$$

Equation (3.48) is the fundamental equation to develop an in-house coded FORTRAN program named “Gel Swelling Program (GSP)” (see Appendix A). It is a fully coupled equation about displacement and chemical potential. Newton

iterations are required to finally obtain accurate result. In each numerical iteration, the displacement and chemical potential value are updated. Using this program, various complex problems could be solved and studied in subsequent chapters.

3.3. NUMERICAL SWELLING EXAMPLES

In this section several numerical examples are studied using the previously described numerical method. Again, free-energy density and stress is normalized by kT/v and the chemical potential is normalized by kT. The theory has no intrinsic length scale or intrinsic time scale. Let L be a characteristic length in a boundary-value problem and normalize all the other lengths by L, and normalize the time by L^2/D.

A representative value of the volume per solvent molecule $v = 10^{-28}\,\mathrm{m}^3$ is used. At room temperature, $kT = 4\times10^{-21}\,\mathrm{J}$ and in this case $kT/v = 4\times10^{7}$ Pa. The Flory-Rehner free energy density function introduces two dimensionless material parameters: Nv and χ. The dry network has a shear modulus NkT under the small-strain conditions, with the representative values $NkT = 10^{4} \sim 10^{7}$ $\mathrm{N/m}^2$, which gives the range $Nv = 10^{-4} \sim 10^{-1}$. The parameter χ is a dimensionless measure of the enthalpy of mixing, with representative values χ = 0 ~ 1.2. For applications that prefer gels with large swelling ratios, materials with low values of χ are used. In the numerical examples below, the values $Nv = 10^{-3}$ and $\chi = 0.2$ are used. Diffusion coefficient for water $D = 8\times10^{-10}\,\mathrm{m}^2/\mathrm{s}$ is adopted.

The performance of the finite element method is first benchmarked by comparing finite element results with those using a finite difference method for a creep problem(2008).

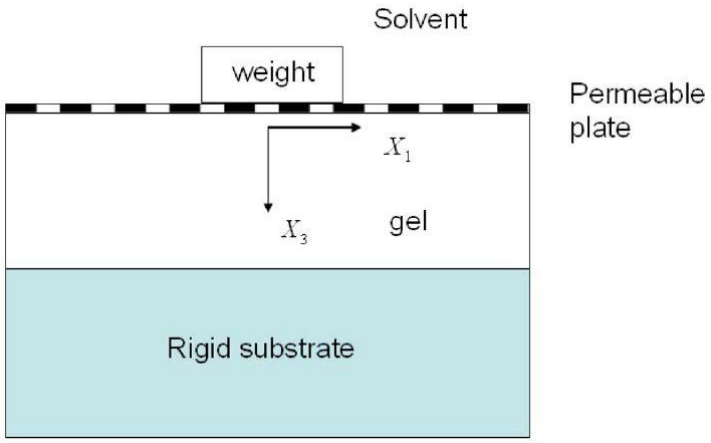

Figure 3.1. A fully swelling gel bonded to a rigid substrate and subject to an applied weight via a permeable plate

Figure 3.1 illustrates a thin layer of a gel immersed in a pure liquid solvent. The gel first undergoes free swelling subject to no constraint and no applied forces. The swollen gel is then bonded to a rigid substrate, and subject to an applied weight. The solvent can migrate out from the top surface of the gel, and the gel thins down. The layer will eventually attain a new state of equilibrium. Let L be thickness of the dry network subject to no mechanical forces. This dry and undeformed configuration is used as the reference configuration, where a marker has the coordinates X_1 and X_2 in the plane of the layer, and the coordinate X_3 normal to the layer and pointing downwards. After free swelling and equilibrating

with the pure liquid solvent, the layer swells by an isotropic stretch, $\lambda_1 = \lambda_2 = \lambda_3 = 3.215$. The gel is then bonded to the rigid substrate, and subjected to a surface traction, i.e., the weight divided by the area of the dry polymer. When the solvent migrates out, λ_1 and λ_2 remain unchanged, but λ_3 changes with time and position. The thickness of the gel is taken to be much smaller than the lateral dimensions of the gel, such that the field in gel is independent of X_1 and X_2. The functions $\lambda_3(X_3,t)$ and $\mu(X_3,t)$ could be determined.

In a finite element model, twenty 8-node brick elements are used. They stacked up one on top of another in the direction of the thickness. To model the full layer of the gel, vanishing displacements and flux in lateral directions are imposed. The top surface of the gel is prescribed with the traction and the vanishing chemical potential, while the bottom surface of the gel is prescribed with the vanishing displacement and flux.

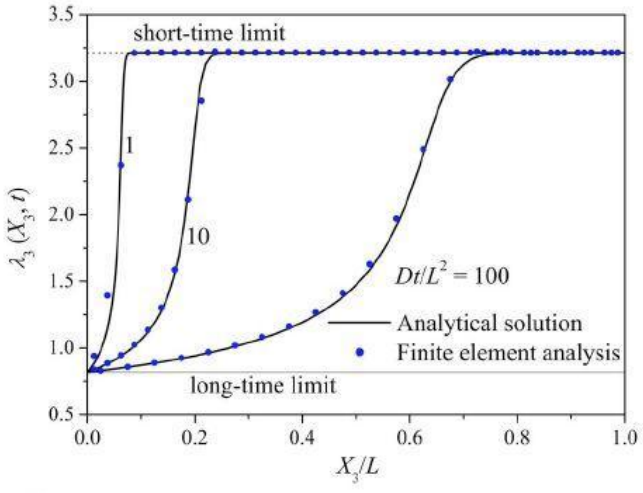

Figure 3.2. Stretch evolution during the creep test

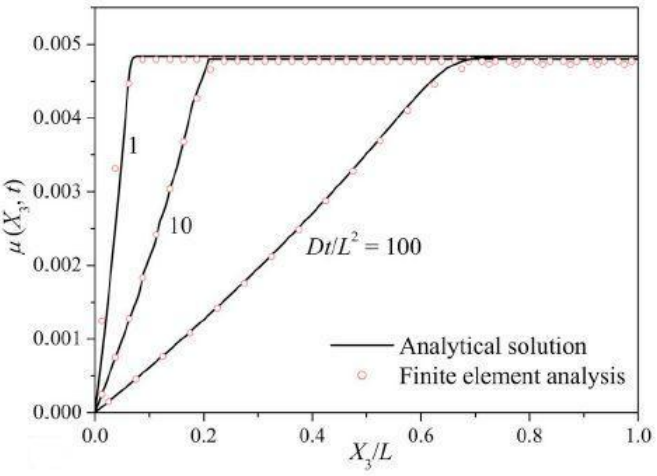

Figure 3.3. Chemical potential evolution during the creep test

Figure 3.2 and Figure 3.3 compare the functions $\lambda_3(X_3,t)$ and $\mu(X_3,t)$ obtained from the finite element method in this paper and that from a finite difference method by Hong et al. (2008). As shown in the figures, the agreement is good. At the short-time limit, the weight is applied, but the solvent has no time to migrate out, so that the stretch is unchanged, $\lambda_3(X_3,0)=3.215$, but the chemical potential jumps to a value higher than that of the external solvent, $\mu(X_3,0)>0$. At the long-time limit, the chemical potential in the gel equilibrates with that of the solvent, $\mu(X_3,0)=0$, and the stretch reduces to a new value.

As a consequence of the conditions of local equilibrium, the top surface of the gel $(X_3=0)$ reaches the long-time limit instantaneously, with the vanishing

chemical potential as fixed by the external solvent. In a short time, the interior of the gel is still largely in the state of short-time limit. As the time processes, the solvent migrates out gradually, and the entire gel evolves toward the long-time limit.

The second example is free swelling of a cube of a gel with size L in the dry state is studied. The dry cubic gel is dropped into a solvent bath with all surfaces contact with solvent. Because all the surfaces have the same chance to absorb solvent and geometrically equivalent, conditions of symmetry are imposed, so that only one-eighth of the cube is modeled. 1,000 brick elements with chemical potential degree of freedom were used to simulate the whole swelling process and Figure 3.4 showed several key steps.

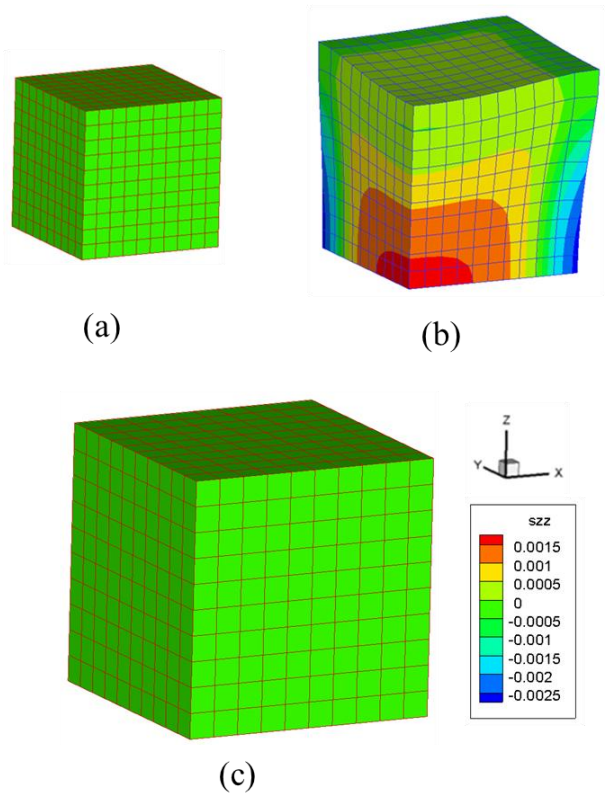

Figure 3.4. Different stage of swelling of a quarter of the gel (a) initial shape $Dt / L^2 = 0$ (c) transient swelling shape at $Dt / L^2 = 3.0$ (c) equilibrium swelling shape $Dt / L^2 = \infty$

Figure 3.4(a) is the initially dry state, with the dimension in all direction be the same. Figure 3.4(b) is a transient state relates to $Dt / L^2 = 3.0$ and Figure 3.4(c) is the state for swelling equilibrium. Again, the figure in Figure 3.4 is only one-eighth of the whole geometry, i.e., full cubic. As shown from the swelling process, it is observed that the gel first swells to a bowl-like shape, where the corner swells more than the center. The reason is because the corner has more contact with solvent. And the pulling stress in the center is larger than the corner,

which serves as the driven force for the center to match up with the swelling of the corner. More intuitively, the dry region (center region) has larger tendency to absorb solvent. But at the final stage, i.e., given enough time, the gel swelling reaches equilibrium. The final shape is flat which indicates that a homogeneous swelling state is reached due to the lack of constraint for this cubic gel. In any material point inside the gel, it bears the same amount of swelling along any direction. As observed from the swelling process, extensional stress have been developed, indicating that the gel have the "tendency" to be stretched, or namely, swell. This inhomogeneous swelling process is very common in the swelling of gels and have also been observed in experiments(Achilleos et al. 2000).

3.4. SUMMARY AND DISCUSSIONS

In this chapter, the status of numerical methods toward gel swelling is introduced. Numerical method for equilibrium gel swelling and transient gel swelling is presented. In this method, coupling equation regarding deformation and chemical potential change is obtained. Based on this method, an ABAQUS user material program UMAT that is capable to study gel equilibrium swelling is built and an in-house FORTRAN program named "Gel Swelling Program (GSP)" that is capable to study both transient and equilibrium swelling is developed and attached in Appendix A. GSP is capable to solve very complex program and allows flexibility for future editing. In the gel community, where new applications come out rapidly(Xue et al. 2011, ; Costa et al. 2012), it meets the demands of numerical tools in swelling simulation. The validity of the numerical method is

benchmarked via a creep test problem and visualized by a simple cubic swelling example.

4 SWELLING INDUCED BUCKLING IN GELS

4.1. INTRODUCTION TO GEL BUCKLING

Buckling instability has been studied extensively for the past few decades as one of the most critical structural failure modes (Timoshenko and Gere 1961). This conventional theme is recently gaining new attention as a useful way for creation and transformation of patterns because buckling is often accompanied with large deformation and radical shape change of the structure. Nature has already developed such techniques to leverage mechanical instability to create a wealth of complex patterns. As biological tissues and organisms grow non-uniformly or under constraints, plane features transform into rich patterns with complexity as found in such examples as wavy edges of plant leaves(Sharon, Marder, and Swinney 2004), fine annular patterns in fingerprints(Kucken and Newell 2005, ; Liang and Mahadevan 2009), inter-connected creases of brain cortex(Bayer and Altman 2005) and buckling of microtubules(Shen 2010, ; Gao and Lei 2009, ; Jiang and Zhang 2008).

This elegant approach to achieve pattern transformation by harnessing mechanical instability has not been much explored until recent progress in material science and manufacturing technologies for soft materials such as elastomers and hydrogels. Particularly, swelling gels have attracted increasing interest because they can actively grow and shrink depending on environmental conditions such as humidity, temperature and pH(Beebe et al. 2000, ; Dong et al. 2006, ; Sidorenko et al. 2007). Hydrogel-based structures, therefore, can

spontaneously create and reversibly pose different patterns via buckling without the need for external load to trigger mechanical instability. This holds great potential in development of self-operating devices with switchable functionalities.

4.2. EXPERIMENTAL STUDY AND FINITE ELEMENT SIMULATION

4.2.1 Experimental Study

A novel 3D micro-fabrication technology, projection micro-stereolithography (PμSL)(Sun et al. 2005), is used to fabricate hydrogel micro tubes. All the experiments in this chapter are done by Dr. Howon Lee. The bottom of the hydrogel tube is fixed to impose constraints against swelling as shown in Figure 4.1.

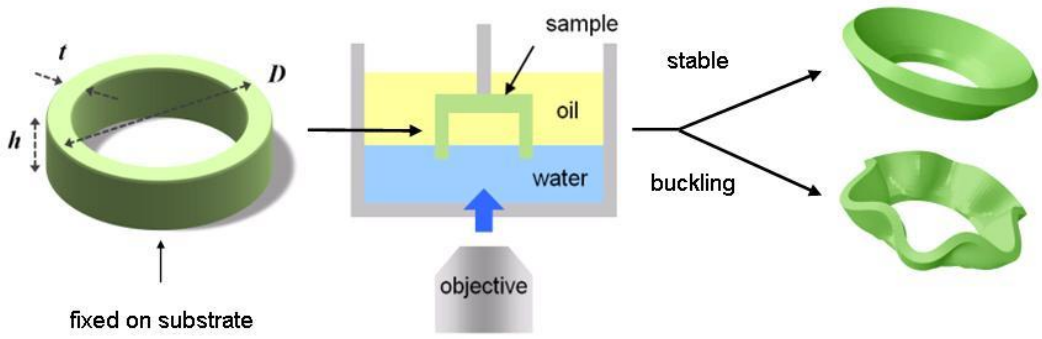

Figure 4.1. Illustration of the ring buckling experimental setup and buckling process

Characteristic dimensional parameters, t, h and D represent thickness, height, and diameter of the model structure in dry state, respectively. Subjected to

the fixed boundary condition on the bottom, the gel develops inhomogeneous stress when allowed to swell. By appropriate selection of dimension, constrained swelling can be made to exhibit buckling instability, causing the circular wall to transform into wrinkled patterns with different wave numbers.

To demonstrate pattern formation, The tubular gel samples are fabricated in different dimensions using poly(ethylene glycol) diacrylate (PEGDA). Four groups of samples (I-IV) with different levels of normalized thickness t/h were prepared, with group I being thicker and group IV being more slender (upper image in Figure 4.2). Each group consists of six samples (i-vi) with different levels of normalized height h/D, with the sample i being shorter and the sample vi being taller. For swelling experiment, a sample is placed upside down and put in the bath with water covered with oil layer on top as illustrated in Figure 4.1. Then the sample was brought into contact with water surface for swelling, while base substrate part on which the gel tube was fixed stayed in the top oil layer. In this way, water can diffuse into the tube wall allowing the sample swell before the constraining base relaxes by wetting. Circular tubes transformed into a wide variety of rich patterns as swelling proceeded.

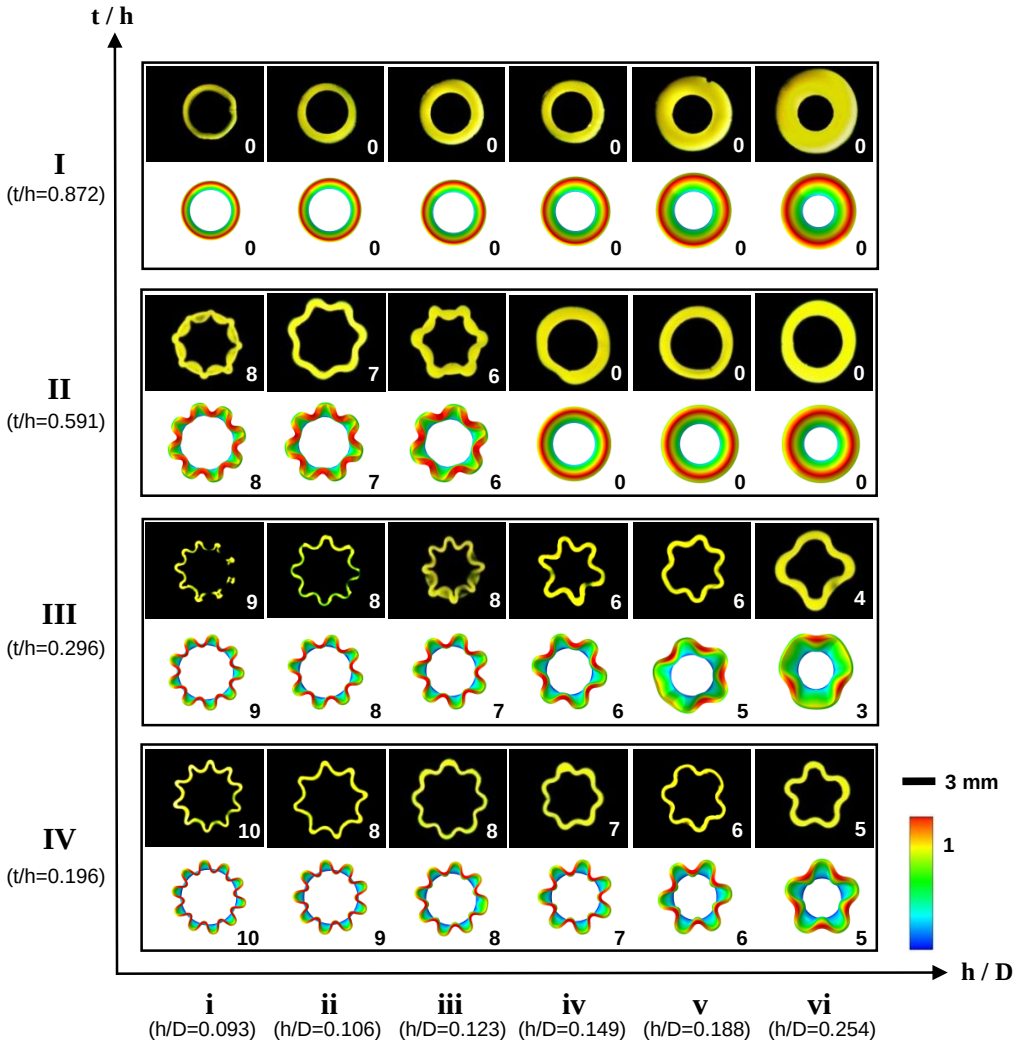

Figure 4.2. Comparison of finite element simulated buckling pattern and experimental buckling pattern. Color bar indicates normalized height of samples.

Figure 4.2 presents swelling patterns obtained in the swelling experiment from different samples. Images with dark background are experimental results and with white background are finite element simulation results. Experiment

agrees with simulation very well. These results suggest strong connection between the normalized thickness t/h and stability, and between the normalized wall height h/D and buckling pattern. Samples in group I and II had tendency to remain stable during swelling, while samples in group III and IV underwent mechanical instability and transformed into wrinkled patterns. More interestingly, samples with the same normalized height h/D transformed into instability patterns with the number of wrinkles close to each other, regardless of the normalized wall thickness t/h. The same trend was observed when the same experiment using hydrogel with different stiffness and swelling ratio was repeated, confirming that dimension plays a dominant role in spontaneous buckling in swelling gel.

4.2.2 Finite Element Simulation

The simulation follows much with the method described in chapter 3. And a user material program UMAT implemented in ABAQUS software is used to study the gel swelling. In the UMAT, the gel is programmed as a user material and chemical potential is an adjustable parameter. Swelling is realized via coupled-temperature displacement analysis by changing chemical potential. To simulate the buckling process, an initial perturbation analysis is performed to generate the buckling wave followed by a subsequent post-buckling analysis to produce the final wave shape. 0.1% of the first three buckling modes magnitude from a thermal expansion perturbation analysis (expansion ratio=1.75) is added as an initial geometric imperfection for the post-buckling analysis. Different small

initial imperfection is tested and exhibits no significant influence over the post-buckling result. This agrees well with the general understanding that initial geometric imperfection is merely a "trigger" for post-buckling study. Parameters used in the simulation contain $k_B T / v = 138$ Mpa for water molecules. And $Nv = 3.06 \times 10^{-4}$ corresponds to gel elastic modulus 0.11 Mpa . Polymer solvent interaction parameter is $\chi = 0.57$. Degree of swelling is adjusted (based on deformation estimation) by increasing chemical potential gradually, from $\mu / kT = -2.02$ ($\lambda_0 = 1.01$) to $\mu / kT = 0$ (corresponds to $\lambda = 1.75\lambda_0$) while maintaining Nv and χ . Typically 1000~3000 incremental steps in ABAQUS are required to complete a single simulation due to the strong divergence occurred. Several thousands of 3-D brick elements with temperature degree of freedom (C3D8T) are used for most of the calculations and result reaches convergence by mesh refinement. Finite element results are shown in Figure 4.2 to compare with experiment and showed good agreement as stated before.

4.3. THEORETICAL FORMULATION

In this section, principle behind the pattern formation is explained by simple energy analysis and design criteria to control instability pattern is presented.

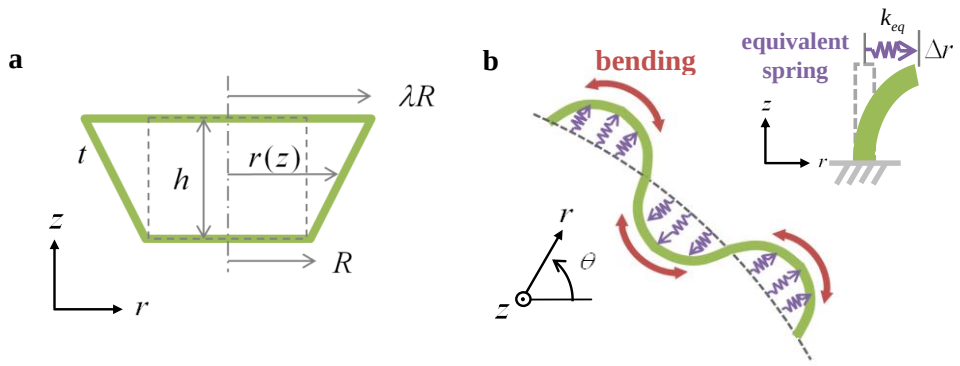

Figure 4.3. Model geometry (a) compressed configuration (side view) (b) buckled configuration (top view), deflection away from central axis modeled as equivalent springs

A cylindrical-walled hydrogel tube with diameter D, height h, and wall thickness t is shown in Figure 4.3. Cylindrical coordinate system (r,θ,z) is used to describe deformation. Fully swollen state is considered as stress-free and zero strain energy state. Therefore, any deformation from it increases potential energy of the system. The system poses a shape that minimizes the total potential energy. With the given boundary condition, there are two possible configurations for the swollen tube to adopt in order to accommodate expanded geometry in the original dimension: compression and buckling. The elastic energy for each configuration is analyzed to predict stability as well as post-buckling pattern.

4.3.1 Stable Configuration

For stable configuration, cross-section of the tube remains circular with the radius being a function of height only. It is assumed that radius is linearly varying from the dry radius $R = D/2$ at the fixed bottom to the fully swollen radius λR at the top as shown in Figure 4.3 (a). Then, radius can be written as

$$r = r(z) = R\left[1 + (\lambda - 1)\frac{z}{h}\right] \tag{4.1}$$

Since only in-plane compression is involved, total elastic energy in the stable configuration is obtained as

$$U_{stable} = \int \frac{1}{2} E\varepsilon_{\theta\theta}^2 dV = \frac{1}{24}\pi EDth \bullet b(\lambda) \tag{4.2}$$

Where $\varepsilon_{\theta\theta}(z) = \frac{r - \lambda R}{\lambda R} = -\left(1 - \frac{1}{\lambda}\right)\left(1 - \frac{z}{h}\right)$ is strain in circumferential direction and $b(\lambda) = (1 - 1/\lambda)^2 (3 + \lambda)$.

4.3.2 Buckled Configuration

Once the structure becomes mechanically unstable, it buckles and creates wrinkles along its circumference. Due to the confinement of the tube at its bottom surface, the gel tube swells more near its upper end than near its bottom end. Two parts of energy should be considered in this case. The first part is the elastic energy due to the wavy bending along the circumferential direction. This energy

contribution increases with bucking mode because the wall undergoes more bending with large curvature in higher buckling mode. This part of energy is referred to circumferential energy. The second part is the elastic energy due to the deflection of the wall in axial direction. As the gel swells more near its free upper end than near its confined bottom, the gel wall has to deflect outwards or inwards in axial direction depending on the position on the wave. This energy contribution decreases with buckling mode because higher buckling mode results in smaller wave amplitude in given length, thus less deflection in axial direction is necessary. This part of energy is referred to axial energy. It should be noted that the name of energy is purely for purpose of analysis and simplification. With the two energy contributions working together, there exists an optimum buckling mode that yields minimum total potential energy.

The closed form wave amplitude could also be derived. In order to describe the wavy pattern of buckled configuration in an analytical form, one should be able to express the wave amplitude with known variables. Assuming that wavy pattern follows sinusoidal function along the circumference, amplitude of sinusoidal wave for given contour length can be calculated and obtained in a closed form using approximation for the elliptic integral (Luke 1968).

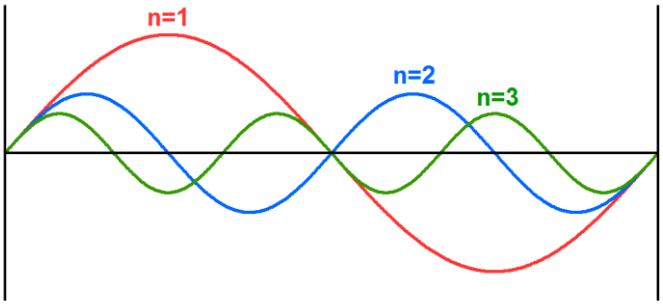

Figure 4.4. Given arc-length of sinusoidal wave function, wave amplitude becomes smaller as wave number increases

Given overall wave contour length, wave amplitude is inversely proportional to the number of waves as shown is Figure 4.4. First, radius on the top end of the wrinkled tube could be written as

$$r\left(\theta, z=h\right)=R+A\cos n\theta \tag{4.3}$$

where A is amplitude of the wave to be determined and n is mode number, i.e. the number of waves along the circumference. The contour length of the waves could be integrated as

$$L=4n\int_0^{\pi/2n}\sqrt{dr^2+\left(rd\theta\right)^2} \tag{4.4}$$

Substituting equation (4.3) into equation (4.4) under small strain assumption, and using the approximation for elliptic integral given by (Luke 1968)

$$\int_0^{\pi/2} \sqrt{1+k^2\cos^2 x}\,dx \approx \frac{\pi}{2}\left(3-\frac{2}{\sqrt{1+k^2/4}}\right) = L \tag{4.5}$$

The arc-length of the wave can be obtained by

$$\begin{aligned} L &= 4n\int_0^{\pi/2n} \sqrt{1+\left(\frac{nA}{R}\right)^2 \sin^2 n\theta}\,R\,d\theta \\ &= 4R\bullet\left[\frac{\pi}{2}\left(3-\frac{2}{\sqrt{1+\left(nA/R\right)^2/4}}\right)\right] \end{aligned} \tag{4.6}$$

From stable buckling, the contour length is

$$L = 2\pi\lambda R \tag{4.7}$$

Combine eqns. (4.6) and (4.7), solve for A yields

$$A = \frac{D}{h}a(\lambda) \tag{4.8}$$

Where $a(\lambda) = \sqrt{\left(\frac{2}{3-\lambda}\right)^2 - 1}$.

Then wrinkled radius at the free top end (i.e. $z = h$) can be now expressed with given parameters as follows.

$$r(\theta, z=h) = R\left\{1+\frac{2}{n}a(\lambda)\cos n\theta\right\} \tag{4.9}$$

The elastic energy for buckled configuration could be derived as follows. Radial wave amplitude varies with height and here we assume that it follows a bending profile of cantilever beam subjected to point load at the free end, $z^2(3h-z)/(2h^3)$, where h is the height of the cantilever beam and z is the specific location along the height direction. Then, radius of wrinkled cross-section can be written as

$$r(\theta,z)=R\left\{1+\frac{2}{n}a(\lambda)\cos n\theta\bullet\frac{z^2(3h-z)}{2h^3}\right\} \tag{4.10}$$

Elastic energy from bending along the circumferential direction is obtained by (Landau 1986)

$$U_c=\frac{1}{2}\int EI\kappa^2 dV=\frac{11}{140}\frac{\pi Et^3a^2(\lambda)h}{D}n^2 \tag{4.11}$$

where $I=\frac{t^3Rd\theta}{12}$ and $\kappa\approx\frac{1}{R^2}\frac{\partial^2 r(\theta,z)}{\partial\theta^2}$ are bending moment of inertia and curvature of the wave. Note that energy is proportional to n^2, which means that lower mode is energetically favorable.

Next, elastic energy along the axial direction is considered. This part of energy is modeled as bending of a set of cantilever beams surrounding the central axis. For simplicity, equivalent springs for cantilever beams are introduced as shown in Figure 4.3(b). Then each spring undergoes stretching by the distance to

the neutral circumferential line, which is the wave amplitude at each point, $\Delta r = r(\theta; z = h) - R$. From beam theory, equivalent spring constant of each cantilever beam is given by (Timoshenko and Woinowsky-Krieger 1959)

$$k_{eq} = \frac{Et^3 R d\theta}{4h^3} \tag{4.12}$$

Energy for the wall is obtained by integration of energy of each individual cantilever beam:

$$U_a = \int \frac{1}{2} k_{eq} (\Delta r)^2 = \frac{\pi E t^3 D^3 a^2(\lambda)}{16h^3} \bullet \frac{1}{n^2} \tag{4.13}$$

Note that the energy in this case is inversely proportional to n^2, which means that higher mode is energetically favorable. Combining Eq. (4.11)and Eq.(4.13), total elastic energy for buckled configuration, therefore, is given by

$$U_{unstable} = U_c + U_a = \frac{\pi E t^3 h a^2(\lambda)}{D} \left[\frac{11}{140} n^2 + \frac{1}{16(h/D)^4} \bullet \frac{1}{n^2} \right] \tag{4.14}$$

Minimization of $U_{unstable}$ will give an optimum mode number n for buckling. It is interesting to find that two terms are proportional to n^2 and $1/n^2$, respectively. The former is from circumferential bending (lower energy for lower mode) and the latter is from axial deflection (lower energy for higher mode). We find that this opposite dependence on mode number from two energy contributions brings

the system to a certain buckling mode in the event of buckling. Moreover, it is surprising to see that dimensional parameters involved in this competition in the bracket in (4.14) are h and D only. In other words, other parameters such as t, λ and E have no impact on the determination of buckling mode. This trend is verified by experiments shown in Figure 4.2. Once the tube buckles, the buckling mode does not depend on t, but only on h/D.

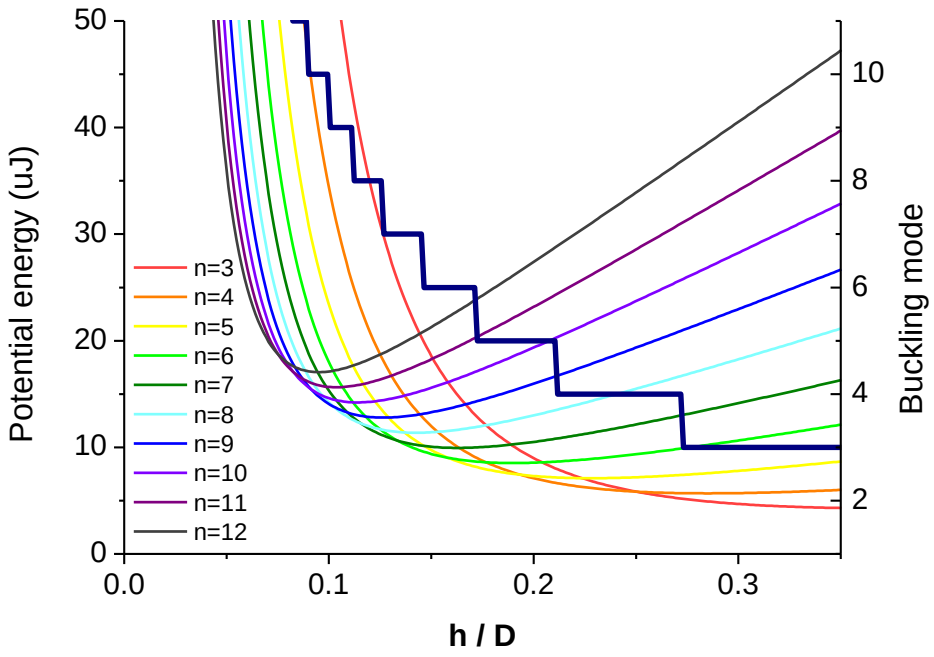

Figure 4.5. Potential energy as a function of height diameter ratio for different buckling mode

Figure 4.5 plots the total potential energy for different possible buckling modes as a function of h/D. We can clearly see that for each h/D, there is a

mode number $\tilde{n}$ which brings the potential energy to the minimum, suggesting corresponding buckling patterns for given dimension. Taking $\partial U_{unstable}/\partial n = 0$ yields

$$\tilde{n} = \left(\frac{35}{44}\right)^{\frac{1}{4}} \cdot \frac{1}{(h/D)} = \frac{0.944}{(h/D)} \tag{4.15}$$

The actual buckling mode number n is an integer, its value is either $n = \lfloor \tilde{n} \rfloor$ or $n = \lceil \tilde{n} \rceil$, depending on which one gives lower potential energy. "$\lfloor\ \rfloor$" and "$\lceil\ \rceil$" represent the floor and ceiling functions which map a real number to its largest previous or smallest following integer, respectively.

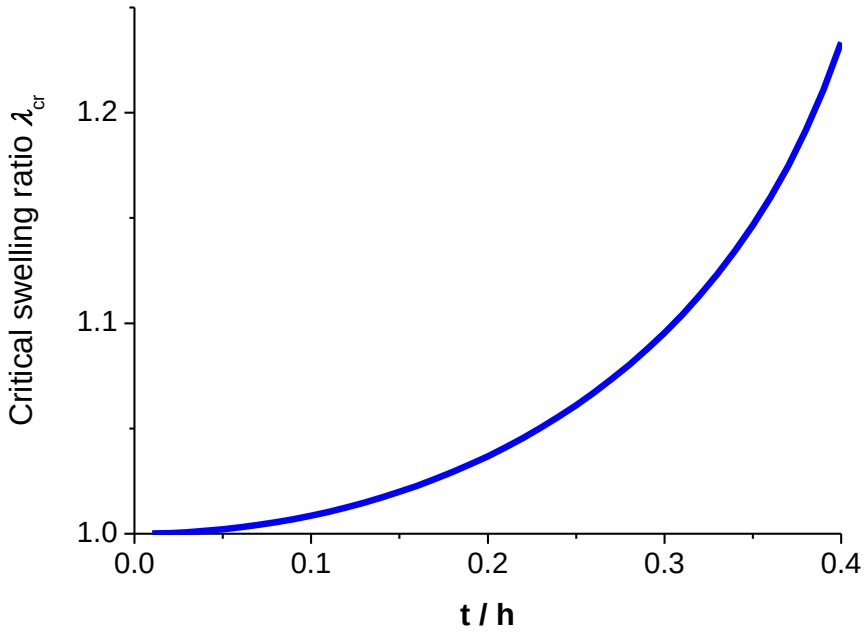

Figure 4.6. Critical swelling ratio as a function of thickness height ratio

Between stable and buckled state, the system chooses the configuration at the lower energy level. Instability index is defined as follows to characterize relative magnitude of the energy levels,

$$\gamma = \frac{U_{stable}}{U_{unstable}\Big|_{n=\tilde{n}}} = \frac{1}{(t/h)^2} \cdot c(\lambda) \tag{4.16}$$

Where $c(\lambda) = \left(\sqrt{35/11}/6\right)\left[b(\lambda)/a^2(\lambda)\right]$ is a swelling factor increasing monotonically with λ. $\gamma > 1$ means $U_{stable} > U_{unstable}$, thus the system opts to buckle, while $\gamma < 1$ means $U_{stable} < U_{unstable}$, thus the system remains stable. This result implies that stability is determined by the square of the aspect ratio of tube wall t/h and swelling ratio λ. This also matches well with the result found in the literature(Mora and Boudaoud 2006) ($\lambda_{cr} = 0.867 \cdot t^2/h^2$). λ_{cr} required to trigger buckling instability is plotted as a function of the wall aspect ratio in Figure 4.6, suggesting that slender walled tube becomes mechanically unstable at smaller swelling ratio.

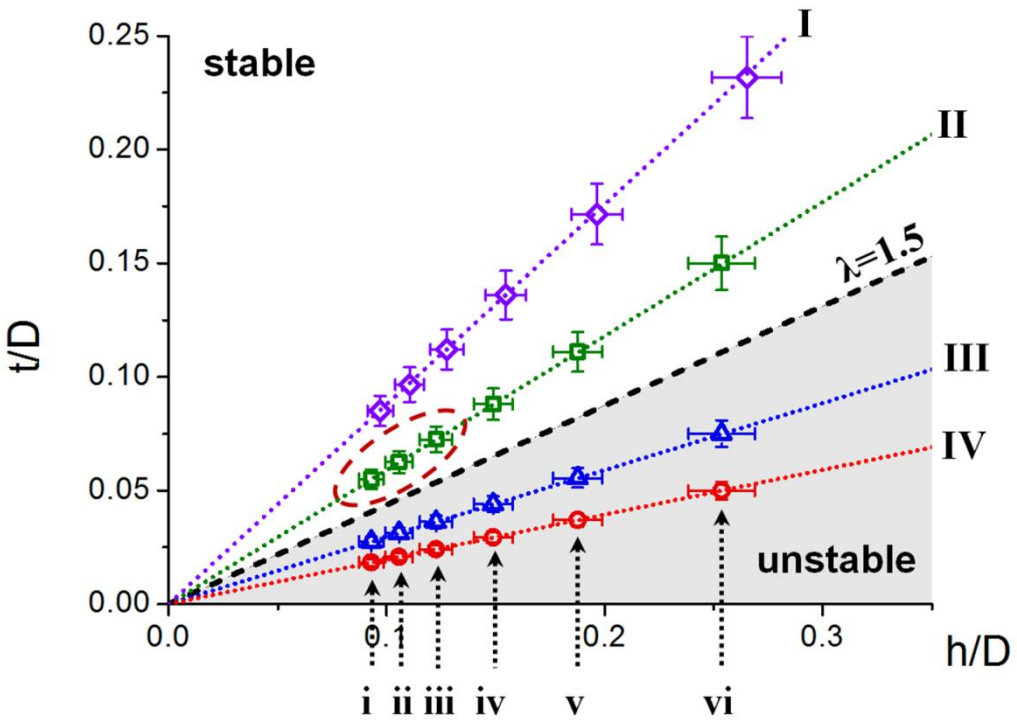

Figure 4.7. Critical thickness height line divides upper stable region and shaded unstable region below

Figure 4.7 is a stability map that can predict stability and buckling pattern together. With the horizontal and vertical axes representing h/D and t/D, respectively. Any tube geometries can be mapped onto this plot. For given equilibrium swelling ratio λ, corresponding critical wall aspect ratio $(t/h)_{cr}$ for instability from equation (4.16) can be represented by a straight line drawn from the origin. The shaded area under this line is unstable region where $\gamma > 1$, hence samples fall into this region are expected to buckle. The slope of this boarder line increases with λ, making the unstable region larger. Furthermore, since buckling mode depends only on h/D as shown in equation (4.15), the buckling mode

number can be determined based on the horizontal position of the sample on this map. Collectively, stability of the swelling gel tube as well as buckling pattern can be predicted together from this plot. In Figure 4.7, the critical stability line is drawn for $\lambda = 1.5$. Samples on the same sloped line (I-IV) have the same instability index. Instability indices defined by equation (4.16) for each line are 0.25, 0.55, 2.18, and 4.98, respectively, which means that group I and II above the stability line should remain circular while group III and IV below the stability line are expected to create wrinkles. This prediction agrees with experimental result shown in Figure 4.2, except for a few cases of II-(i-iii) (in the dotted circle).

From equation (4.15), it is suggested that samples aligned on the same vertical line (i-vi) should transform into patterns in the same buckling mode regardless of t. This was also experimentally observed in Figure 4.2. Samples on the same column in Figure 4.2 have the same h/D and their buckling modes are close to each other. The small difference across different groups should come from the thickness effect. For samples with thick wall, in-plane strain energy along the circumferential direction should also be considered, whereas this term is negligible for thin wall tube buckling where only out-of-plane strain energy along the circumferential direction is dominant. The experimental results for buckling mode numbers are plotted in Figure 4.8.

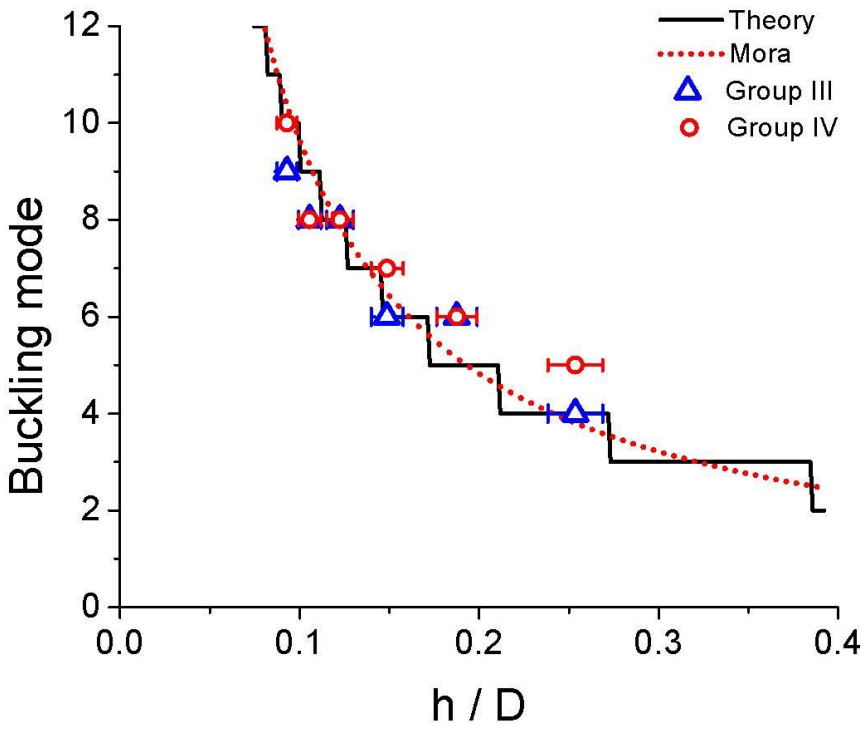

Figure 4.8. Buckling mode number for different height over diameter values for unstable sample

Instability patterns from samples spanning a wide range of dimension collapse well around theoretical prediction. This shows that we demonstrated full control over the pattern of gel tubes formed by mechanical instability.

4.4. DISCUSSIONS

In summary, well-controlled wrinkle formation of confined hydrogel tube using swelling-induced circumferential buckling are produced. Simple theory based on elastic energy is built and suggests that key dimensional parameters

sensitive to stability and buckling pattern formation are thickness to height ratio and height to diameter ratio, respectively. Experimental results showed good quantitative agreement with theoretical prediction as well as FEM simulation. In this study, it has been demonstrated that spontaneous formation of complex patterns can be achieved in a controlled manner by making use of mechanical instability of hydrogel. Furthermore, reversible nature of swelling and shrinking of hydrogel offers unique opportunities to develop versatile devices with tunable properties. It is believed that the study on buckling of swelling gels will contribute to increasing the breadth of possible application of soft materials in many emerging fields where complex morphologies and dramatic pattern shift are of critical importance, such as tissue engineering.

5 SWELLING INDUCED CRACK CLOSURE IN GELS

5.1. INTRODUCTION TO FRACTURE OF GELS

Gels are soft materials where the three dimensional polymer network is immersed in a typical liquid environment. The dual attributes of a solid and a liquid, their environmental sensitivities and some other superior properties, such as biocompatibility, biodegradability and non-toxic nature make the gel a material of choice in nature and in engineering for a variety of applications, from our daily life(Pilnik and Rombouts 1985), sustained drug delivery(Qiu and Park 2001), tissue engineering scaffolds(Drury and Mooney 2003), and oil industry(Gomez, Mamora, and Lilledal 2002, ; Kleverlaan, van Noort, and Jones 2005). Though some recent improvements on strengthening of gels have been made by double-networking(Gong et al. 2003), many gels are mechanically fragile(Levental, Georges, and Janmey 2007). Thus, it is important to understand the fracture behavior of gels.

Recently, the fracture behavior of gels has aroused some interests in the soft materials community. Hui et al.(2003) have found that unlike hard materials, soft elastomers showed a blunted crack shape. Krishnan et al.(2008) numerically studied the crack tip field of elastomers in mode I fracture and showed different stress singularities compared with linear elastic materials. Solvent also plays an important role in gel fracture. It affects crack propagation dynamics, as evidenced by Baumberger(2006) and Seitz et al.(2009)

This chapter studies another aspect of the influence of the solvent on gel

fracture. The solvent swells the gel and thus modifies the stress distribution within the gel. Under this circumstance, swelling-induced healing occurs. This chapter studies the healing process using finite element simulations and experiments.

5.2. SIMULATION OF THE CRACK CLOSURE PROCESS

The finite element simulation follows the method described in chapter 3, using the in-house FORTRAN program as attached in APPENDIX A. Part of the simulation is accomplished using a user-defined hyperelastic material (UHYPER) in ABAQUS(Hong, Liu, and Suo 2009).

Parameters $Nv = 0.001$ and $\chi = 1.13$ are used in most of the simulations, which give the equilibrium swelling ratio $\lambda_{eq} = 1.1$. Here the relatively smaller swelling ratio is used for the sake of easier convergence and less computational efforts. As discussed earlier, the characteristic time scale is given by L_{rep}^2 / D, where L_{rep} is the characteristic length in a boundary value problem. In the following simulation, all lengths are normalized by L_{rep} and the time is normalized by L_{rep}^2 / D.

Figure 5.1 illustrates the geometry of model. The boundary conditions are vanishing displacement at the rightmost ($u_1(x = L/2) = u_2(x = L/2) = u_3(x = L/2) = 0$) and a prescribed displacement load is applied at $x = -L/2$ and $y = \pm W$, i.e., $u_2(x = -L/2, y = W) = u_0$ and $u_2(x = -L/2, y = -W) = -u_0$. In order to study the stress and displacement fields at the crack tip before and after the solvent is applied, a two-step process is used.

In the first step, a dry gel (i.e., chemical potential $\mu = -\infty$) is subjected to a displacement load $\pm u_0$ at $x = -L/2$ and $y = \pm W$, respectively. Then a droplet of solvent (chemical potential $\mu = 0$) is applied at the crack tip ($x = y = 0$) while the prescribed displacement remains at $x = -L/2$ and $y = \pm W$. Thus, in the second step, the fields of displacement of chemical potential of the gel will evolve. The displacement u_3 is set to be zero.

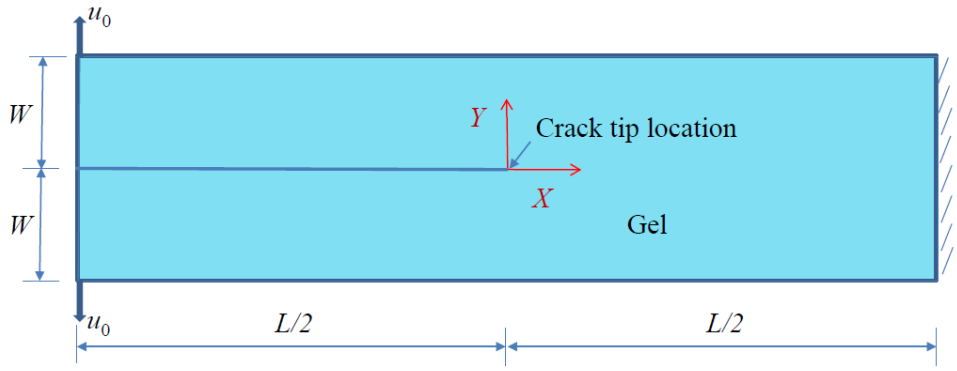

Figure 5.1. A gel model with a rectangle geometry $2W \times L$ is used in the analysis. Prescribed displacements u_0 are applied at the upper and lower left corners of the model.

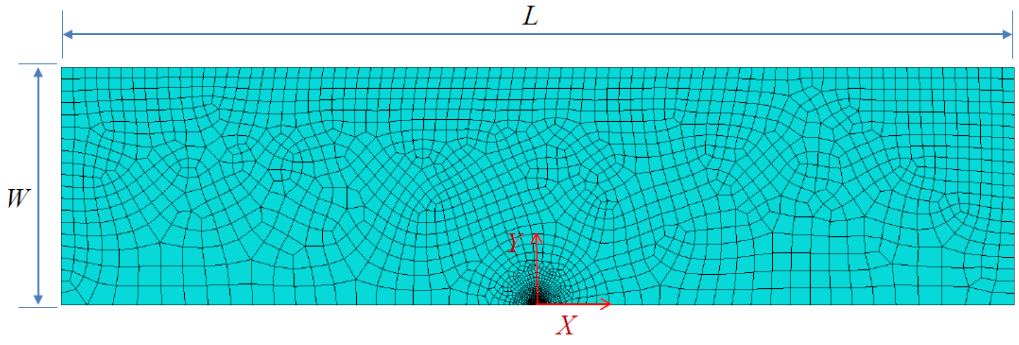

Figure 5.2. Finite element mesh for half of the global model with a rectangle geometry $W \times L$. The symmetric displacement boundary conditions are applied at

$Y = 0$ and $X > 0$.

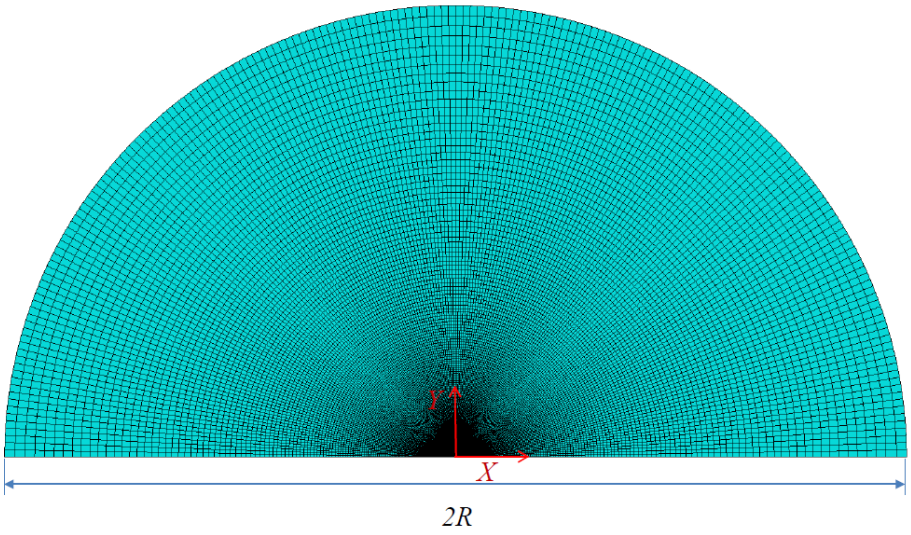

Figure 5.3. Finite element mesh for the submodel near the crack tip. The center of the circle is the crack tip and the radius of the submodel is R.

The symmetry of the model is utilized and Figure 5.2 shows a representative mesh that contains 3,861 three-dimensional brick elements. The symmetric boundary conditions are applied at $Y = 0$ and $X > 0$ and the crack faces are traction free. This model is considered as the global model. We take a circular domain of radius R centered at the crack tip as our submodel (Figure 5.3) to obtain finer resolution at the crack tip. The submodel is subjected to a prescribed displacement boundary condition provided by the global model. In the following simulation, we take $L = 80$ and $W = 20$ and the size of the submodel R is 1.25×10^{-2}. The submodel zone contains 28,950 three-dimensional brick elements. A very fine mesh is used near the crack tip. Thus, the largest element size is approximately 2.0 (Figure 5.2) and the smallest element size is 1.3×10^{-5} (Figure 5.3), which provides a ratio of 10^5 between the largest element size to

smallest element size. Efforts are made to ensure that elements have an aspect ratio close to 1. Mesh refinement and comparison of different meshes have ensured that the numerical results are accurate.

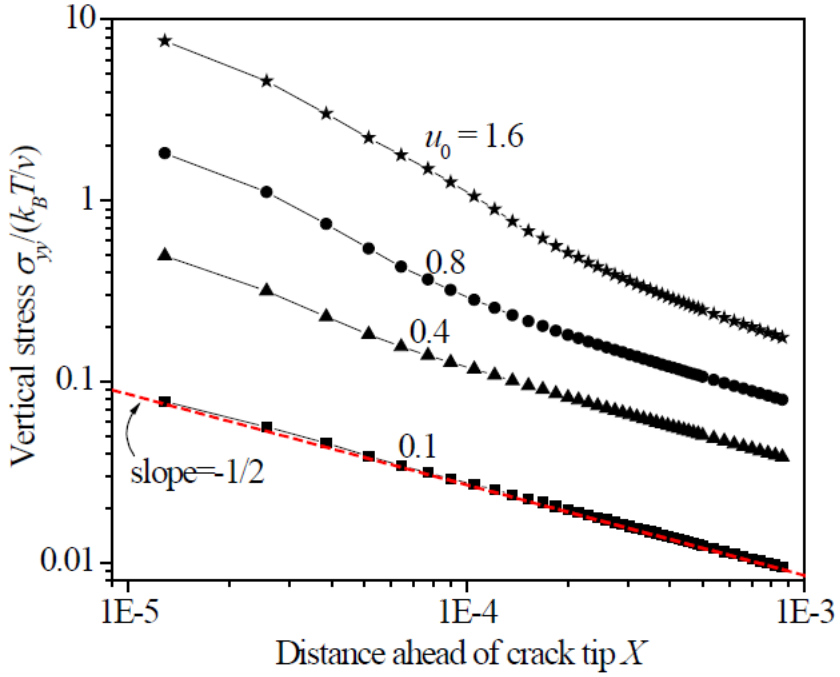

Figure 5.4. The distribution of normalized vertical stress $\sigma_{yy}/(k_BT/v)$. Ahead of the crack tip for dry gel subjected to different loading $u_0 = 0.1$, 0.4, 0.8 and 1.6.

Figure 5.4 shows the normalized vertical stress ($\sigma_{yy}/(k_BT/v)$) of the dry gel versus the normalized distance to the crack tip X , ahead of the crack tip during the first step for four sets of prescribed load, $u_0 = 0.1$, 0.4, 0.8, and 1.6. It is observed that for smaller loading (e.g., $u_0 = 0.1$), the stress profile follows a straight line with slope -1/2 near the crack tip, this is known as square root singularity in linear elastic fracture mechanics stating that stress varies as -1/2 order of the distance from the crack tip. As the increase of the load, the stress

around the crack tip ($X < 1\times10^{-4}$) is evaluated and shows a stronger singularity compared with linear elasticity. This stronger singularity has been attributed to the effect of hyperelasticity(Krishnan, Hui, and Long 2008, ; Hui et al. 2003). As away from the crack tip, the stress still shows -1/2 singularity and a transition exists. The following simulations use $u_0 = 0.1$ for the sake of computational simplicity, though similar results have been found for large prescribed displacement (e.g., $u_0 = 0.4$).

Solvent is then dropped at the crack tip in the second step. The wetting process is simulated using the submodel mesh. The nodes on the outer half circle are subjected to the displacement field obtained from the global mesh and the symmetric boundary conditions are applied along the crack extension. Since the solvent will swell the elements, stiff spring elements are employed to prevent element penetration through the symmetric axis ($Y = 0$). Thus, in the second step, some regions of the crack faces do not have traction free boundary conditions depending on the swelling of the gel.

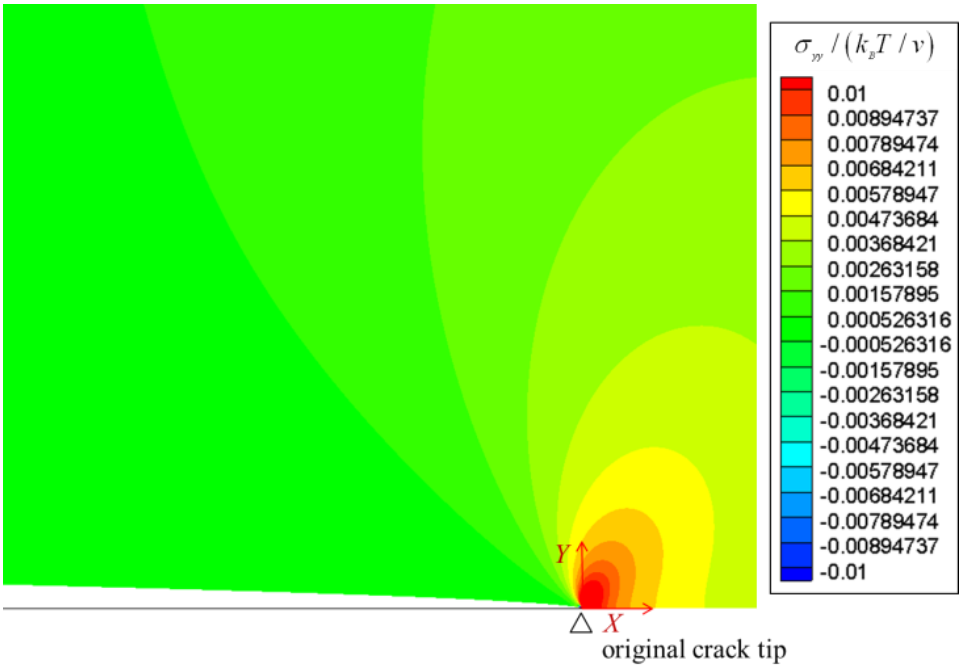

Figure 5.5. Contour of the normalized vertical stress $\sigma_{yy}/(k_BT/v)$ at $Dt/R^2 = 0.31$. The tensile stress at the original crack tip is reduced and the location of crack tip does not change.

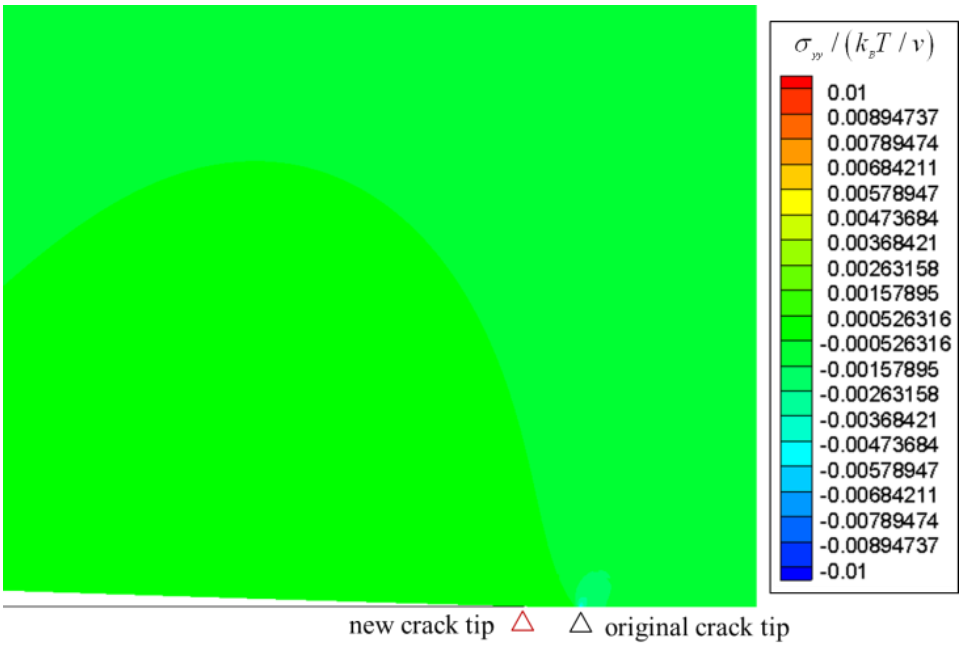

Figure 5.6. Contour of the normalized vertical stress $\sigma_{yy}/\left(k_B T/v\right)$ at $Dt/R^2 = 1.53$. The compressive stress appears at the original crack tip and the location of crack tip changes

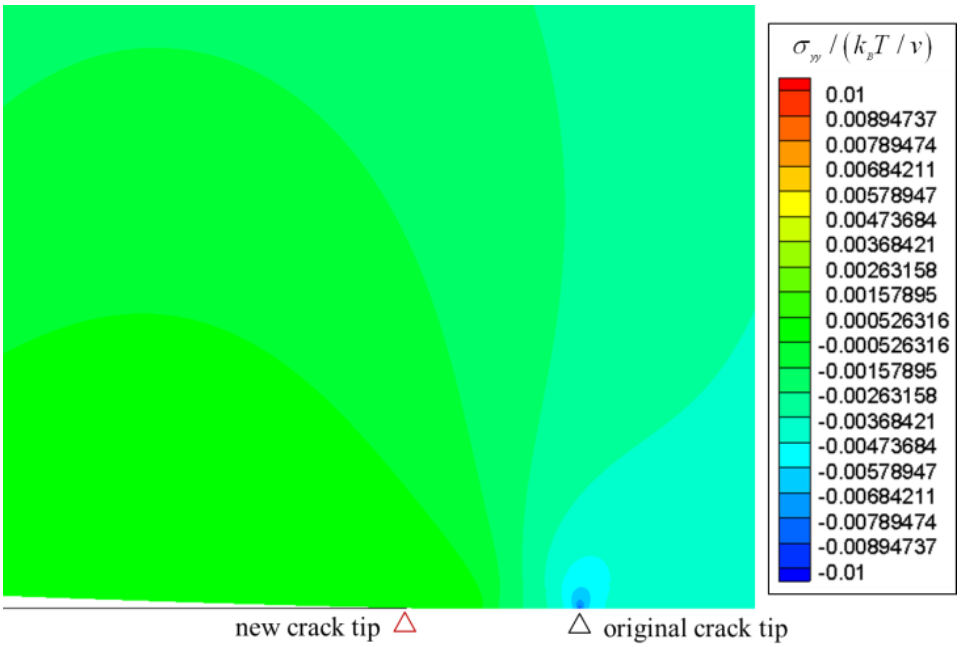

Figure 5.7. Contour of the normalized vertical stress $\sigma_{yy}/\left(k_B T/v\right)$ at $Dt/R^2 = 2.15$. A compressive zone appears around the original crack tip and the location of crack tip moves further

Figure 5.5 to Figure 5.7 show the stress contours near the crack tip at different time after the solvent droplet is applied at the crack tip. In order to have a fair comparison, the same scale bar is used in all the contours. Since the submodel is used in this simulation, the radius of the submodel R is chosen as the representative length. As shown in Figure 5.5 at $Dt/R^2 = 0.31$, the tensile stress still dominates the stress field at the crack tip, though the stress level is slightly diminished because of the swelling of the crack tip. At $Dt/R^2 = 1.53$ as shown in

Figure 5.6, the tensile stress has been further reduced and the stress at the original crack tip turns to compressive. The stress singularity at the crack tip disappears. It is also interesting to note that due to the swelling of the crack tip, the crack is healed as a new crack tip ($X = -1.293\times10^{-4}$) is generated to the left of the original crack tip. Since the new crack tip is generated by the swelling of the gel but tensile load, the stress singularity does not exist at the new crack tip. The swelling induced healing in some polymers have been observed(Toohey et al. 2007). Figure 5.7 shows that as time evolves, at $Dt / R^2 = 2.15$, the crack continues to close and the new crack tip has travelled to $X = -0.00163$. The compressive stress at the original crack tip increase and creates compressive zone near the original crack tip. In the present analysis, the influence of the submodel to the global model is assumed to be insignificant so that the time is limited to a point at which the swelling is still localized near the crack tip and does not affect the global model. The entire crack closure process is still foreseen based on the trends shown in Figure 5.5 to Figure 5.7.

The localized swelling at the crack tip results in a tensile to compressive stress transition and crack closure. After very short time since the solvent is applied at the crack tip, the crack tip does not have time to swell such that the tensile stress still dominates (Figure 5.5). As swelling goes, material near to the crack tip absorbs large amount of solvent and generates an inhomogeneous swelling field. Swelling at the crack tip releases the tensile stress and even turns it to a compressive stress as the swollen elements push each other (Figure 5.6). This process repeats and generates a compressive zone near the original crack tip, as

shown in Figure 5.7.

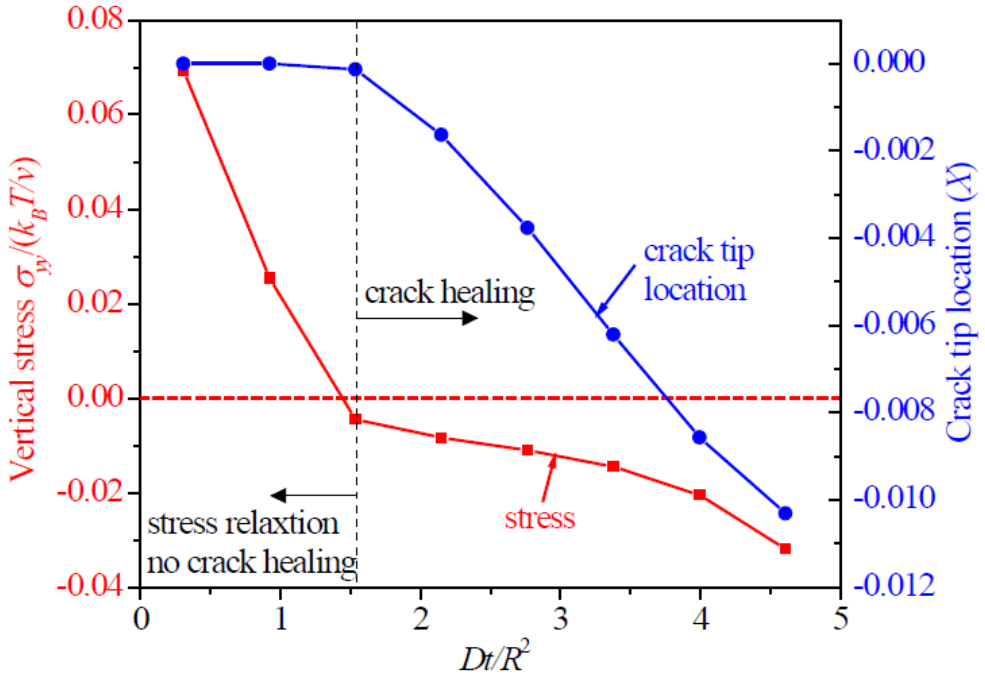

Figure 5.8. Normalized vertical stress $\sigma_{yy}/(k_BT/v)$ at the original crack and the location of the crack tip versus the normalized time (Dt/R^2).

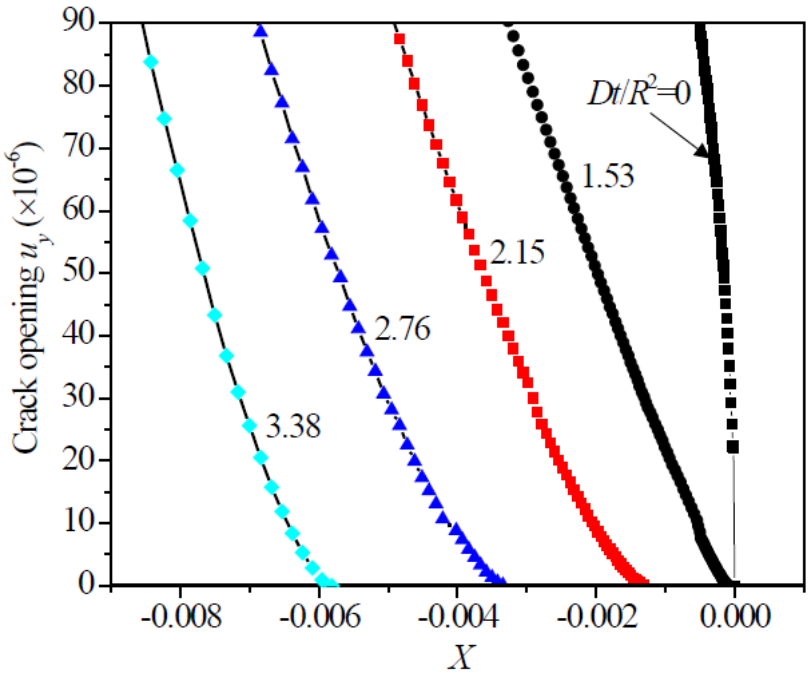

Figure 5.9. Crack opening profile $u_y(X)$ at different time (Dt/R^2).

The evolution of stress at the original crack tip and the position of the new crack tip with time are also studied and shown in Figure 5.8. It is found that it only takes a short time to release the tensile stress at the original crack tip and change it to compressive stress. This suggests that even a small amount of solvent present at the crack tip will help to eliminate the stress singularity at the crack tip. Once the stress at the original crack tip turns to compressive, the crack starts to close. It is also observed that once the crack closure is initiated, the location of new crack tip evolves approximately linearly with time. In other words, a constant crack healing speed occurs in the present analysis. The same constant healing speed is also observed in experiment when Poly(methyl methacrylate) swelled in co-solvent of methanol and ethanol(Hsieh, Yang, and Lee 2001).

The constant crack closure speed can be explained by the crack opening u_y at different time Dt/R^2 shown in Figure 5.9. The crack opening u_y at $Dt/R^2 = 0$ corresponds to the case of the dry gel. It is observed that the crack opening profile significantly changes at the onset of crack healing (time $Dt/R^2 = 1.53$). Once the crack healing starts, for equal time interval ($Dt/R^2 = 0.62$), the crack opening profiles are self-similar with approximately equal separation in X. Thus, the crack healing is propagating with a constant speed in a similar manner as that of the stress wave.

We also study the effect of the equilibrium swelling ratio of a gel on the crack healing. Thus the static simulations are conducted here. The global model is

subjected to the previously mentioned loading. The obtained displacement fields are applied to the submodel as the prescribed displacement boundary conditions. Then the crack closure is studied in the submodel. Gels with different equilibrium swelling ratio have been used and relative crack healing (healed length versus submodel size) is plotted as a function of equilibrium swelling ratio in Figure 5.10. It can be observed that a very small swelling ratio is insufficient to heal the crack. As the equilibrium swelling ratio increases, the percentage of the healing increased drastically. When equilibrium swelling ratio is 1.1 (i.e., the equilibrium swelling ratio used in the previous analysis), most of the crack has been healed. This result suggests that for a given crack, a corresponding equilibrium swelling ratio exists to ensure that the crack can be healed completely by gel swelling. The equilibrium swelling ratio depends on the polymer crosslink density, the polymer-solvent affinity, and the ambient humidity as well.

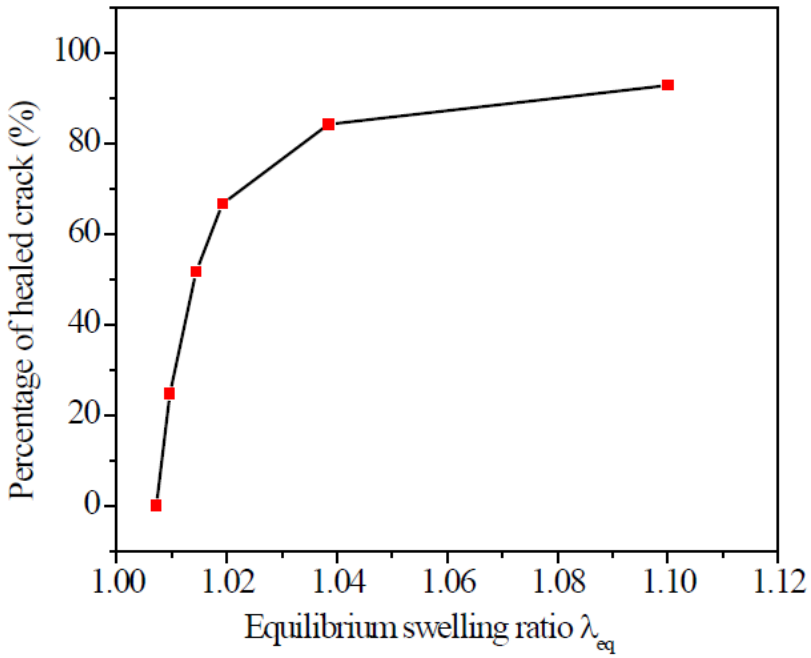

Figure 5.10. Percentage of healed crack versus equilibrium swelling ratio λ_{eq}

5.3. EXPERIMENTAL STUDY

Despite that the involvement of the solvent decreases the fracture toughness of the gel as shown in Baumberger et al.'s experiement(2006), the swelling of the gel may compensate this decrease and still lead to crack closure as shown in the simulation and to be shown in the following experiments. All the experiment in this chapter should be credited to Dr. Kyle Yazzie when he was completing his ph.D. supervised by Prof. Nikhilesh Chawla.

The solvent aided self-healing process of gel was validated by experiments as well. A Poly(ethylene glycol) diacrylate(PEGDA) gel slab with 15mm in length and 10mm in width was prepared. The gel was prepared with the solution containing a 1:1 (by weight) mixture cross-linker of PEGDA and polyethylene glycol(PEG), together with 2 wt% photoinitiator, Irgacure 819. The solution was put in a petri dish and exposed to ultraviolet light with wavelength 365 nm. Both sides were exposed for 15 seconds to ensure uniform crosslinking. Equilibrium swelling ratio of the gel was measured to be 1.3. The square, dry, PEGDA gel stab is cut by a razor blade to create a crack, followed by 0.4 mm displacement loading as illustrated in Figure 5.1. A drop of water was then dropped in the crack tip. Then the digital image correlation (DIC) technique was used to measure the displacement and to calculate the strain field. DIC uses a correlation algorithm to compare successive images of a deforming speckle pattern. The speckle pattern is applied to the sample surface, and provides a high contrast pattern that can be

easily correlated by the DIC algorithm. The algorithm computes a displacement field based on local correlation of the positions of individual speckles. The speckle pattern was applied to the gel specimen surface as follows. The gel surface was coated with a thin layer of white matte-finish spray paint. Black matte-finish spray paint was sprayed on the white base coat to create a stochastic pattern of speckles on the order of $200\ \mu m$ wide, or about 4 pixels by 4 pixels in area. The test was recorded by taking 8-bit tiff images. The strain produced in the specimen during the tensile test was analyzed by importing the 8-bit tiffs into commercially available digital image correlation software (ARAMIS, Trillion Quality System, Plymouth Meeting, PA, USA).

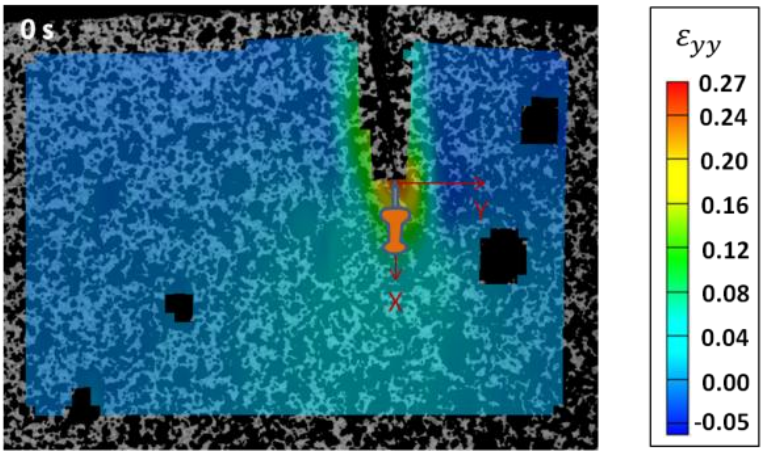

Figure 5.11. Strain field right after the square gel slab is subjected to a displacement loading $u_0 = 0.4$ mm

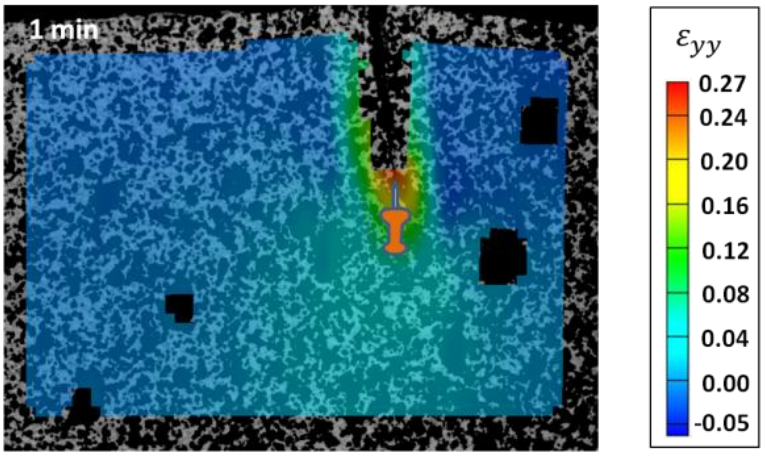

Figure 5.12. Strain field at 1 minute after adding solvent

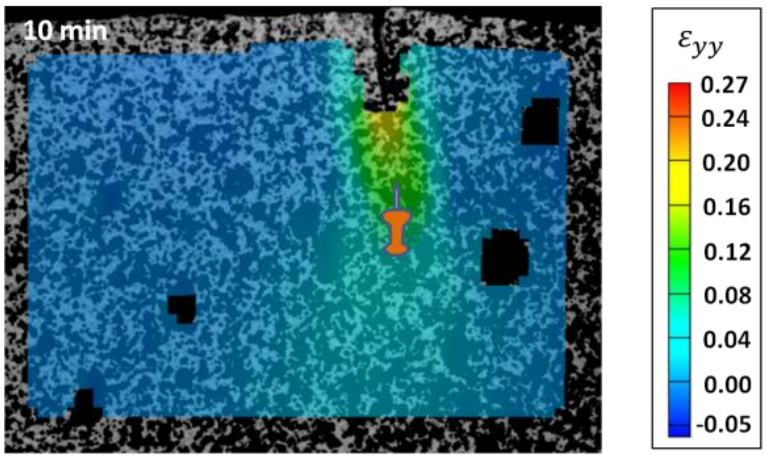

Figure 5.13. Strain field at 10 minutes after adding solvent

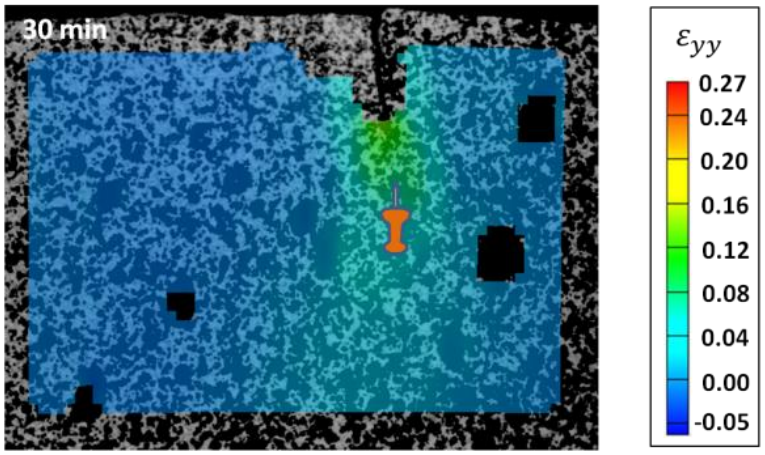

Figure 5.14. Strain field 30 minutes after adding solvent

Figure 5.11 to Figure 5.14 show the strain field at different time after the water droplet is applied at the crack tip. At $t = 0$ (Figure 5.11), i.e., the prescribed displacement load is just applied, and a high tensile strain field is observed around the crack tip. One minute after the water droplet is applied at the crack tip (Figure 5.12), part of the original crack has been closed and the strain field around the original crack tip is reduced. Ten minutes later (Figure 5.13), most of the crack has been closed due to swelling. Thirty minutes later (Figure 5.14), the healing process is complete and the strain field is tremendously reduced. The experimental healing process directly proved that the solvent were able to swell the crack tip of the gel and finally heal the crack, and at the same time, reduce the high stress zone near the original crack tip.

5.4. DISCUSSION OF GEL CRACK CLOSURE

In summary, this study shows that the presence of a solvent at the crack tip swells the gel and releases the tensile stress around the crack tip. Crack closure occurs due to gel swelling and the fraction of crack healing depends on the equilibrium swelling ratio of a gel. Future work on the solvent involved gel fracture, such as the evolution of stress field at the crack tip as solvent diffuses using the asymptotic analysis would be of interest. This work also sheds some light on the practical application of self-healing, though the actual healing process is a much more complicated process that involves polymerization of the healing agent assisted by a catalyst(White et al. 2001). However, one critical step in healing is to bring the cracked faces in contact(Wool 2008, ; Wang et al. 2010)

and the present analysis provides a means to analyze this problem. Once the crack faces come into contact, subsequent healing steps may involve molecular interdiffusion(Wool and Oconnor 1981) or reversible bonding(Wu, Meure, and Solomon 2008) such as ionic bonding and hydrogen bonding. Moreover, swelling-induced self-healing may provide an alternative way for heat(Chen et al. 2002) or light(Burnworth et al. 2011) based healing. In this spirit, healing by solvent swelling is a promising way to improvXe the structural integrity of gels, to extend product lifetime, and to broaden their applications.

6 CASE II DIFFUSION-MODELING AND EXPERIMENT

6.1. INTRODUCTION TO CASE II DIFFUSON

As stated in previous chapters, there are many efforts to develop mechanics theories to capture the coupled deformation and diffusion of gels (Tanaka and Fillmore 1979, ; Durning and Morman 1993, ; Dolbow, Fried, and Jia 2004, ; Tsai, Pence, and Kirkinis 2004, ; Li et al. 2007, ; Hong, Zhao, and Suo 2010). A recent work by Hong et al. (2008) developed a rigorous framework to describe the coupled large deformation and diffusion in gels. The deformation of the polymeric network was described by the deformation gradient $\mathbf{F}$ that maps the material point from a reference configuration to a current configuration. From a free-energy function of Flory and Rehner (1943), the gel stress was calculated as the work conjugate with respect to the deformation gradient $\mathbf{F}$. The kinetic law of diffusion follows the Fickian law and was presented in a rigorous manner by differentiating the different configurations. This theory was used to study some interesting phenomena(Zhou et al. 2010, ; Kim, Yoon, and Hayward 2010, ; Zhao, Hong, and Suo 2008) and a few numerical tools were developed based on it (Zhang, Zhao et al. 2009, ; Hong, Liu, and Suo 2009).

The dynamic behavior of gels is controlled by the deformation of the polymeric network (e.g., physical gels that exhibit phase transitions (An, Solis, and Jiang 2010)) and/or diffusion of the solvent into the polymeric network. It is a complex and interesting problem to accurately describe the diffusion of solvents into a polymeric network. This interest has been last for several decades. For most

glassy polymers, at temperatures far above the glass transition temperature of the polymer, the diffusion follows Fickian law. However, near or below the glass transition temperature, a non-Fickian behavior was observed. One particular instance of non-Fickian diffusion is Case II diffusion which is characterized by a sharp diffusion front that separates the swollen rubbery part and the dry glassy part of the polymer (Alfrey, Gurnee, and Lloyd 1966). Many solvent/polymer systems exhibit the Case II diffusion behavior, for example, methanol diffusion in Poly(methyl methacrylate) (Weisenberger and Koenig 1990), acetone in poly(vinyl chloride) (Perry et al. 1994), dioxane in polystyrene (Ilg et al. 1994) and iodoalkane into polystyrene (Gall, Lasky, and Kramer 1990).

Our recent experiment also clearly shows the sharp front when the solvent diffuses into a polymeric rod. We prepared a poly(ethylene glycol) diacrylate (PEG-DA) gel rod by photo-polymerization. Crosslinking density of PEG-DA gel was controlled in such a way that the transparent gel in dry state becomes white and opaque when it swells, facilitating the visual distinction between dry and wet area. The PEG-DA rod was brought into contact with a droplet of deionized (DI) water on the tip. Then water started to diffuse into the polymer network, creating a visible boundary indicating the location of diffusion front. This experiment was carried out in oil bath to prevent possible evaporation of water through the side wall of the wet part, ensuring that solvent migration is primarily in the direction along the axis only. The locations of the diffusion front and the tip of the rod were measured by a digital camera over the course of diffusion process.

Many efforts have been made to develop various models for case II diffusion based on different assumptions and physical pictures (Astarita and Sarti 1978, ; Hui et al. 1987, ; Fu and Durning 1993, ; Govindjee and Simo 1993, ; Edwards and Cohen 1995, ; Argon, Cohen, and Patel 1999, ; El Afif and Grmela 2002, ; Durning and Tabor 1986, ; Rossi, Pincus, and Degennes 1995, ; Lee and Kim 1992). A meaningful mechanism to explain the case II diffusion is the competition between the rate of relaxation of the polymeric network and the diffusion of solvent into the network. Thomas and Windle (1982) adopted this physical picture and modeled the gel as a viscous material and suggested that both the viscosity and diffusivity depend on solvent uptake, which has been qualitatively and quantitatively verified by experiments (Lasky, Kramer, and Hui 1988, ; Gall, Lasky, and Kramer 1990, ; El Afif and Grmela 2002). Wu and Peppas (1993) improved Thomas and Windle's model by modeling the gel as a viscoelastic material via a Maxwell model.

Given various theories and complexity of the coupled large deformation and diffusion, as well as a large number of applications, ample room exists for more theoretical work to connect principles of mechanics, constitutive relations of polymeric network, and kinetics of diffusion to experimental characterization and to validation. Specifically, we will develop a rigorous mechanics model to describe the deformation of the network, constitutive relations, equilibrium, and kinetic of diffusion, in the framework of continuum mechanics. The parameters

involved are experimentally measured and the model is validated by comparing with experiments.

6.2. A PHENOMENOLOGICAL MODEL

6.2.1 Configurations and Field Variables

Let $X_A\left(A=\text{I, II, III}\right)$ and $x_i\left(i=1,2,3\right)$ denote the coordinates of a material point in the reference configuration (e.g., dry state) and current configuration (e.g., swollen state), respectively. The mapping between the two configurations is given by the deformation gradient $\mathbf{F}$ as

$$\mathbf{F}\left(\mathbf{X},t\right)=\frac{\partial\mathbf{x}\left(\mathbf{X},t\right)}{\partial\mathbf{X}} \tag{6.1}$$

Here $\left(\mathbf{X},t\right)$ is used to emphasize that this variable $\mathbf{x}$ is under Lagrangian description and has temporal (t) dependence.

The corresponding gradient operators in the reference and current configurations are denoted by $\overset{<}{\nabla}$ and $\overset{>}{\nabla}$, respectively,

$$\overset{<}{\nabla}=\frac{\partial}{\partial X_A}\mathbf{e}_A,\qquad \overset{>}{\nabla}=\frac{\partial}{\partial x_i}\mathbf{e}_i \tag{6.2}$$

where $\mathbf{e}_A\left(A=\text{I, II, III}\right)$ and $\mathbf{e}_i\left(i=1,\,2,\,3\right)$ are unit vectors along coordinate axes X_A and x_i, respectively. Field variables can be expressed in both configurations

as subjected to "push-forward" and "pull-back" operations defined by $\mathbf{F}$ or its related operators.

The mechanical forces do the work and deform the gel. In the current configuration, the stress traction $\mathbf{t}$ per unit area on the surface a does the work and deforms the gel with displacement $\mathbf{u}$ and stress $\boldsymbol{\sigma}$ (the body force is ignored here). The gel stress $\boldsymbol{\sigma}$ in the current configuration is given by

$$\boldsymbol{\sigma} = \boldsymbol{\sigma}^{def} - P\mathbf{I} \tag{6.3}$$

where $\boldsymbol{\sigma}^{def}$ is the gel stress due to the deformation of the polymeric network, $-P\mathbf{I}$ is the osmotic pressure due to the migration of the solvent molecules, and $\mathbf{I}$ is the identity tensor. Hong et al. (2008) used the similar form by introducing the Lagrangian multiplier. The counterpart of the stress in the reference configuration is the second Piola-Kirchhoff stress $\mathbf{T}$ given by

$$\mathbf{T} = \det(\mathbf{F})\mathbf{F}^{-1} \cdot \boldsymbol{\sigma} \cdot \mathbf{F}^{-T} \tag{6.4}$$

and the gel stress due to the deformation of the polymeric network is then $\mathbf{T}^{def}$. Here $\det(\mathbf{F})$ is the determinant of $\mathbf{F}$. $\mathbf{F}^{-1}$ and $\mathbf{F}^{-T}$ are the reciprocal and the reciprocal transpose of deformation gradient $\mathbf{F}$, respectively.

The chemical potential μ pumps solvent molecules into the polymeric network. In the current configuration, the solvent volume fraction, i.e., volume of

the solvent molecules per unit volume, is given by $\phi(\mathbf{X},t)$, and the flux is expressed by $\mathbf{j}(\mathbf{X},t)$. Here it should be emphasized that both ϕ and $\mathbf{j}$ are not Eulerian description but updated Lagrangian description since specific materials points are fixed as clearly indicated by $\mathbf{X}$. Thus in the current configuration, the volume of the solvent molecules in a volume element dv is ϕdv and the change of solvent volume due to the migration of solvents crossing an area element $d\mathbf{a}$ in the gel per unit time is $\mathbf{j}\cdot d\mathbf{a} = j_i n_i da$, where $\mathbf{n}$ is the unit vector of an area element.

In the reference configuration, the volume fraction (per unit volume V) is $\Phi(\mathbf{X},t)$ and the flux is $\mathbf{J}(\mathbf{X},t)$. Thus the volume of the solvent molecules in a volume element dV is ΦdV and the change of solvent volume due to the migration of solvents crossing an area element $d\mathbf{A}$ in the gel per unit time is $\mathbf{J}\cdot d\mathbf{A} = J_K N_K dA$, where $\mathbf{N}$ is the unit vector of an area element. It should be noted that the variables in the current and reference configurations actually describe the identical physics, i.e.,

$$\begin{aligned} &\text{volume of solvent molecules : } \phi dv = \Phi dV, \\ &\text{volume change due to diffusion crossing an area element: } \mathbf{j}\cdot d\mathbf{a} = \mathbf{J}\cdot d\mathbf{A}. \end{aligned} \tag{6.5}$$

Therefore, the variables defined in two configurations are related through the deformation gradient and Nanson's formula,

$$\Phi = \phi \det(\mathbf{F}) \tag{6.6}$$

and

$$\mathbf{J} = \det(\mathbf{F})\,\mathbf{j}\cdot\mathbf{F}^{-T} = \det(\mathbf{F})\,\mathbf{F}^{-1}\cdot\mathbf{j} \tag{6.7}$$

6.2.2 Principle of Virtual Work: Equilibrium Equations and Boundary Conditions

The equilibrium equations and boundary conditions are established from the principle of virtual work in this section. The principle of virtual work in the current configuration can be established via the virtual velocity $\delta\mathbf{v}$ and the virtual rate of deformation $\delta\mathbf{d} = \frac{1}{2}\left(\overset{>}{\nabla}\delta\mathbf{v} + \delta\mathbf{v}\overset{>}{\nabla}\right)$ as

$$\int_v (\boldsymbol{\sigma} : \delta\mathbf{d})\,dv = \int_a (\mathbf{t}\cdot\delta\mathbf{v})\,da \tag{6.8}$$

Apply the divergence theorem, the equilibrium equations and traction boundary conditions in the current configuration can be established as

$$\overset{>}{\nabla}\cdot\boldsymbol{\sigma} = 0, \text{ or } \overset{>}{\nabla}\cdot\boldsymbol{\sigma}^{def} = \overset{>}{\nabla} P \text{ In volume } v \tag{6.9}$$

$$\mathbf{n}\cdot\boldsymbol{\sigma} = \mathbf{t} \text{ On area } a \tag{6.10}$$

The corresponding principle of virtual work in the reference configuration can be obtained by replacing the virtual rate of deformation $\delta\mathbf{d}$ with virtual rate of the Green strain $\mathbf{E} = \frac{1}{2}\left(\mathbf{F}^T\cdot\mathbf{F} - \mathbf{I}\right)$ in the left-hand side of Eq. (6.8) as

$$\int_V \left(\mathbf{T} : \delta \dot{\mathbf{E}} \right) dV = \int_A \left(a_N \mathbf{t} \right) \bullet \delta \mathbf{v} dA \tag{6.11}$$

where $a_N = \det(\mathbf{F}) \left(\mathbf{N} \cdot \mathbf{F}^{-1} \cdot \mathbf{F}^{-T} \cdot \mathbf{N} \right)^{\frac{1}{2}}$ is the area ratio da / dA from the Nanson's formula. Thus the equilibrium equations and boundary conditions in the reference configurations are

$$\overset{<}{\nabla} \cdot \left(\mathbf{T} \cdot \mathbf{F}^T \right) = 0, \text{ or } \overset{<}{\nabla} \cdot \left(\mathbf{T}^{def} \cdot \mathbf{F}^T \right) = \det(\mathbf{F}) \mathbf{F}^{-T} \cdot \overset{<}{\nabla} P \text{ in V} \tag{6.12}$$

$$\mathbf{N} \cdot \mathbf{T} \cdot \mathbf{F}^T = a_N \mathbf{t} \text{ on A} \tag{6.13}$$

6.2.3 Mass Conservation Law

Due to the invariance of framework, it is convenience to express the conservation law in the reference configuration, while its counterpart in the current configuration can be obtained by transformation of configurations. In the reference configuration, the variation of the volume of solvent molecules with time is due to the flux across the area, as expressed by

$$\frac{\partial}{\partial t} \int \Phi(\mathbf{X}, t) dV = -\int_A \mathbf{J}(\mathbf{X}, t) \bullet \mathbf{N} dA \tag{6.14}$$

Because Eq. (6.14) holds for any choice of the volume, using the divergence theorem, the conservation law in the differential form can be obtained as

$$\frac{\partial}{\partial t}\Phi(\mathbf{X},t)+\overset{<}{\nabla}\cdot\mathbf{J}(\mathbf{X},t)=0 \text{ in } V \tag{6.15}$$

The number of solvent molecules across an interface provides the boundary condition of the mass conservation law, i.e.,

$$\mathbf{J}(\mathbf{X},t)\cdot\mathbf{N}=\bar{J}(\mathbf{X},t) \text{ on A} \tag{6.16}$$

where $\bar{J}(\mathbf{X},t)$ is the prescribed flux across the surface.

6.2.4 Constitutive Relation of the Polymeric Network

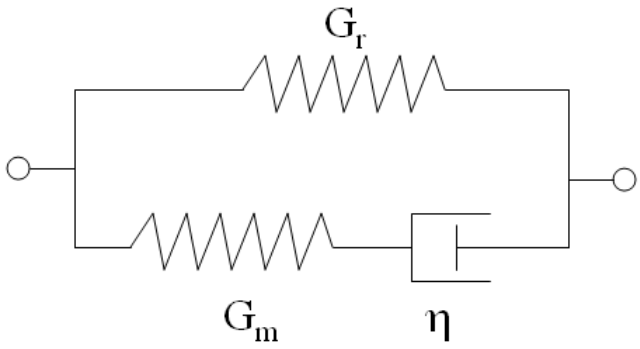

Figure 6.1. Standard Linear Solid viscoelastic model

Glassy polymers have time-dependent viscoelastic behavior. Viscous and viscoelastic models have been adopted (e.g., by Thomas and Windle 1982, ; Durning 1985, ; Wu and Peppas 1993) to describe the polymeric network in gels. The standard linear solid (SLS) model (also known as the Zener model) is the simplest model to describe both creep and stress relaxation for viscoelastic material. A pictorial representation of the SLS model is shown in Figure 6.1, in

which a linear combination of two linear springs (G_r and G_m) and a dashpot (η) represents elastic and viscous components, respectively. The constitutive relation is given by

$$\frac{\partial \sigma}{\partial t} + \frac{G_m}{\eta}\sigma = \left(G_m + G_r\right)\frac{\partial \varepsilon}{\partial t} + \frac{G_m G_r}{\eta}\varepsilon \tag{6.17}$$

, where the material parameters G_r and G_m are the modulus, and η is the extensional viscosity.

To extend this one-dimensional small-deformation constitutive relation to three-dimensional large deformation, one needs to consider the objective rate in large deformation and the nonlinear springs for the polymeric network. Because of the invariance of the framework, the rate of second Piola-Kirchhoff stress $\mathbf{T}$ with respect to time is objective; therefore, we here use the second Piola-Kirchhoff stress $\mathbf{T}$ and only express the constitutive relations in the reference configuration. The counterpart in the current configuration can also be obtained by introducing some objective stress rates (e.g., Truesdell stress rate), though it is complicated and omitted here.

The constitutive relation for polymeric materials is usually nonlinear, with pictorial representation of nonlinear springs, is given by

$$\mathbf{T}^{def} = \frac{\partial W}{\partial \mathbf{E}} \tag{6.18}$$

Various models are available to express this nonlinearity, such as Neo-Hookean model, Mooney-Rivlin model, and Flory's model. Here we adopt the Flory's model, in which the strain energy is given by

$$W = \frac{E}{6}\left\{I_1(\mathbf{C}) - 3 - \ln\left[I_3(\mathbf{C})\right]\right\} \tag{6.19}$$

Where E is the modulus of the dry polymer, and $I_i(\mathbf{C})(i = 1,2,3)$ is the ith invariance of the right Cauchy-Green tensor $\mathbf{C} = \mathbf{F}^T \cdot \mathbf{F}$. The second Piolar-Kirchhoff stress $\mathbf{T}^{def}$ is then obtained as

$$\mathbf{T}^{def} = \frac{E}{3}\left(\mathbf{I} - \mathbf{C}^{-1}\right) = \frac{2E}{3}\mathbf{E}^{(-1)} \tag{6.20}$$

where $\mathbf{C}^{-1}$ is the inverse of $\mathbf{C}$, and

$$\mathbf{E}^{(-1)} = \frac{1}{2}\left(\mathbf{I} - \mathbf{C}^{-1}\right) \tag{6.21}$$

is the Alamnsi strain tensor. By the analogy of Newton's law of viscous deformation, the constitutive relation for viscous materials can be expressed as

$$\mathbf{T}^{def} = \frac{2\eta}{3}\frac{\partial \mathbf{E}^{(-1)}}{\partial t} \tag{6.22}$$

Combining Eqs. (6.17), (6.20) and (6.22), the three-dimensional, large-deformation viscoelastic constitutive relation is given by a SLS-typed model:

$$\frac{\partial \mathbf{T}^{def}}{\partial t} + \frac{G_m}{\eta}\mathbf{T} = \left(G_m + G_r\right)\frac{\partial \mathbf{E}^{(-1)}}{\partial t} + \frac{G_m G_r}{\eta}\mathbf{E}^{(-1)} \tag{6.23}$$

The relaxed modulus (i.e., long-time limit) is given by G_r and the short-time limit is given by $G_r + G_m$. Therefore, the gel stress due to the deformation of polymeric network at the long-time limit is

$$\mathbf{T}^{def} = G_r \mathbf{E}^{(-1)} \tag{6.24}$$

and the short-time limit

$$\mathbf{T}^{def} = \left(G_m + G_r\right)\mathbf{E}^{(-1)} \tag{6.25}$$

The relaxation time of the gel is given by

$$\tau_{relax} = \frac{\eta}{G_m} \tag{6.26}$$

6.2.5 Diffusion Law

The diffusion is driven by the gradient of the chemical potential(Feynman, Leighton, and Sands 1964), i.e.,

$$\mathbf{j} = -\frac{\phi D}{kT}\overset{>}{\nabla}\mu \tag{6.27}$$

, where D is the diffusivity (unit length^2/time), $k = 1.38\times10^{-23}$ JK^{-1} is the Boltzmann constant and T is temperature. The chemical potential (per solvent molecule) in the gel is given by

$$\mu = kT\left[\ln\phi + (1-\phi) + \chi(1-\phi)^2\right] + Pv \tag{6.28}$$

,where the first term is from the mixing between the polymeric network and solvents (Flory 1953), χ is the Flory interaction parameter; and the second term denotes the external work done by the osmotic pressure P on a solvent molecule with unit volume v. An equivalent form was also adopted by Hong et al.(2008). Then the flux is explicitly expressed as

$$\mathbf{j} = -D_{12}\left[\frac{v\phi}{kT(1-\phi)(1-2\chi\phi)}\vec{\nabla}\cdot\boldsymbol{\sigma}^{def} + \vec{\nabla}\phi\right] \tag{6.29}$$

where

$$D_{12} = \frac{\phi D}{kT}\frac{\partial\mu}{\partial\phi} = D(1-\phi)(1-2\chi\phi) \tag{6.30}$$

is the mutual diffusivity (Wu and Peppas 1993) and the equilibrium equation Eq. (6.9) has been applied. Flux is driven by both the gradient of gel stress resulted from the deformation of the polymeric network and the volume fraction of solvent. The mutual diffusivity D_{12} is the pre-factor of the gradient of volume fraction of solvent to the flux.

Suggested by Thomas and Windle (1982) and Wu and Peppas (1993), the mutual diffusivity D_{12} has a strong dependence on the solvent concentration and can be expressed in an exponential form as

$$D_{12} = D_0 \exp\left(a_d \phi\right) \tag{6.31}$$

where D_0 is the diffusivity of solvent into the dry polymer and $a_d\,(>0)$ is a phenomenological parameter that describes the solvent concentration dependence. Comparison between Eq. (6.30) and Eq. (6.31) suggests that the diffusivity D is also a function of solvent concentration. The empirical expression (6.31) will be characterized in the next section and the phenomenological parameter a_d will be measured.

The flux defined in the reference configuration can be obtained by

$$\mathbf{J} = -D_{12}\left\{\frac{v\Phi \det\left(\mathbf{F}\right)\mathbf{F}^{-1}\cdot\left[\overset{<}{\nabla}\cdot\left(\mathbf{T}^{def}\cdot\mathbf{F}^{T}\right)\right]}{kT\left(\det\mathbf{F}-2\chi\Phi\right)}+\mathbf{F}^{-1}\cdot\left[\overset{<}{\nabla}\cdot\left(\mathbf{F}^{-1}\Phi\right)\right]\right\} \tag{6.32}$$

Here the ideal mixing is assumed, i.e., there is no volume change during the diffusion process, which gives

$$\det\left(\mathbf{F}\right) = 1+\Phi \tag{6.33}$$

In other words, both polymer and solvent molecules are incompressible during the mixing process but the gel is compressible.

6.2.6 Time Scales

Besides the intrinsic relaxation time scale (Eq. (6.26)) due to the viscoelastic effect of the polymeric network, there also exists another time scale, the diffusion time scale defined by

$$\tau_{diffusion} = \frac{L^2}{D_{12}} = \frac{L^2}{D_0 \exp\left(a_d \phi\right)} \tag{6.34}$$

where L is the characteristic length scale. A more practically meaningful definition is the diffusion time scale in the region where the polymeric network reaches the equilibrium swelling state,

$$\tau_{diffusion,eq} = \frac{L^2}{D_0 \exp\left(a_d \phi_{eq}\right)} \tag{6.35}$$

where ϕ_{eq} is the solvent volume fraction at the equilibrium swelling state.

Following Vrentas et al. (1975), Vrentas and Duda (1977), and Wu and Peppas (1993), a differential Deborah number is defined as

$$De = \frac{\tau_{relax}}{\tau_{diffusion,eq}} = \frac{D_0 \exp\left(a_d \phi_{eq}\right)\eta}{G_m L^2} \tag{6.36}$$

, which is the ratio of the relaxation rate in the glassy polymer region (i.e., without solvent or dry state) and the characteristic diffusion time. The differential Deborah number provides a simple means to identify the diffusion process. For example, in case II diffusion, the relaxation time in the glassy polymer region is much longer than the diffusion time in the rubbery region; thus the Deborah number is greater than unity. On the other hand, if the polymer is elastic, i.e., no extensional viscosity ($\eta = 0$), the relaxation time is zero, which gives a vanishing Deborah number and therefore corresponds to Fickian diffusion.

6.3. EXPERIMENTS: PARAMETERS CHARACTERIZATION

The model presented in Section 6.2 involves a set of parameters, including:

(1) Young's modulus of the dry polymer G_r and G_m,

(2) Extensional viscosity of the polymer η,

(3) Diffusivity of the solvent into the dry polymer D_0,

(4) Solvent-dependent diffusion constant a_d.

In order to validate the theory and practically utilize the theory on applications, this section presents the experiments to quantitatively characterize these parameters. Compression test was carried out to measure the viscoelastic material parameters (1) and (2). MRI was used to measure solvent diffusivity in polymer network, i.e., parameters (3) and (4).

6.3.1 Material Synthesis

All the experiments here are done by Dr. Howon Lee. Porous PEG-DA hydrogel was synthesized by mixing PEG-DA prepolymer (MW575, Sigma Aldrich) with PEG (MW200, Sigma Aldrich) in a weight ratio of 1:3 followed by addition of 0.5%wt. of photo-initiator (phenylbis(2,4,6-trimethylbenzoyl) phosphine oxide, Sigma Aldrich) for photo-polymerization under UV illumination ($\lambda = 365$ nm). Not being polymerized, PEG contributes to reducing crosslinking density by occupying intermolecular space between PEG-DA during photo-polymerization, resulting in low modulus and large swelling ratio.

6.3.2 Viscoelastic Material Characterization

Modulus G_r and G_m and viscosity η of the polymer were measured by compression test as shown in Figure 6.2. Gel disks were made for compression test. 1 mm gap between two glass slides was filled with prepolymer solution. Sample was photo-polymerized for 10 s in UV oven, followed by another 10 s exposure after flipping over for uniform crosslinking. Then the film was punched to obtain a set of gel disks. Samples were put in acetone bath for rinse for 3 hours to remove remaining uncrosslinked PEG after polymerization. The gel samples were allowed to dry for 1 hour in a vacuum desiccator.

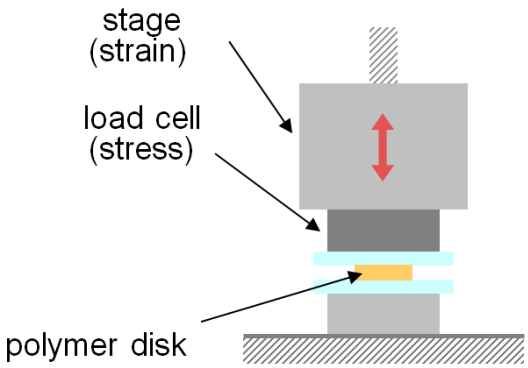

Figure 6.2. Experimental setup for compression test to measure viscoelastic parameters

A dry gel disk was compressed between two parallel glass plates, one of which is fixed and the other is connected to a load cell and then to a computer-controlled stage, as illustrated in Figure 6.2. Oil is applied between the sample and the compression plates for lubrication to facilitate lateral expansion of the sample under compression.

For time dependent material properties of the polymer, ramp-and-hold compressive stress input was applied and time varying stress was measured and fitted to the response of SLS model to obtain the moduli G_r and G_m, and extensional viscosity η. Ramp-and-hold compressive strain input is described as

$$\varepsilon(t) = \begin{cases} b_0 t & (t \le t_0) \\ b_0 t_0 & (t \ge t_0) \end{cases} \tag{6.37}$$

,where b_0 is a pre-factor and t_0 is the time when the loading stops to change. From the constitutive relation of SLS model Eq. (6.17), stress response to input Eq. (6.37) is obtained as

$$\sigma(t) = b_0 \left\langle \left[G_r t + \tau_{relax} G_m \left(1 - e^{-t/\tau_{relax}} \right) \right] - \left\{ G_r (t - t_0) + \tau_{relax} G_m \left[1 - e^{-(t-t_0)/\tau_{relax}} \right] \right\} H(t - t_0) \right\rangle \tag{6.38}$$

where the relax time τ_{relax} is given by Eq. (6.26) and $H(x)$ is the Heaviside function.

Stress data was read from the load cell and then fitted to Eq. (6.38) to extract Young's modulus G_r , G_m and viscosity of the polymer η. Obtained values of the viscoelastic parameters are $G_r = 2.90$ Mpa , $G_m = 0.58$ Mpa and $\eta = 3.91 \times 10^{-6}$ N•s/m^2.

6.3.3 Diffusivity Characterization

Magnetic resonance imaging (MRI) provides a unique opportunity to quantify diffusion properties. Being able to non-invasively characterize diffusion behavior, MRI has been a powerful method to probe biological samples (Johansen-Berg and Behrens 2009). Recently, use of MRI has been extended to studies of gels as a tool for measuring diffusion behavior of solvent molecules in polymer network(Naji, Chudek, and Baker 2008). Because concentration

dependent diffusivity D_{12} plays a crucial role in the present model, MRI is employed in this work to probe in situ water diffusivity in PEG-DA gels.

For concentration dependent diffusivity, gel samples with different solvent concentration was needed. Instead of using many different gels samples with different solvent concentration to acquire as many as possible concentration data points, a gel sample with varying solvent concentration was prepared. The sample preparation is shown in Figure 6.3.

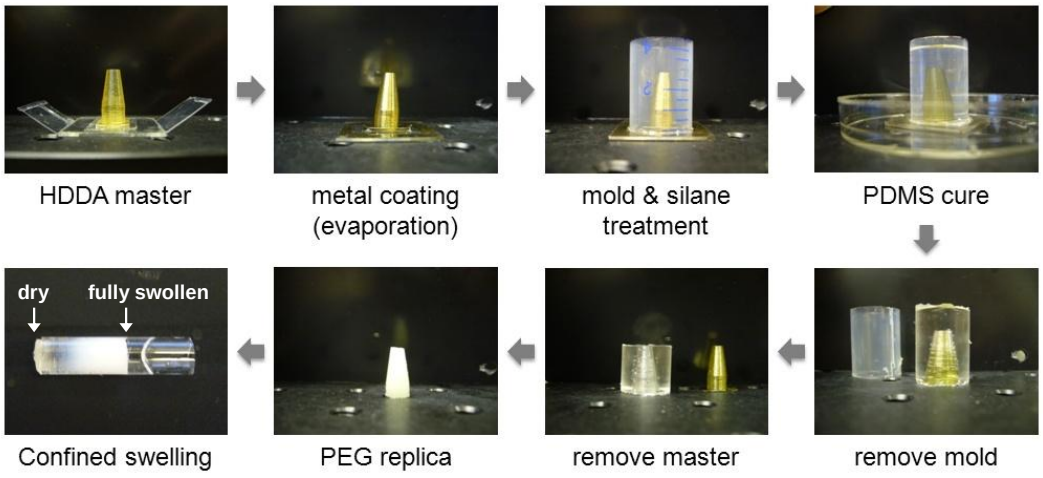

Figure 6.3. Tapered sample preparation procedure to create solvent concentration gradient in swollen hydrogel

A tapered cylindrical master was fabricated by projection micro-stereolithography(Sun et al. 2005), using hard polymeric material, hexanediol diacrylate (HDDA) (step 1). Thin metal layer was coated on the master (step 2),

followed by silane treatment for easy demolding process (step 3). Then poly(dimethylsiloxane) (PDMS) was poured and cured for 4 hours at 80 ℃ to make transparent complementary mold (steps 4-6). The PDMS mold was filled with prepolymer solution and illuminated for 10 s in UV oven, followed by another 10 s exposure after flipping over for uniform crosslinking. A gel rod was then retrieved out of the PDMS mold (step 7) and put in acetone bath for rinse for 3 hours, followed by 1 hour dry in a vacuum desiccator. This tapered gel rod was then inserted into a glass tube and let swell in water for MRI measurement. Taper dimension was designed in such a way that thicker side fits to the glass tube in dry state, whereas the thinner side fits to the glass tube in fully swollen state. Therefore, once the gel swells inside the MRI glass tube, continuous solvent concentration gradient was created along the gel sample axis because one side of the gel is fully swollen, whereas the other side of the gel sample remained almost dry due to the confinement from the MRI glass tube (step 8).

Local diffusivity and water concentration profile in the gel sample was measured by nuclear magnetic resonance (NMR) scanner (600MHz). The local diffusivity was determined using a standard pulsed field gradient spin-echo sequence with different diffusion sensitivity factors (Raguin et al. 2006). The local water concentration was measured via two spin-echo images with long repetition time (TR) to eliminate T1-weighting and two values for echo time (TE) in order to account for T2-weighting. Continuous profile of diffusivity and water concentration was obtained by taking the cross sectional MRI image along the

axial direction. Acquired local water concentration and diffusivity at each point was mapped to construct the diffusivity profile as a function of water concentration, as shown in Figure 6.4.

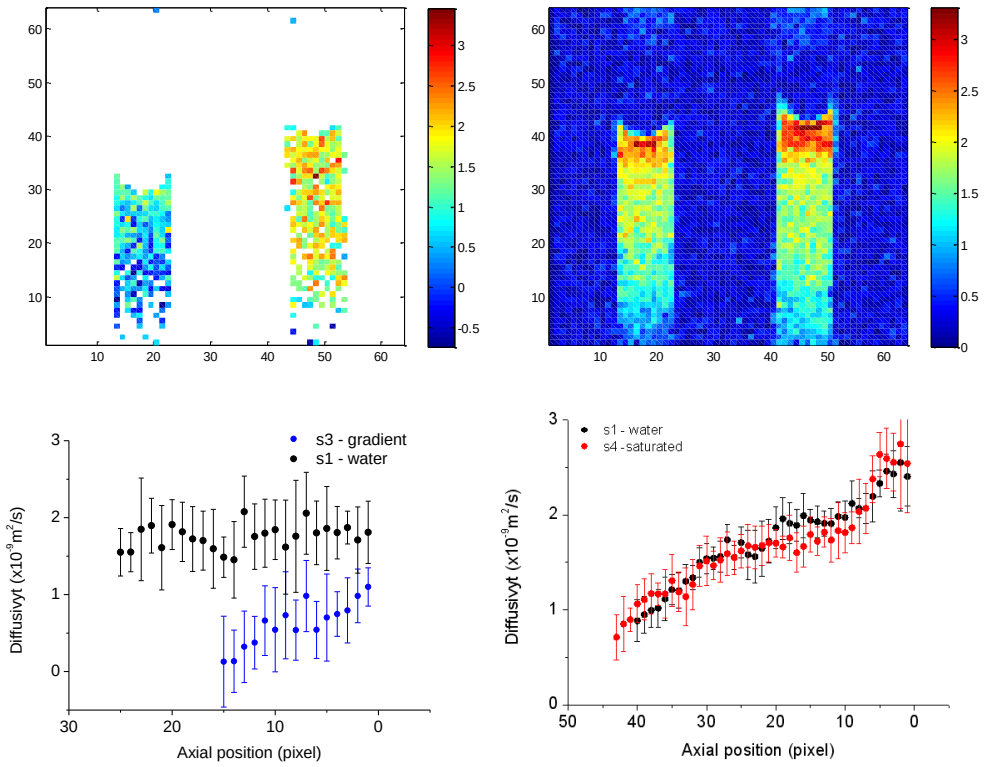

Figure 6.4. Local diffusivity and water concentration measurement result. The result is fitted to phenomenological diffusivity function to obtain diffusivity parameters

This curve was fitted to Eq. (6.31) to obtain diffusivity of the solvent into the dry polymer D_0 and solvent-dependent diffusion constant a_d. A reasonable good

agreement is observed when the following values are used,

$D_0 = 1.94\times10^{-12}\ m^2/s$ and $a_d = 17.34$.

6.3.4. Flory Interaction Parameter

Flory interaction parameter χ can be calculated by the experimentally measured equilibrium swelling ratio λ_{eq}. The equilibrium swelling is reached at the long-time limit, at which $\boldsymbol{\sigma} = 0$, $\mu = 0$ and $\mathbf{F} = \lambda_{eq}\mathbf{I}$. Using Eqs. (6.3), (6.4), (6.24), and (6.28) and eliminating P, we obtain that

$$\frac{G_r}{2}\left(\frac{1}{\lambda_{eq}} - \frac{1}{\lambda_{eq}^3}\right) + \frac{kT}{v}\left[\ln\left(1-\frac{1}{\lambda_{eq}^3}\right) + \frac{1}{\lambda_{eq}^3} + \frac{\chi}{\lambda_{eq}^6}\right] = 0 \tag{6.39}$$

, which can be used to determine the Flory interaction parameter χ. A gel disk that was prepared following the same procedure for compression test was used to measure the swelling ratio. The diameter of the gel disk was measured in dry state and in full swelling state in water at the room temperature to obtain the equilibrium swelling ratio, $\lambda_{eq} = 1.75$. For room temperature $kT = 4.14\times10^{-21}$ J, and for water molecules $v = 0.3\times10^{-28}$ m^3, which gives $kT/v = 138$ MPa Combined with previously measured modulus $G_r = 2.90$ MPa, , solve equation (6.39) and the Flory interaction parameter could be obtained as $\chi = 0.456$.

6.4. A DIFFUSION EXAMPLE

Using the measured materials parameters previously, we apply the model to study gel rod swelling examples and compare with experiments. PEG-DA polymer synthesized for this study dramatically changes optical property from transparent to opaque as it swells. This helps visualize the evolution of interface between dry and wet regions in diffusion experiment.

The solvent diffuses into a rod from two ends, as illustrated in Figure 6.5. $2L$ is the initial length of the rod. Denote X_1 and X_2 as the material coordinates in the cross section of the rod, and X_3 as the material coordinate in the length direction defined at the center of the rod and pointing upwards. The solvent diffuses from the top ($X_3 = L$) and bottom ($X_3 = -L$) to the center ($X_3 = 0$).

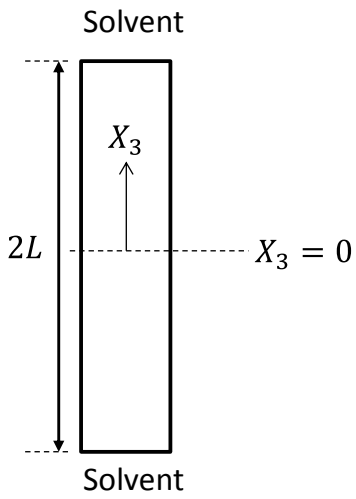

Figure 6.5. Gel rod with length $2L$ swelling from two ends to the center

Because the dimension in the in-plane direction is much smaller than L, the stretches in the in-plane direction keep symmetric $\lambda_1 = \lambda_2$ and only depend on X_3, i.e., $\lambda_1 = \lambda_1(X_3, t)$. The stretch in X_3 direction is $\lambda_3 = \lambda_3(X_3, t)$. The non-vanishing Alamnsi strain is $E^{(-1)}{}_{11}(X_3, t) = E^{(-1)}{}_{22}(X_3, t) = \frac{1}{2}\left(1 - \lambda_1^{-2}\right)$, $E^{(-1)}{}_{33}(X_3, t) = \frac{1}{2}\left(1 - \lambda_3^{-2}\right)$; and the incompressibility condition of dry polymer and solvent molecules (Eq. (6.33)) becomes $1 + \Phi = \lambda_1^2 \lambda_3$. Then the constitutive equations (Eq. (6.23)) are specified to

$$\frac{\partial T_{11}^{def}}{\partial t} + \frac{G_m}{\eta} T_{11}^{def} = \left(G_m + G_r\right)\lambda_1^{-3}\dot{\lambda}_1 + \frac{G_m G_r}{2\eta}\left(1 - \lambda_1^{-2}\right) \tag{6.40}$$

$$\frac{\partial T_{33}^{def}}{\partial t} + \frac{G_m}{\eta} T_{33}^{def} = \left(G_m + G_r\right)\lambda_3^{-3}\dot{\lambda}_3 + \frac{G_m G_r}{2\eta}\left(1 - \lambda_3^{-2}\right) \tag{6.41}$$

The gel stress is given by

$$\begin{aligned} \sigma_{11} &= \sigma_{22} = \frac{1}{\lambda_3} T_{11}^{def} - P \\ \sigma_{33} &= \frac{\lambda_3}{\lambda_1^2} T_{33}^{def} - P \end{aligned} \tag{6.42}$$

In lateral directions and X_3 direction, tractions are free, which leads to $\sigma_{11} = \sigma_{22} = \sigma_{33} = 0$. Eliminating P from Eq. (6.42) and the relation

$\lambda_1^2 T_{11}^{def} = \lambda_3^2 T_{33}^{def}$ is obtained. Combining Eqs. (6.40) with Eqs. (6.41), we obtain that

$$\lambda_1 = \lambda_3 = \lambda \tag{6.43}$$

and then apply the incompressibility condition is $\lambda^3 = 1+\Phi$. The polymer constitutive relation Eq. (6.41) becomes

$$\frac{\partial T_{33}^{def}}{\partial t} + \frac{G_m}{\eta} T_{33}^{def} = \left(G_m + G_r\right) \frac{\Phi}{3\left(1+\Phi\right)^{5/3}} + \frac{G_m G_r}{2\eta} \left[1 - \frac{1}{\left(1+\Phi\right)^{2/3}} \right] \tag{6.44}$$

The mass conservation law Eq. (6.15) becomes

$$\begin{aligned} &\frac{\partial \Phi}{\partial t} - D_0 \frac{\partial}{\partial X_3} \left\langle \exp\left(a_d \frac{\Phi}{1+\Phi} \right) \left\{ \frac{1}{\left(1+\Phi\right)^{1/3}} \frac{\partial \left[\dfrac{\Phi}{\left(1+\Phi\right)^{1/3}} \right]}{\partial X_3} \right.\right. \\ &\left.\left. + \frac{v\Phi\left(1+\Phi\right)^{2/3}}{kT\left(1+\Phi-2\chi\Phi\right)} \frac{\partial \left[T_{33}^{def} \left(1+\Phi\right)^{1/3} \right]}{\partial X_3} \right\} \right\rangle = 0 \end{aligned} \tag{6.45}$$

Two differential equations (6.44) and (6.45) evolve two fields, $T_{33}^{def}\left(X_3, t\right)$ and $\Phi\left(X_3, t\right)$, which could be solved with appropriate initial conditions and boundary conditions as illustrated below.

At time $t<0$, the rod rests at a stress-free state and is completely dry; so that the initial conditions are

$$T_{33}^{def}\left(X_3,0\right)=0,\qquad \Phi\left(X_3,0\right)=0 \tag{6.46}$$

The traction-free boundary condition holds all the time at the end. And this boundary condition corresponds to $\sigma_{33}\left(L,t\right)=0$. Once the solvent contacts the rod at the end ($X_3=L$), the exchange of solvent molecules between the external solvent and the rod occurs in a rate much faster than the diffusion process of migrating solvent molecules into the rod. Therefore, the chemical equilibrium remains unchanged all the time at the top, i.e., $\mu\left(L,t\right)=0$. Combining these two boundary conditions and Eqs. (6.28) and (6.42), we eliminate P and obtain

$$\frac{T_{33}^{def}}{\left(1+\Phi\right)^{1/3}}+\frac{kT}{v}\left[\ln\left(\frac{\Phi}{1+\Phi}\right)+\frac{1}{1+\Phi}+\frac{\chi}{\left(1+\Phi\right)^2}\right]=0 \tag{6.47}$$

at the boundary $X_3=L$ over any time t. This is a time-dependent equation for $\Phi\left(X_3,t\right)$ because T_{33}^{def} is governed by Eq. (6.44). At the short-time limit, apply Eq.(6.25), the elasticity of the gel responses instantaneously so that we could obtain

$$\frac{G_m+G_r}{2}\left[\frac{1}{\left(1+\Phi\right)^{1/3}}-\frac{1}{1+\Phi}\right]+\frac{kT}{v}\left[\ln\left(\frac{\Phi}{1+\Phi}\right)+\frac{1}{1+\Phi}+\frac{\chi}{\left(1+\Phi\right)^2}\right]=0 \tag{6.48}$$

Equation (6.48) provides a nonlinear equation to determine the boundary condition $\Phi(L,0)$. Substitute this boundary condition into the constitutive relation Eq. (6.44) and the boundary condition for T_{33}^{def} is obtained as

$$T_{33}^{def}(L,0)=\frac{G_m+G_r}{2}\left\{1-\left[1+\Phi(L,0)\right]^{-2/3}\right\} \tag{6.49}$$

Note that the boundary conditions here ($\Phi(L,0)$ and $T_{33}^{def}(L,0)$) differ from the common boundary conditions that remain at any time t. Specifically, these boundary conditions only hold at the beginning $t=0$. In fact, this type of boundary condition is common in viscoelastic problems. With time evolves, the viscosity comes into play in the evolution of Φ and T_{33}^{def}. The symmetric boundary conditions at the center ($X_3=0$) are

$$\frac{\partial\Phi(0,t)}{\partial X_3}=0, \qquad \frac{\partial T_{33}^{def}(0,t)}{\partial X_3}=0 \tag{6.50}$$

The partial differential equations (6.44) and (6.45) subjected to the aforementioned initial and boundary conditions are solved numerically, specifically by finite difference method.

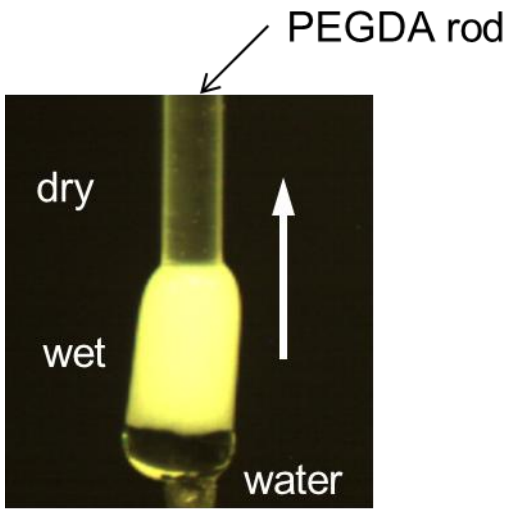

Figure 6.6. Water diffuses inside a PEGDA rod. Transparent polymer becomes white when it gets wet. A sharp boundary separating dry and wet region is clearly observed.

The experiment was conducted using the gel rod configuration as shown in Figure 6.6. Water diffused from the bottom to the top of the gel rod with length $L = 468\,\mu\text{m}$. Unswollen region was transparent and swollen region was opaque. There exists an apparent boundary separates the unswollen region and swollen region. The boundary moved upward almost at a constant velocity until the full rod became swollen. The boundary is so called "sharp front". Also from Figure 6.6 and from the comparison of unswollen region and swollen region, we can also see that the volumetric swelling ratio of the gel is large, which indicates that large deformation should be considered and that the volumetric change of the polymer network is negligible compared with the whole volume change of the gel which is mostly caused by the change of the water content.

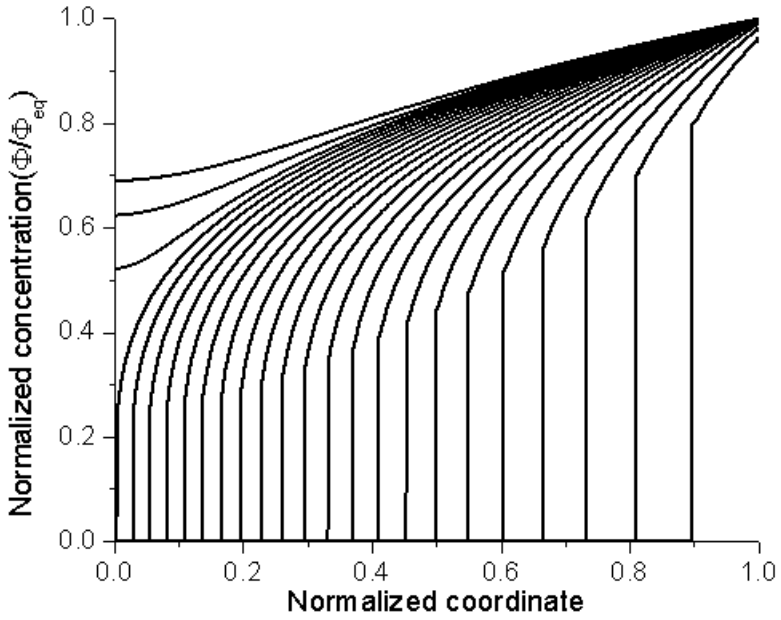

Figure 6.7. Normalized concentration distributions at different location for several time intervals, sharp diffusion fronts are observed.

Based on the model we proposed previously, and the parameters measured, we are able to simulate the diffusion process using the evolution equations (6.44) and equation (6.45) with the aid of finite difference discretization. Figure 6.7 plots the normalized concentration profile $\Phi(X_3,t)/\Phi_{eq}$ with respect to the location measured from the original gel rod. In this example, equilibrium swelling ratio $\lambda_{eq}=1.75$ corresponds to $\Phi_{eq}=4.36$ by the relation of $\lambda^3=1+\Phi$. Multiple lines are plotted at equivalent time interval 42 seconds. It shows that there is a sharp transition differentiating the wet region (with concentration close to the equilibrium value) and the dry region (with zero concentration), which defines the

sharp front. With time evolving, the front moves inside the gel and eventually the wet the entire gel.

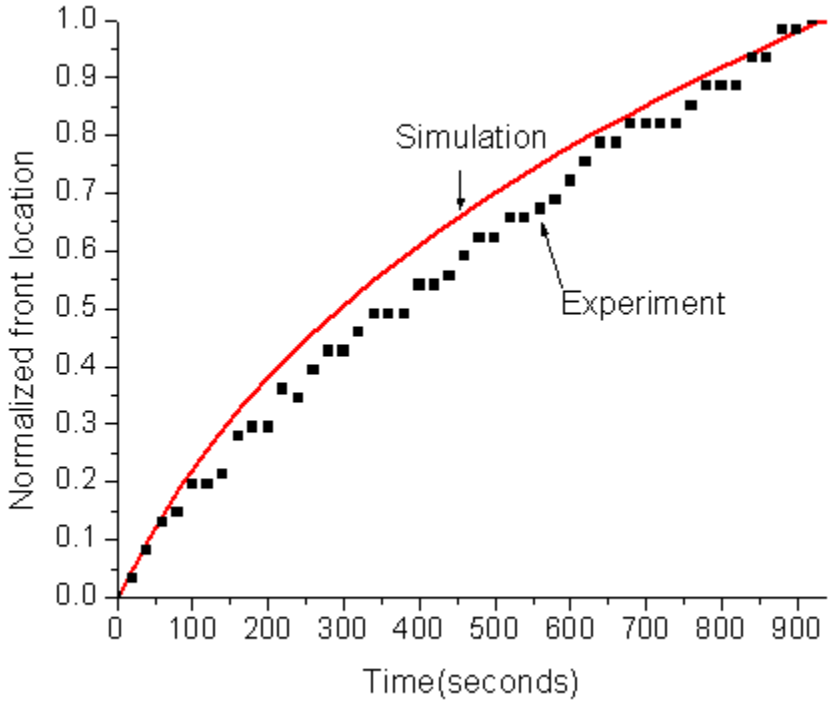

Figure 6.8. Sharp front location as a function of time

The sharp front location as a function of time is plotted in Figure 6.8. Simulation results are compared with experiments and showed good agreement. The slope is close to linear but not exactly because the diffusion is not ideally case II diffusion. The length is normalized by the total original length of the gel rod which is $L = 468\,\mu\text{m}$. After about 900 seconds, the entire gel rod is swollen, which gives a constant speed about $0.52\,\mu\text{m/s}$.

After swelling, the total length of the rod changed. The new gel rod length could be obtained by integration

$$l(t)=\int_0^L\left[1+\Phi\left(X_3,t\right)\right]^{1/3}dX_3 \tag{6.51}$$

Figure 6.9 compares the normalized length profile $l(t)/L$ calculated from Eq. (6.51) and measurement from experiments. It also showed reasonably good agreement between experiment and simulation, which again validates the theory.

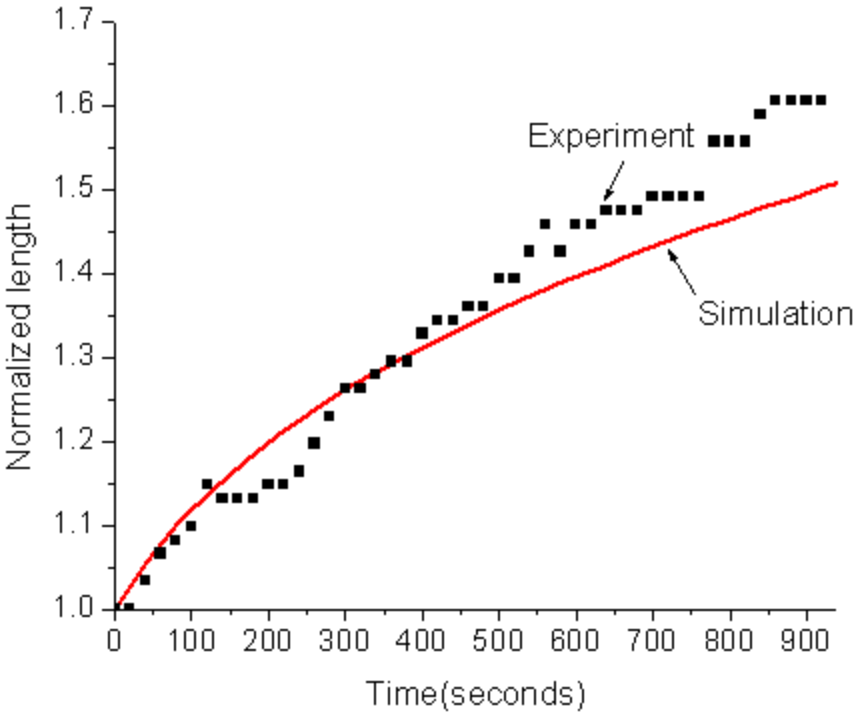

Figure 6.9. Normalized gel rod length as a function of time

6.5. SUMMARY AND DISCUSSIONS

In this chapter, a coupled large deformation model for case II diffusion is presented. The total stress of the gel is separated to polymer network stress and solvent osmotic pressure. The polymer network stress relates to the strain via a viscoelastic standard linear solid model which contains both elastic and viscous components. Solvent flow in the polymer network is governed by diffusion equation with diffusion coefficient strongly depends on the solvent concentration. Under large deformation regime, the solvent flux depends both on local solvent concentration gradient and local polymer stress gradient. Diffusion time scale is compared with polymer relaxation scale to investigate the underlying principle that the case II diffusion could be explained by the lag of the polymer relaxation. Compression test and MRI experiment are conducted to measure the parameters introduced in the model. Simulation results are compared with experiment results and showed good agreement. Sharp diffusion front is observed and solvent diffusion along a gel rod follows almost a constant speed. All these facts validate the theory.

The modeling and simulation of case II diffusion in gels enhance our understanding of solvent diffusion in polymers, not only phenomenological, but also physically. In fact, given the fact that the variety of different types of polymers and solvent exist, a large part of solvent diffusion in polymers is anomalous diffusion(De Kee, Liu, and Hinestroza 2005) which is a diffusion type between Fickian diffusion and case II diffusion, both of whom are ideal cases.

Tunable parameters such as concentration dependent diffusivity would allow the theory to consider more general cases. As a simple example, the numerical simulation of the gel rod diffusion also encourages further investigation in the numerical simulation of the anomalous diffusion and numerical simulation will certainly aid the design process for gel devices.

7 CONCLUSIONS

7.1. SUMMARY AND DISCUSSIONS

In this dissertation, the material about gels and their applications are introduced. Specifically, the swelling of gels is an interesting topic that deserves extensive attention. During the swelling process, the volume of the gel is changed by adding more solvent that expands the original gel polymer network. This is a coupled deformation and diffusion process and various theories are proposed to solve, each with their different advantages and limitations. In chapter 2, we listed several theories with simple format and clear physics. Among them include Biot theory, THB theory, Flory's theory and Wallmersperger theory. At the same time we introduced a coupled theory proposed by Hong et al.(2008). In the theory, physically simple equations such as equilibrium equation for the whole gel and diffusion equation for solvent are introduced. In the theory, two processes occur simultaneously: solvent diffusion and polymer network stretching. Solvent diffusion is governed by diffusion law and polymer network stretching is governed by mechanical equilibrium. Surprisingly, common physical properties such as crosslink density of the polymer network and polymer affinity with the solvent come in the model through two key parameters. And they dominate the degree of swelling. Stress inside the gel is derived by a free energy based on Flory's theory which takes into account both the polymer stretching and polymer solvent mixing. Diffusion equation is considered in the large deformation regime where the actual diffusion coefficient depends on deformation. Deformation and

diffusion is correlated directly via an molecular incompressibility condition which states that the polymer network is incompressible and the volumetric change is of the gel is caused by the amount of solvent that enters. Then in chapter 3, numerical methods are introduced to implement the coupled theory. Starting from the free energy, Cauchy stress which depends on chemical potential is derived and tangential modulus are obtained through the rate of stress. These two parameters come into an ABAQUS user material code (UMAT) and an in-house coding as well and they are capable to solve equilibrium swelling problems where the solvent properties chemical potential does not change. By considering the diffusion equation which evolves the time change of the chemical potential, the in-house program is extended to be able to study the transient swelling of gels and has been applied to study a creep problem for benchmark and a free swelling of a cubic.

In chapter 4, the swelling of a ring confined in the bottom surface is investigated. It showed that buckling would happen given appropriate conditions. A simple model based on energy minimization is conducted and showed a correlation between the criterion for buckling, wavenumber if buckled and the geometry of the ring. Finite element analysis is conducted to verify experiment and testify the model. In chapter 5, the in-house finite element code is applied to study the swelling-induced healing in gels. Solvent are dropped to the crack tip of a gel slab which is originally subjected to tensile loading. The gel near the crack tip absorbs water and swells and finally closes the gap between the crack surfaces.

This process is also visualized by experiment. The healing study showed a promising way to reduce the stress singularity of fractured gels through adding solvent and to estimate the time to heal an existing crack. In chapter 6, a diffusion model is proposed to consider the diffusion of solvent in some glassy polymers near the glass transition temperature. In this model, instead of consider the diffusion as fickian-diffusion where the diffusion map is continuous, a concentration dependent diffusion law is proposed and is able to predict the diffusion which has discontinuous diffusion map called case II diffusion. In case II diffusion, a sharp diffusion front separates the swollen region and the unswollen region. The model assumes that the swollen region has much larger diffusion coefficient than the unswollen region and has been validated by experimental measurement. In this case, the solvent flux both depends on concentration gradient and stress gradient. A viscoelastic material constitutive relation is used for the polymer network, which is believed to be more practical for polymers. Applying this model, the reason behind the case II diffusion is explained by the physics that the polymer network relaxation time is slow compared with the solvent diffusion time, thus it blocks the diffusion and accumulate a lot of solvent once a near a relaxed polymer segment. In this way, the sharp front is created near the newly relaxed polymer segment. Simulation results is compared with experimental result for a rod swelling experiment and showed good agreement. Sharp concentration profile and near-constant diffusion front is predicted as well. This study bridges the gap for different combinations of polymer-solvent diffusion, which spans from Fickian diffusion to anomalous

diffusion to case II diffusion. Under these circumstances, a clear picture is created for coupled large deformation and diffusion modeling. By providing specific diffusion law, by providing the specific polymer constitutive, the model is able to simulate the diffusion of solvent in polymers.

7.2. FUTURE WORK

The present study provides a method to study various swelling phenomenon related to swelling of gels. Given the fact that different kinds of gels with different polymer network properties and transport laws for the solvent, future work are encouraged to extend the current large deformation model to be able to simulate different polymer-solvent systems. Another aspect is from the application side, the current model is expected to study fascinating swelling phenomenon, such as swelling-induced surface instability(Kang and Huang 2010), buckling and creasing(Cai et al. 2010), programmable gel(Zhang, Guo, and Zhang 2011), swelling under constraint and loading(Zhang, Zeng et al. 2009) and so on. Temperature-sensitive gel and pH-sensitive gel are two most widely used categories of gels in real applications. Theories regarding temperature-sensitive gel(Chester and Anand 2011, ; Cai and Suo 2011) and pH-sensitive gel(Marcombe et al. 2010) are developed, subsequent extension of the current numerical method to these theories should enable more applications be studied. The fracture characteristic regarding gel is studied(Baumberger, Caroli, and Martina 2006, ; Baumberger and Ronsin 2010) but still require further study. Though so many modeling and simulation toward gel have been performed in

recent years, it is believed that it is far from maturity. Multi-physics nature of this smart material is expected to attracting increasing attention in the near future.

REFERENCES

Achilleos, E. C., R. K. Prud'homme, I. G. Kevrekidis, K. N. Christodoulou, and K. R. Gee. 2000. Quantifying deformation in gel swelling: Experiments and simulations. *Aiche Journal* 46 (11):2128-2139.

Alfrey, T., E. F. Gurnee, and W. G. Lloyd. 1966. Diffusion in Glassy Polymers. *Journal of Polymer Science Part C-Polymer Symposium* (12PC):249-253.

An, Y., F. J. Solis, and H. Jiang. 2010. A Thermodynamic Model of Physical Gels. *Journal of the Mechanics and Physics of Solids* 58:2083-2099.

Argon, A. S., R. E. Cohen, and A. C. Patel. 1999. A mechanistic model of case II diffusion of a diluent into a glassy polymer. *Polymer* 40 (25):6991-7012.

Arruda, E. M., and M. C. Boyce. 1993. A 3-Dimensional Constitutive Model for the Large Stretch Behavior of Rubber Elastic-Materials. *Journal of the Mechanics and Physics of Solids* 41 (2):389-412.

Astarita, G., and G. C. Sarti. 1978. Class of Mathematical-Models for Sorption of Swelling Solvents in Glassy Polymers. *Polymer Engineering and Science* 18 (5):388-395.

Baek, S., and A. R. Srinivasa. 2004. Diffusion of a fluid through an elastic solid undergoing large deformation. *International Journal of Non-Linear Mechanics* 39 (2):201-218.

Baumberger, T., C. Caroli, and D. Martina. 2006. Solvent control of crack dynamics in a reversible hydrogel. *Nature Materials* 5 (7):552-555.

Baumberger, T., and O. Ronsin. 2010. A convective instability mechanism for quasistatic crack branching in a hydrogel. *European Physical Journal E* 31 (1):51-58.

Bayer, Shirley Ann, and Joseph Altman. 2005. *The human brain during the second trimester*. Boca Raton: Taylor & Francis.

Beebe, D. J., J. S. Moore, J. M. Bauer, Q. Yu, R. H. Liu, C. Devadoss, and B. H. Jo. 2000. Functional hydrogel structures for autonomous flow control inside microfluidic channels. *Nature* 404 (6778):588-590.

Biot, M. A. 1941. General theory of three-dimensional consolidation. *Journal of Applied Physics* 12 (2):155-164.

Birgersson, E., H. Lib, and S. Wua. 2008. Transient analysis of temperature-sensitive neutral hydrogels. *Journal of the Mechanics and Physics of Solids* 56 (2):444-466.

Bonet, Javier, and Richard D. Wood. 1997. *Nonlinear Continuum Mechanics for Finite Element Analysis*. Cambridge: Cambridge University Press.

Burnworth, M., L. M. Tang, J. R. Kumpfer, A. J. Duncan, F. L. Beyer, G. L. Fiore, S. J. Rowan, and C. Weder. 2011. Optically healable supramolecular polymers. *Nature* 472 (7343):334-337.

Cai, S. Q., K. Bertoldi, H. M. Wang, and Z. G. Suo. 2010. Osmotic collapse of a void in an elastomer: breathing, buckling and creasing. *Soft Matter* 6 (22):5770-5777.

Cai, S. Q., and Z. G. Suo. 2011. Mechanics and chemical thermodynamics of phase transition in temperature-sensitive hydrogels. *Journal of the Mechanics and Physics of Solids* 59 (11):2259-2278.

Chen, X. X., M. A. Dam, K. Ono, A. Mal, H. B. Shen, S. R. Nutt, K. Sheran, and F. Wudl. 2002. A thermally re-mendable cross-linked polymeric material. *Science* 295 (5560):1698-1702.

Chester, S. A., and L. Anand. 2011. A thermo-mechanically coupled theory for fluid permeation in elastomeric materials: Application to thermally responsive gels. *Journal of the Mechanics and Physics of Solids* 59 (10):1978-2006.

Costa, D., J. Queiroz, M. G. Miguel, and B. Lindman. 2012. Swelling behavior of a new biocompatible plasmid DNA hydrogel. *Colloids and Surfaces B-Biointerfaces* 92:106-112.

De Kee, D., Q. Liu, and J. Hinestroza. 2005. Viscoelastic (non-fickian) diffusion. *Canadian Journal of Chemical Engineering* 83 (6):913-929.

Doi, M. 2009. Gel Dynamics. *Journal of the Physical Society of Japan* 78 (5):19.

Dolbow, J., E. Fried, and H. D. Jia. 2004. Chemically induced swelling of hydrogels. *Journal of the Mechanics and Physics of Solids* 52 (1):51-84.

Dong, L., A. K. Agarwal, D. J. Beebe, and H. R. Jiang. 2006. Adaptive liquid microlenses activated by stimuli-responsive hydrogels. *Nature* 442 (7102):551-554.

Drury, J. L., and D. J. Mooney. 2003. Hydrogels for tissue engineering: scaffold design variables and applications. *Biomaterials* 24 (24):4337-4351.

Durning, C. J. 1985. Differential Sorption in Viscoelastic Fluids. *Journal of Polymer Science Part B-Polymer Physics* 23 (9):1831-1855.

Durning, C. J., and K. N. Morman. 1993. Nonlinear Swelling of Polymer Gels. *Journal of Chemical Physics* 98 (5):4275-4293.

Durning, C. J., and M. Tabor. 1986. Mutual Diffusion in Concentrated Polymer-Solutions under a Small Driving Force. *Macromolecules* 19 (8):2220-2232.

Edwards, D. A., and D. S. Cohen. 1995. A Mathematical-Model for a Dissolving Polymer. *Aiche Journal* 41 (11):2345-2355.

El Afif, A., and M. Grmela. 2002. Non-Fickian mass transport in polymers. *Journal of Rheology* 46 (3):591-628.

Feynman, R. P., R. B. Leighton, and M. Sands. 1964. *The Feynman Lectures on Physics*. Boston: Addison–Wesley.

Flory, P. J., and J. Rehner. 1943. Statistical mechanics of cross-linked polymer networks I Rubberlike elasticity. *Journal of Chemical Physics* 11 (11):512-520.

Flory, P.J. 1953. *Principles of Polymer Chemistry*. New York: Cornell University Press.

Forterre, Y., J. M. Skotheim, J. Dumais, and L. Mahadevan. 2005. How the Venus flytrap snaps. *Nature* 433 (7024):421-425.

Fu, T. Z., and C. J. Durning. 1993. Numerical-Simulation of Case-Ii Transport. *Aiche Journal* 39 (6):1030-1044.

Gall, T. P., R. C. Lasky, and E. J. Kramer. 1990. Case-Ii Diffusion - Effect of Solvent Molecule Size. *Polymer* 31 (8):1491-1499.

Gao, Y. W., and F. M. Lei. 2009. Small scale effects on the mechanical behaviors of protein microtubules based on the nonlocal elasticity theory. *Biochemical and Biophysical Research Communications* 387 (3):467-471.

George, M., and T. E. Abraham. 2007. pH sensitive alginate-guar gum hydrogel for the controlled delivery of protein drugs. *International Journal of Pharmaceutics* 335 (1-2):123-129.

Gernandt, J., G. Frenning, W. Richtering, and P. Hansson. 2011. A model describing the internal structure of core/shell hydrogels. *Soft Matter* 7 (21):10327-10338.

Gomez, J. A., D. D. Mamora, and L. O. Lilledal. 2002. Full-scale well-model tests of a new chemical plug system for zone isolation in horizontal wells. *Spe Drilling & Completion* 17 (2):82-86.

Gong, J. P., Y. Katsuyama, T. Kurokawa, and Y. Osada. 2003. Double-network hydrogels with extremely high mechanical strength. *Advanced Materials* 15 (14):1155-1163.

Govindjee, S., and J. C. Simo. 1993. Coupled Stress Diffusion - Case-Ii. *Journal of the Mechanics and Physics of Solids* 41 (5):863-887.

Hong, W., Z. S. Liu, and Z. G. Suo. 2009. Inhomogeneous swelling of a gel in equilibrium with a solvent and mechanical load. *International Journal of Solids and Structures* 46 (17):3282-3289.

Hong, W., X. H. Zhao, and Z. G. Suo. 2010. Large deformation and electrochemistry of polyelectrolyte gels. *Journal of the Mechanics and Physics of Solids* 58 (4):558-577.

Hong, W., X. H. Zhao, J. X. Zhou, and Z. G. Suo. 2008. A theory of coupled diffusion and large deformation in polymeric gels. *Journal of the Mechanics and Physics of Solids* 56 (5):1779-1793.

Hsieh, H. C., T. J. Yang, and S. Lee. 2001. Crack healing in poly(methyl methacrylate) induced by co-solvent of methanol and ethanol. *Polymer* 42 (3):1227-1241.

Hughes, T. J. R. 1980. Generalization of Selective Integration Procedures to Anisotropic and Non-Linear Media. *International Journal for Numerical Methods in Engineering* 15 (9):1413-1418.

Hui, C. Y., A. Jagota, S. J. Bennison, and J. D. Londono. 2003. Crack blunting and the strength of soft elastic solids. *Proceedings of the Royal Society of London Series a-Mathematical Physical and Engineering Sciences* 459 (2034):1489-1516.

Hui, C. Y., K. C. Wu, R. C. Lasky, and E. J. Kramer. 1987. Case-Ii Diffusion in Polymers .1. Transient Swelling. *Journal of Applied Physics* 61 (11):5129-5136.

Ilg, M., B. Pfleiderer, K. Albert, W. Rapp, and E. Bayer. 1994. Investigation of the Diffusion Process in Cross-Linked Polystyrenes by Means of Nmr Imaging and Solid-State Nmr-Spectroscopy. *Macromolecules* 27 (10):2778-2783.

Jeong, B., Y. H. Bae, D. S. Lee, and S. W. Kim. 1997. Biodegradable block copolymers as injectable drug-delivery systems. *Nature* 388 (6645):860-862.

Ji, H. D., H. Mourad, E. Fried, and J. Dolbow. 2006. Kinetics of thermally induced swelling of hydrogels. *International Journal of Solids and Structures* 43 (7-8):1878-1907.

Jiang, H. Q., and J. P. Zhang. 2008. Mechanics of Microtubule Buckling Supported by Cytoplasm. *Journal of Applied Mechanics-Transactions of the ASME* 75 (6).

Jin, L. H., S. Q. Cai, and Z. G. Suo. 2011. Creases in soft tissues generated by growth. *Epl* 95 (6).

Johansen-Berg, Heidi, and Timothy E.J. Behrens. 2009. *Diffusion MRI: From Quantitative Measurement to In vivo Neuroanatomy*. Boston: Elsevier.

Kang, M. K., and R. Huang. 2010. Swell-induced surface instability of confined hydrogel layers on substrates. *Journal of the Mechanics and Physics of Solids* 58 (10):1582-1598.

Repeated Author. 2010. A Variational Approach and Finite Element Implementation for Swelling of Polymeric Hydrogels Under Geometric Constraints. *Journal of Applied Mechanics-Transactions of the ASME* 77 (6).

Kim, J., J. Yoon, and R. C. Hayward. 2010. Dynamic display of biomolecular patterns through an elastic creasing instability of stimuli-responsive hydrogels. *Nature Materials* 9 (2):159-164.

Kissel, T., Y. X. Li, and F. Unger. 2002. ABA-triblock copolymers from biodegradable polyester A-blocks and hydrophilic poly(ethylene oxide) B-blocks as a candidate for in situ forming hydrogel delivery systems for proteins. *Advanced Drug Delivery Reviews* 54 (1):99-134.

Kleverlaan, M, R. H. van Noort, and I. Jones. 2005. Deployment of swelling elastomer packers in Shell E&P. Paper read at SPE/IADC conference, February 2005, at Amsterdam, Netherlands.

Krishnan, V. R., C. Y. Hui, and R. Long. 2008. Finite Strain Crack Tip Fields in Soft Incompressible Elastic Solids. *Langmuir* 24 (24):14245-14253.

Kucken, M., and A. C. Newell. 2005. Fingerprint formation. *Journal of Theoretical Biology* 235 (1):71-83.

Lai, W. M., J. S. Hou, and V. C. Mow. 1991. A Triphasic Theory for the Swelling and Deformation Behaviors of Articular-Cartilage. *Journal of Biomechanical Engineering-Transactions of the Asme* 113 (3):245-258.

Landau, Lev Davidovich. 1986. *Theory of Elasticity*. Oxford, New York: Pergamon Press.

Lasky, R. C., E. J. Kramer, and C. Y. Hui. 1988. Temperature-Dependence of Case-Ii Diffusion. *Polymer* 29 (6):1131-1136.

Lee, K. Y., and D. J. Mooney. 2001. Hydrogels for tissue engineering. *Chemical Reviews* 101 (7):1869-1879.

Lee, P. I., and C. J. Kim. 1992. Effect of Geometry on Solvent Front Penetration in Glassy-Polymers. *Journal of Membrane Science* 65 (1-2):77-92.

Levental, I., P. C. Georges, and P. A. Janmey. 2007. Soft biological materials and their impact on cell function. *Soft Matter* 3 (3):299-306.

Li, B., Y. P. Cao, X. Q. Feng, and H. J. Gao. 2011. Surface wrinkling of mucosa induced by volumetric growth: Theory, simulation and experiment. *Journal of the Mechanics and Physics of Solids* 59 (4):758-774.

Li, H., R. Luo, E. Birgersson, and K. Y. Lam. 2007. Modeling of multiphase smart hydrogels responding to pH and electric voltage coupled stimuli. *Journal of Applied Physics* 101 (11):11490501-11490507.

Repeated Author. 2007. Modeling of multiphase smart hydrogels responding to pH and electric voltage coupled stimuli. *Journal of Applied Physics* 101 (11):7.

Li, H., and S. S. Mulay. 2011. 2D simulation of the deformation of pH-sensitive hydrogel by novel strong-form meshless random differential quadrature method. *Computational Mechanics* 48 (6):729-753.

Li, J., X. Li, X. P. Ni, X. Wang, H. Z. Li, and K. W. Leong. 2006. Self-assembled supramolecular hydrogels formed by biodegradable PEO-PHB-PEO

triblock copolymers and alpha-cyclodextrin for controlled drug delivery. *Biomaterials* 27 (22):4132-4140.

Liang, H. Y., and L. Mahadevan. 2009. The shape of a long leaf. *Proceedings of the National Academy of Sciences of the United States of America* 106 (52):22049-22054.

Liu, Z. S., S. Swaddiwudhipong, F. S. Cui, W. Hong, Z. Suo, and Y. W. Zhang. 2011. Analytical Solutions of Polymeric Gel Structures under Buckling and Wrinkle. *International Journal of Applied Mechanics* 3 (2):235-257.

Luke, Yudell L. 1968. Approximations for Elliptic Integrals. *Mathematics of Computation* 22:627-634.

Marcombe, R., S. Q. Cai, W. Hong, X. H. Zhao, Y. Lapusta, and Z. G. Suo. 2010. A theory of constrained swelling of a pH-sensitive hydrogel. *Soft Matter* 6 (4):784-793.

Mora, T., and A. Boudaoud. 2006. Buckling of swelling gels. *The European Physical Journal E* 20 (2):119-124.

Nagtegaal, J.C.;Parks D.M.;Rice J.R. 1974. On numerically accurate finite element solutions in the fully plastic range. *Computer Methods in Applied Mechanics and Engineering* 4 (2):153-177.

Naji, L., J. A. Chudek, and R. T. Baker. 2008. Magnetic resonance imaging study of a soft actuator element during operation. *Soft Matter* 4 (9):1879-1886.

Perry, K. L., P. J. Mcdonald, E. W. Randall, and K. Zick. 1994. Stray Field Magnetic-Resonance-Imaging of the Diffusion of Acetone into Poly(Vinyl Chloride). *Polymer* 35 (13):2744-2748.

Pilnik, W., and F. M. Rombouts. 1985. Polysaccharides and Food-Processing. *Carbohydrate Research* 142 (1):93-105.

Qiu, Y., and K. Park. 2001. Environment-sensitive hydrogels for drug delivery. *Advanced Drug Delivery Reviews* 53 (3):321-339.

Raguin, Guy, Cibele V. Falkenberg, Shaurya Prakash, Heather R. FitzHenry, Glennys Mensing, Luisa Ciobanu, John G. Georgiadis, and Mark A. Shannon. 2006. Magnetic Resonance Imaging (MRI) of Water Diffusion in Hydroxyethyl Methacrylate (HEMA) Gels. Paper read at Mater. Res. Soc. Symp. Proceedings.

Rossi, G., P. A. Pincus, and P. G. Degennes. 1995. A Phenomenological Description of Case-Ii Diffusion in Polymeric Materials. *Europhysics Letters* 32 (5):391-396.

Seitz, M. E., D. Martina, T. Baumberger, V. R. Krishnan, C. Y. Hui, and K. R. Shull. 2009. Fracture and large strain behavior of self-assembled triblock copolymer gels. *Soft Matter* 5 (2):447-456.

Sharon, E., M. Marder, and H. L. Swinney. 2004. Leaves, flowers and garbage bags: Making waves. *American Scientist* 92 (3):254-261.

Shen, H. S. 2010. Nonlocal shear deformable shell model for postbuckling of axially compressed microtubules embedded in an elastic medium. *Biomechanics and Modeling in Mechanobiology* 9 (3):345-357.

Sidorenko, A., T. Krupenkin, A. Taylor, P. Fratzl, and J. Aizenberg. 2007. Reversible switching of hydrogel-actuated nanostructures into complex micropatterns. *Science* 315 (5811):487-490.

Slaughter, B. V., S. S. Khurshid, O. Z. Fisher, A. Khademhosseini, and N. A. Peppas. 2009. Hydrogels in Regenerative Medicine. *Advanced Materials* 21 (32-33):3307-3329.

Suematsu, N., K. Sekimoto, and K. Kawasaki. 1990. 3-Dimensional Computer Modeling for Pattern-Formation on the Surface of an Expanding Polymer Gel. *Physical Review A* 41 (10):5751-5754.

Sultan, E., and A. Boudaoud. 2008. The buckling of a swollen thin gel layer bound to a compliant substrate. *Journal of Applied Mechanics-Transactions of the ASME* 75 (5).

Sun, C., N. Fang, D. M. Wu, and X. Zhang. 2005. Projection micro-stereolithography using digital micro-mirror dynamic mask. *Sensors and Actuators a-Physical* 121 (1):113-120.

Tanaka, T. 1978. Collapse of Gels and Critical Endpoint. *Physical Review Letters* 40 (12):820-823.

Tanaka, T., and D. J. Fillmore. 1979. Kinetics of Swelling of Gels. *Journal of Chemical Physics* 70 (3):1214-1218.

Tanaka, T., L. O. Hocker, and G. B. Benedek. 1973. Spectrum of Light Scattered from a Viscoelastic Gel. *Journal of Chemical Physics* 59 (9):5151-5159.

Thomas, N. L., and A. H. Windle. 1982. A Theory of Case-Ii Diffusion. *Polymer* 23 (4):529-542.

Timoshenko, S., and S. Woinowsky-Krieger. 1959. *Theory of Plates and Shells*. New York: McGraw-Hill Companies.

Timoshenko, Stephen P., and James M. Gere. 1961. *Theory of Elastic Stability*. New York: McGraw-Hill Companies.

Toohey, K. S., N. R. Sottos, J. A. Lewis, J. S. Moore, and S. R. White. 2007. Self-healing materials with microvascular networks. *Nature Materials* 6 (8):581-585.

Treloar, L.R.G. 2005. *The physics of rubber elasticity*. Oxford: Oxford University Press.

Tsai, H., T. J. Pence, and E. Kirkinis. 2004. Swelling induced finite strain flexure in a rectangular block of an isotropic elastic material. *Journal of Elasticity* 75 (1):69-89.

Vrentas, J. S., and J. L. Duda. 1977. Diffusion in Polymer-Solvent Systems .3. Construction of Deborah Number Diagrams. *Journal of Polymer Science Part B-Polymer Physics* 15 (3):441-453.

Vrentas, J. S., C. M. Jarzebski, and J. L. Duda. 1975. Deborah Number for Diffusion in Polymer-Solvent Systems. *AICHE Journal* 21 (5):894-901.

Wallmersperger, T., B. Kroplin, and R. W. Gulch. 2004. Coupled chemo-electro-mechanical formulation for ionic polymer gels - numerical and experimental investigations. *Mechanics of Materials* 36 (5-6):411-420.

Wang, Q., J. L. Mynar, M. Yoshida, E. Lee, M. Lee, K. Okuro, K. Kinbara, and T. Aida. 2010. High-water-content mouldable hydrogels by mixing clay and a dendritic molecular binder. *Nature* 463 (7279):339-343.

Weisenberger, L. A., and J. L. Koenig. 1990. Nmr Imaging of Diffusion-Processes in Polymers - Measurement of the Spatial Dependence of Solvent Mobility in Partially Swollen Pmma Rods. *Macromolecules* 23 (9):2445-2453.

Westbrook, K. K., and H. J. Qi. 2008. Actuator designs using environmentally responsive hydrogels. *Journal of Intelligent Material Systems and Structures* 19 (5):597-607.

White, S. R., N. R. Sottos, P. H. Geubelle, J. S. Moore, M. R. Kessler, S. R. Sriram, E. N. Brown, and S. Viswanathan. 2001. Autonomic healing of polymer composites. *Nature* 409 (6822):794-797.

Wong, W. H., T. F. Guo, Y. W. Zhang, and L. Cheng. 2010. Humidity-driven bifurcation in a hydrogel-actuated nanostructure: A three-dimensional computational analysis. *International Journal of Solids and Structures* 47 (16):2034-2042.

Wool, R. P. 2008. Self-healing materials: a review. *Soft Matter* 4 (3):400-418.

Wool, R. P., and K. M. Oconnor. 1981. Craze Healing in Polymer Glasses. *Polymer Engineering and Science* 21 (14):970-977.

Wu, D. Y., S. Meure, and D. Solomon. 2008. Self-healing polymeric materials: A review of recent developments. *Progress in Polymer Science* 33 (5):479-522.

Wu, J. C., and N. A. Peppas. 1993. Modeling of Penetrant Diffusion in Glassy-Polymers with an Integral Sorption Deborah Number. *Journal of Polymer Science Part B-Polymer Physics* 31 (11):1503-1518.

Xue, Z. X., S. T. Wang, L. Lin, L. Chen, M. J. Liu, L. Feng, and L. Jiang. 2011. A Novel Superhydrophilic and Underwater Superoleophobic Hydrogel-Coated Mesh for Oil/Water Separation. *Advanced Materials* 23 (37):4270-4273.

Zhang, J. P., X. H. Zhao, Z. G. Suo, and H. Q. Jiang. 2009. A finite element method for transient analysis of concurrent large deformation and mass transport in gels. *Journal of Applied Physics* 105 (9): 09352201-09352209.

Zhang, X. X., T. F. Guo, and Y. W. Zhang. 2011. Instability analysis of a programmed hydrogel plate under swelling. *Journal of Applied Physics* 109 (6).

Zhang, X. X., K. Y. Zeng, J. Li, and Y. W. Zhang. 2009. Instability pathways of hydrogel microlenses under concentrated loadings. *Journal of Applied Physics* 106 (2).

Zhao, X. H., W. Hong, and Z. G. Suo. 2008. Inhomogeneous and anisotropic equilibrium state of a swollen hydrogel containing a hard core. *Applied Physics Letters* 92 (5).

Zhao, Z. X., Z. Li, Q. B. Xia, E. Bajalis, H. X. Xi, and Y. S. Lin. 2008. Swelling/deswelling kinetics of PNIPAAm hydrogels synthesized by microwave irradiation. *Chemical Engineering Journal* 142 (3):263-270.

Zhou, J. X., G. Y. Huang, M. E. Li, and A. K. Soh. 2010. Stress evolution in a phase-separating polymeric gel. *Modelling and Simulation in Materials Science and Engineering* 18 (2).

APPENDIX A

GEL SWELLING PROGRAM (GSP)

Note: The FORTRAN program is used study the coupled large deformation and diffusion in gels. The example used in the program is a free swelling example with 27 elements, 1/8 of a whole cubic (6*6*6 in dimension), with initial homogeneous swelling ratio 1.01. Compaq FORTRAN complier is used with IMSL library. For parallel implementation, PARDISO, MUMPS (with MPI) solver is available.

Copyright goes to Prof. Hanqing Jiang's group and the reader is responsible for his/her own result. Any questions regarding this program should go to Prof. Jiang by email and this program is highly expected to be used in gel community to study interesting swelling phenomenon.

```
C-----------------------------------------------------------------------------------
      PROGRAM MAIN
C     ---use compaq fortran imsl library---
      USE IMSL

      IMPLICIT DOUBLE PRECISION (A-H,O-Z)
      OPEN (1,FILE='PARS.TXT')
C     ---NTOTAL: Total Nodes
C     ---NELEM:  Total Elements
C     ---NDISBOU_DEF: #of displacement boundaries
C     ---NDISBOU_DEF: #of diffusion boundaries
      READ
(1,*)NTOTAL,NELEM,NDISBOU_DEF,NDISBOU_DIFF
      CLOSE(1)
c     ---MCRD: 3 dimensional problem---
C     ---NNODE: # of nodes in each element
      MCRD=3
      NNODE=8
      NDOFEL=MCRD*NNODE

      CALL
MAINPROGRAM(NTOTAL,NELEM,MCRD,NNODE,NDOFEL,
     &    NDISBOU_DEF,NDISBOU_DIFF)

      END

c     ---Main Program for gel swelling---
      SUBROUTINE
MAINPROGRAM(NTOTAL,NELEM,MCRD,NNODE,NDOFEL,
     &    NDISBOU_DEF,NDISBOU_DIFF)

      IMPLICIT DOUBLE PRECISION (A-H,O-Z)
     ALLOCATABLE:: GLB_COORDS(:,:),GLB_COORDS_NEW(:,:)
     ALLOCATABLE:: GLB_FORCE_DEF(:),GLB_STIFF_DEF(:,:)
     ALLOCATABLE:: GLB_FORCE_DEF_T(:),GLB_STIFF_DEF_T(:,:)
```

```
            ALLOCATABLE:: U_DEF(:),U_DEF_T(:)
            ALLOCATABLE:: DIS_DEF(:),U_DIFF_T(:)
            ALLOCATABLE:: NBP_DEF(:),DNBP_DEF(:)
            ALLOCATABLE:: NBP_TOTAL(:),DNBP_TOTAL(:)
          ALLOCATABLE:: GLB_FORCE_DIFF(:),GLB_STIFF_DIFF(:,:)
          ALLOCATABLE::
GLB_FORCE_DIFF_T(:),GLB_STIFF_DIFF_T(:,:)
            ALLOCATABLE:: U_DIFF(:)
            ALLOCATABLE:: DIS_DIFF(:)
            ALLOCATABLE:: NBP_DIFF(:),DNBP_DIFF(:)
            ALLOCATABLE:: GLB_STIFF_UT_T(:,:)
            ALLOCATABLE:: GLB_STIFF_TU_T(:,:)
            ALLOCATABLE:: GLB_FORCE_TU_T(:)
            ALLOCATABLE:: GLB_STIFF_TT_T(:,:)
            ALLOCATABLE:: GLB_STIFF_TOTAL_T(:,:)
            ALLOCATABLE:: GLB_STIFF_TOTAL(:,:)
            ALLOCATABLE:: GLB_FORCE_TOTAL_T(:)
            ALLOCATABLE:: GLB_FORCE_TOTAL(:)
            ALLOCATABLE:: DIS_TOTAL(:)
            ALLOCATABLE:: GLB_STIFF_TOTAL_BACKUP(:,:)
            ALLOCATABLE:: EVAL(:)
            ALLOCATABLE:: GLB_STRESS(:,:)

            DIMENSION NODE_IN_ELEMENT(NELEM,NNODE)
            DIMENSION SIGMA_OLD(NELEM,NNODE,6)
            DIMENSION SIGMA(6)
            DIMENSION SIGMA_NEW(NELEM,NNODE,6)
            DIMENSION SIGMA_NEW2(NELEM,NNODE,6)
            DIMENSION
ELE_STIFF_DEF(NDOFEL,NDOFEL),ELE_FORCE_DEF(NDOFEL)
            DIMENSION
ELE_COORDS_DEF(MCRD,NNODE),ELE_U_DEF(NDOFEL)
            DIMENSION ELE_DU_DEF(NDOFEL)
            DIMENSION DISBOU_DEF(NDISBOU_DEF,3)
            DIMENSION ELE_COORDS_DEF2(MCRD,NNODE)
            DIMENSION ELE_COORDS_DEF0(MCRD,NNODE)
            DIMENSION
ELE_STIFF_DIFF(NNODE,NNODE),ELE_FORCE_DIFF(NNODE)
            DIMENSION
ELE_COORDS_DIFF(NNODE),ELE_U_DIFF(NNODE)
            DIMENSION ELE_DU_DIFF(NNODE)
            DIMENSION DISBOU_DIFF(NDISBOU_DIFF,2)
            DIMENSION ELE_COORDS_DIFF2(NNODE)
            DIMENSION ELE_COORDS_DIFF0(NNODE)
            DIMENSION FTHETAU_T(NNODE)
```

```
      DIMENSION AKTHETATHETA_T(NNODE,NNODE)
      DIMENSION AKTHETAU_T(NNODE,3*NNODE)
      DIMENSION AKUTHETA_T(3*NNODE,NNODE)
      DIMENSION SIGMA_NODE(8,6)
      LOGICAL   JFORCE,JFLUX

      NTDIM_DEF=NTOTAL*MCRD
      NDIM_DEF=NTDIM_DEF-NDISBOU_DEF
      NTDIM_DIFF=NTOTAL
      NDIM_DIFF=NTOTAL-NDISBOU_DIFF
      NTDIM_TOTAL=NTDIM_DIFF+NTDIM_DEF
      NDIM_TOTAL=NDIM_DIFF+NDIM_DEF

      ALLOCATE
(GLB_COORDS(NTOTAL,MCRD+1),GLB_COORDS_NEW(NTOTAL,MCRD
+1))
      ALLOCATE (GLB_FORCE_DEF(NDIM_DEF))
      ALLOCATE (GLB_STIFF_DEF(NDIM_DEF,NDIM_DEF))
      ALLOCATE (GLB_FORCE_DEF_T(NTDIM_DEF))
     ALLOCATE  (GLB_STIFF_DEF_T(NTDIM_DEF,NTDIM_DEF))
      ALLOCATE (GLB_STIFF_UT_T(NTDIM_DEF,NTDIM_DIFF))
      ALLOCATE (GLB_STIFF_TU_T(NTDIM_DIFF,NTDIM_DEF))
      ALLOCATE (GLB_FORCE_TU_T(NTDIM_DIFF))
      ALLOCATE (GLB_STIFF_TT_T(NTDIM_DIFF,NTDIM_DIFF))
      ALLOCATE
(GLB_STIFF_TOTAL_T(NTDIM_TOTAL,NTDIM_TOTAL))
      ALLOCATE
(GLB_STIFF_TOTAL(NDIM_TOTAL,NDIM_TOTAL))
      ALLOCATE (GLB_FORCE_TOTAL_T(NTDIM_TOTAL))
      ALLOCATE (GLB_FORCE_TOTAL(NDIM_TOTAL))
      ALLOCATE (NBP_TOTAL(NTDIM_TOTAL))
      ALLOCATE (DNBP_TOTAL(NTDIM_TOTAL))
      ALLOCATE (U_DEF(NTDIM_DEF))
      ALLOCATE (U_DEF_T(NTDIM_DEF))
      ALLOCATE (DIS_DEF(NDIM_DEF))
      ALLOCATE (NBP_DEF(NTDIM_DEF))
      ALLOCATE (DNBP_DEF(NTDIM_DEF))
      ALLOCATE (GLB_FORCE_DIFF(NDIM_DIFF))
      ALLOCATE (GLB_STIFF_DIFF(NDIM_DIFF,NDIM_DIFF))
      ALLOCATE (GLB_FORCE_DIFF_T(NTDIM_DIFF))
      ALLOCATE
(GLB_STIFF_DIFF_T(NTDIM_DIFF,NTDIM_DIFF))
      ALLOCATE (U_DIFF(NTDIM_DIFF))
      ALLOCATE (U_DIFF_T(NTDIM_DIFF))
      ALLOCATE (DIS_DIFF(NDIM_DIFF))
```

```
            ALLOCATE (NBP_DIFF(NTDIM_DIFF))
            ALLOCATE (DNBP_DIFF(NTDIM_DIFF))
            ALLOCATE (DIS_TOTAL(NDIM_TOTAL))
            ALLOCATE
(GLB_STIFF_TOTAL_BACKUP(NDIM_TOTAL,NDIM_TOTAL))
            ALLOCATE (EVAL(NDIM_TOTAL))
            ALLOCATE (GLB_STRESS(NTOTAL,7))

      C     ---Read initial coordinates---
            OPEN(1,FILE='XYZ.TXT')
            DO WHILE(.NOT.EOF(1))
                  READ(1,*) II,GLB_COORDS(II,1),GLB_COORDS(II,2),
     &            GLB_COORDS(II,3),GLB_COORDS(II,4)
            ENDDO
            CLOSE(1)
      C     ---Read element information---
            OPEN(1,FILE='ELEMENT.TXT')
            DO WHILE(.NOT.EOF(1))
                  READ(1,*)
II,NODE_IN_ELEMENT(II,1),NODE_IN_ELEMENT(II,2),
     &NODE_IN_ELEMENT(II,3),NODE_IN_ELEMENT(II,4),
     &NODE_IN_ELEMENT(II,5),NODE_IN_ELEMENT(II,6),
     &NODE_IN_ELEMENT(II,7),NODE_IN_ELEMENT(II,8)

            ENDDO
            CLOSE(1)
      C     ---Read Boundary conditions---
            NBP_DEF=0
            DNBP_DEF=0.D0
            NBP_DIFF=0
            DNBP_DIFF=0.D0
            OPEN (1,FILE='BOUNDARY.TXT')
      C     ---DEFORMATION BOUNDARY---
                  DO I=1,NDISBOU_DEF
                  READ (1,*)
DISBOU_DEF(I,1),DISBOU_DEF(I,2),DISBOU_DEF(I,3)
                  N1=IDINT(DISBOU_DEF(I,1))
                  N2=IDINT(DISBOU_DEF(I,2))
                  NBP_DEF((N1-1)*MCRD+N2)=1
                  DNBP_DEF((N1-1)*MCRD+N2)=DISBOU_DEF(I,3)
                  ENDDO
      C     ---DIFFUSION BOUNDARY---
                  DO I=1,NDISBOU_DIFF
                  READ (1,*) DISBOU_DIFF(I,1),DISBOU_DIFF(I,2)
                  N1=IDINT(DISBOU_DIFF(I,1))
```

```
            NBP_DIFF(N1)=1
            DNBP_DIFF(N1)=DISBOU_DIFF(I,2)
            ENDDO
      CLOSE(1)

      NBP_TOTAL=0
      DNBP_TOTAL=0.D0
      DO I=1,NTDIM_DEF
            NBP_TOTAL(I)=NBP_DEF(I)
            DNBP_TOTAL(I)=DNBP_DEF(I)
      ENDDO
      DO I=1,NTDIM_DIFF
            NBP_TOTAL(I+NTDIM_DEF)=NBP_DIFF(I)
            DNBP_TOTAL(I+NTDIM_DEF)=DNBP_DIFF(I)
      ENDDO

C     ---PRES: Initial swelling----
      PRES=1.01D0
      ANV=4.833333333D-3
      CHI=0.5190137858D0
C     ---ANV AND CHI VALUE GIVES LAMBDA_EQ=1.75
C     ---with this ANV,CHI AND PRES,
C     ---Initial chempoten=-2.066806650---
C     ---Unit: Length=mm,Time=minute--
C     ---DD: Diffusion coefficient---
C     ---D=8*10^(-10)m^2/s---
C     ---DTIME: total time---
C     ---Multi-time increments is required but omitted---
C     ---for simplicity of author understanding----
C     ---NITERATION: Iteration number---
      DD=0.048D0
      DTIME=1D2
      U_DEF=0.D0
      U_DIFF=0.D0
      NITERATION=1

      OPEN(400,FILE='Message.TXT')
10    CONTINUE
C     ---JFORCE,JFLUX: Convergence indicatior---
      JFORCE=.FALSE.
      JFLUX=.FALSE.

      DIS_DEF=0.D0
      DIS_DIFF=0.D0
      GLB_FORCE_DIFF_T=0.D0
```

```
                GLB_STIFF_DIFF_T=0.D0
                GLB_FORCE_DEF_T=0.D0
                GLB_STIFF_DEF_T=0.D0
                GLB_STIFF_TU_T=0.D0
                GLB_STIFF_UT_T=0.D0
                GLB_STRESS=0.D0

                DO JELEM=1,NELEM !START ELEMENT LOOP
                    DO II=1,NNODE
                        NODE=NODE_IN_ELEMENT(JELEM,II)
                        DO JJ=1,MCRD

        ELE_COORDS_DEF0(JJ,II)=GLB_COORDS(NODE,JJ)

        ELE_COORDS_DEF(JJ,II)=GLB_COORDS(NODE,JJ)
           &                    +(U_DEF(JJ+MCRD*(NODE-1)))/2.D0
        C       ---Strain is defined in t+delta_t/2---

        ELE_COORDS_DEF2(JJ,II)=GLB_COORDS(NODE,JJ)
           &                    +(U_DEF(JJ+MCRD*(NODE-1)))
                                ELE_U_DEF(JJ+MCRD*(II-
1))=U_DEF(JJ+MCRD*(NODE-1))
                                ELE_DU_DEF(JJ+MCRD*(II-
1))=U_DEF(JJ+MCRD*(NODE-1))
                        ENDDO

        ELE_COORDS_DIFF(II)=GLB_COORDS(NODE,4)
                                ELE_DU_DIFF(II)=U_DIFF(NODE)
                    ENDDO
        C       ---Get element stiffness and force vector---
                    CALL
UEL_DEF(ELE_FORCE_DEF,ELE_STIFF_DEF,NDOFEL,MCRD,NNODE,
           &                NITERATION,JELEM,NELEM,DTIME,
           &
        ELE_COORDS_DEF,ELE_COORDS_DEF2,ELE_COORDS_DEF0,
           &
        ELE_DU_DEF,ELE_U_DEF,ELE_DU_DIFF,ELE_COORDS_DIFF,
           &                AKTHETAU_T,AKUTHETA_T,
           &
        ELE_FORCE_DIFF,ELE_STIFF_DIFF,PRES,SIGMA_NODE,
           &                ANV,CHI,DD)
        C       ---Experience:ignore off-diagonal terms gives
        C       ---faster rate of convergence a lof of times---
                                AKTHETAU_T=0.D0
                                AKUTHETA_T=0.D0
```

```
C       ---GET NODE STRESS FOR EACH ELEMENT---
        DO II=1,NNODE
         NODE=NODE_IN_ELEMENT(JELEM,II)

GLB_STRESS(NODE,7)=GLB_STRESS(NODE,7)+1.D0
                                DO J=1,6

      GLB_STRESS(NODE,J)=GLB_STRESS(NODE,J)
     &                                +SIGMA_NODE(II,J)
                                ENDDO
                  ENDDO

                  DO I1=1,NNODE
                        DO IMCRD1=1,MCRD
                                N1=(I1-1)*MCRD+IMCRD1

      NODE1_G=(NODE_IN_ELEMENT(JELEM,I1)-1)*MCRD+IMCRD1

GLB_FORCE_DEF_T(NODE1_G)=GLB_FORCE_DEF_T(NODE1_G)
     &                          +ELE_FORCE_DEF(N1)
                                DO I2=1,NNODE
                                        DO IMCRD2=1,MCRD
                                                N2=(I2-1)*MCRD+IMCRD2

      NODE2_G=(NODE_IN_ELEMENT(JELEM,I2)-1)*MCRD
     &                                  +IMCRD2

      GLB_STIFF_DEF_T(NODE1_G,NODE2_G)=
     &
      GLB_STIFF_DEF_T(NODE1_G,NODE2_G)
     &                                   +ELE_STIFF_DEF(N1,N2)
                                        ENDDO
                                ENDDO
                        ENDDO
                  ENDDO

                  DO I1=1,NNODE

      NODE1_G=NODE_IN_ELEMENT(JELEM,I1)

GLB_FORCE_DIFF_T(NODE1_G)=GLB_FORCE_DIFF_T(NODE1_G)
     &                                +ELE_FORCE_DIFF(I1)
                        DO I2=1,NNODE

      NODE2_G=NODE_IN_ELEMENT(JELEM,I2)
```

```
GLB_STIFF_DIFF_T(NODE1_G,NODE2_G)=
   &
GLB_STIFF_DIFF_T(NODE1_G,NODE2_G)
   &                                          +ELE_STIFF_DIFF(I1,I2)
                     ENDDO
               ENDDO

               DO I1=1,NNODE
                     DO IMCRD1=1,MCRD
                           N1=(I1-1)*MCRD+IMCRD1

NODE1_G=(NODE_IN_ELEMENT(JELEM,I1)-1)*MCRD+IMCRD1
                           DO I2=1,NNODE

NODE2_G=NODE_IN_ELEMENT(JELEM,I2)

GLB_STIFF_UT_T(NODE1_G,NODE2_G)=
   &                       GLB_STIFF_UT_T(NODE1_G,NODE2_G)
   &                             +AKUTHETA_T(N1,I2)
                           ENDDO
                     ENDDO
               ENDDO

               DO I1=1,NNODE
                     NODE1_G=NODE_IN_ELEMENT(JELEM,I1)

GLB_FORCE_TU_T(NODE1_G)=GLB_FORCE_TU_T(NODE1_G)
   &                       +FTHETAU_T(I1)
                     DO I2=1,NNODE
                           DO IMCRD2=1,MCRD
                                 N2=(I2-1)*MCRD+IMCRD2

NODE2_G=(NODE_IN_ELEMENT(JELEM,I2)-1)*MCRD
   &                                          +IMCRD2

GLB_STIFF_TU_T(NODE1_G,NODE2_G)=
   &                       GLB_STIFF_TU_T(NODE1_G,NODE2_G)
   &                             +AKTHETAU_T(I1,N2)
                           ENDDO
                     ENDDO
               ENDDO

         ENDDO !END ELEMENT LOOP
C        ---Assemble global stiffness and force---
```

```
            GLB_STIFF_TOTAL_T=0.D0
            GLB_FORCE_TOTAL_T=0.D0

            DO I=1,NTDIM_DEF
                  DO J=1,NTDIM_DEF
                  GLB_STIFF_TOTAL_T(I,J)=
     &    GLB_STIFF_TOTAL_T(I,J)+GLB_STIFF_DEF_T(I,J)
                  ENDDO
                  DO J=1,NTDIM_DIFF
                  GLB_STIFF_TOTAL_T(I,J+NTDIM_DEF)=
     &
     GLB_STIFF_TOTAL_T(I,J+NTDIM_DEF)+GLB_STIFF_UT_T(I,J)
                  ENDDO
                  GLB_FORCE_TOTAL_T(I)=GLB_FORCE_DEF_T(I)
            ENDDO

            DO I=1,NTDIM_DIFF
                  DO J=1,NTDIM_DEF
                  GLB_STIFF_TOTAL_T(I+NTDIM_DEF,J)=
     &
     GLB_STIFF_TOTAL_T(I+NTDIM_DEF,J)+GLB_STIFF_TU_T(I,J)
                  ENDDO
                  DO J=1,NTDIM_DIFF

     GLB_STIFF_TOTAL_T(I+NTDIM_DEF,J+NTDIM_DEF)=
     &    GLB_STIFF_TOTAL_T(I+NTDIM_DEF,J+NTDIM_DEF)
     &                  +GLB_STIFF_DIFF_T(I,J)
                  ENDDO

     GLB_FORCE_TOTAL_T(I+NTDIM_DEF)=GLB_FORCE_TOTAL_T(I
+NTDIM_DEF)
     &                        +GLB_FORCE_DIFF_T(I)
            ENDDO
C           ---Apply BCs by elimination approach---
            GLB_STIFF_TOTAL=0.D0
            GLB_FORCE_TOTAL=0.D0

            IROW=1
            DO I=1,NTDIM_TOTAL
                  I1=NBP_TOTAL(I)
                  IF(I1.NE.1) THEN

     GLB_FORCE_TOTAL(IROW)=GLB_FORCE_TOTAL_T(I)
                        ICOLUMN=1
                        DO J=1,NTDIM_TOTAL
```

```
                                    J1=NBP_TOTAL(J)
                                    IF(J1.NE.1) THEN

        GLB_STIFF_TOTAL(IROW,ICOLUMN)=
           &                         GLB_STIFF_TOTAL_T(I,J)
                                          ICOLUMN=ICOLUMN+1
                                    ELSE
                                          IF(NITERATION.EQ.1) THEN

        GLB_FORCE_TOTAL(IROW)=GLB_FORCE_TOTAL(IROW)
           &                                    -
DNBP_TOTAL(J)*GLB_STIFF_TOTAL_T(I,J)
                                          ENDIF
                                    ENDIF
                              ENDDO
                              IROW=IROW+1
                        ENDIF
                  ENDDO

        C         ---Calculate the eigenvalue of stiffness ---
                  GLB_STIFF_TOTAL_BACKUP=GLB_STIFF_TOTAL
                  CALL
DEVLSF(NDIM_TOTAL,GLB_STIFF_TOTAL_BACKUP,NDIM_TOTAL,EV
AL)
        C         ---Find minimum---
                  EIGEN_MIN=1D10
                  DO I=1,NDIM_TOTAL
                        IF(EVAL(I).LT.EIGEN_MIN)THEN
                              EIGEN_MIN=EVAL(I)
                        ENDIF
                  ENDDO
        C         ---Add penalty to diagonal of stiffness---
                  FACTOR=3.D0
                  DO I=1,NDIM_TOTAL
                        GLB_STIFF_TOTAL(I,I)=GLB_STIFF_TOTAL(I,I)
           &   +FACTOR*DABS(EIGEN_MIN)
                  ENDDO
        C         ---Solve the equation---
                  CALL
DLSLRG(NDIM_TOTAL,GLB_STIFF_TOTAL,NDIM_TOTAL
           &          ,GLB_FORCE_TOTAL,1,DIS_TOTAL)
                  DEF_MAX=1D-8
                  ICOUNT=1
                  DO I=1,NTDIM_DEF
                        IF(NBP_DEF(I).EQ.1) THEN
```

```
                ELSE

IF(DABS(DIS_TOTAL(ICOUNT)).GE.DABS(DEF_MAX)) THEN

DEF_MAX=DABS(DIS_TOTAL(ICOUNT))
                        ENDIF
                        ICOUNT=ICOUNT+1
                ENDIF
        ENDDO

        DIFF_MAX=1D-8
        ICOUNT=1
        DO I=1,NTDIM_DIFF
                IF(NBP_DIFF(I).EQ.1) THEN
                ELSE
                        IF(DABS(DIS_TOTAL(ICOUNT+NDIM_DEF))
   &            .GE.DABS(DIFF_MAX)) THEN

DIFF_MAX=DABS(DIS_TOTAL(ICOUNT+NDIM_DEF))
                        ENDIF
                        ICOUNT=ICOUNT+1
                ENDIF
        ENDDO

        ICOUNT=1
        DO I=1,NTDIM_DEF
                IF(NBP_DEF(I).EQ.1) THEN
                        U_DEF(I)=DNBP_DEF(I)
                ELSE
                        U_DEF(I)=U_DEF(I)+DIS_TOTAL(ICOUNT)
                        ICOUNT=ICOUNT+1
                ENDIF
        ENDDO

        ICOUNT=1
        DO I=1,NTDIM_DIFF
                IF(NBP_DIFF(I).EQ.1) THEN
                        U_DIFF(I)=DNBP_DIFF(I)
                ELSE

U_DIFF(I)=U_DIFF(I)+DIS_TOTAL(ICOUNT+NDIM_DEF)
                        ICOUNT=ICOUNT+1
                ENDIF
        ENDDO
```

```
c       ---Max displacement and chem potential correction---
        WRITE(400,*)' NITERATION= ',NITERATION
        WRITE(400,*)' DEF_MAX= ',DEF_MAX
        WRITE(400,*)' DIFF_MAX=',DIFF_MAX
C       ---Simple convergence judgement---
        IF(DABS(DEF_MAX).LE.1D-5)  JFORCE=.TRUE.
        IF(DABS(DIFF_MAX).LE.1D-5) JFLUX=.TRUE.

60      FORMAT(10F20.10)
61      FORMAT(8I6)

        OPEN(600,FILE='STRESS_TecplotFormat.DAT')
        IF(JFORCE.AND.JFLUX.AND.NITERATION.GT.2)THEN
          DO I=1,NTOTAL
            DO J=1,6

GLB_STRESS(I,J)=GLB_STRESS(I,J)/GLB_STRESS(I,7)
            ENDDO
          ENDDO

            WRITE(600,*)' TITLE="Gel Swelled Shape"'
            WRITE(600,*)'
variables="x","y","z","CHEM","sxx","syy","szz",
     &                    "syz","sxz","sxy"'
            WRITE(600,*)'ZONE
N=',NTOTAL,',E=',NELEM,',F=FEPOINT,ET=BRICK'
            DO I=1,NTOTAL
              WRITE(600,60)
     &U_DEF((I-1)*MCRD+1)+GLB_COORDS(I,1)+U_DEF_T((I-
1)*MCRD+1),
     &U_DEF((I-1)*MCRD+2)+GLB_COORDS(I,2)+U_DEF_T((I-
1)*MCRD+2),
     &U_DEF((I-1)*MCRD+3)+GLB_COORDS(I,3)+U_DEF_T((I-
1)*MCRD+3),
     &U_DIFF(I)+GLB_COORDS(I,4),
     &GLB_STRESS(I,1),GLB_STRESS(I,2),GLB_STRESS(I,3),
     &GLB_STRESS(I,4),GLB_STRESS(I,5),GLB_STRESS(I,6)
            ENDDO
            DO I=1,NELEM

WRITE(600,61)NODE_IN_ELEMENT(I,1),NODE_IN_ELEMENT(I,2),
     &
NODE_IN_ELEMENT(I,3),NODE_IN_ELEMENT(I,4),
     &
NODE_IN_ELEMENT(I,5),NODE_IN_ELEMENT(I,6),
```

```
            &
NODE_IN_ELEMENT(I,7),NODE_IN_ELEMENT(I,8)
                        ENDDO
                        STOP
                ELSE
                 NITERATION=NITERATION+1
                 GOTO 10
                ENDIF ! END OF IF (JFORCE)
                END


                SUBROUTINE
UEL_DEF(RHS_T,AMATRX_T,NDOFEL,MCRD,NNODE,
            & NITERATION,JELEM,NELEM,DTIME,

&COORDS,COORDS2,COORDS0,ELE_DU_DEF,ELE_U_DEF,DTEMP,TEM
P,
            &AKTHETAU_T,AKUTHETA_T,
            &RHS_DIFF_T,AMATRX_DIFF_T,ALAMBDA0,SIGMA_NODE,
            &                   ANV,CHI,DD)

            IMPLICIT DOUBLE PRECISION (A-H,O-Z)

                PARAMETER (IPNML=8)
                DIMENSION RHS(NDOFEL),AMATRX(NDOFEL,NDOFEL)
                DIMENSION
RHS_T(NDOFEL),AMATRX_T(NDOFEL,NDOFEL)
             DIMENSION U(NDOFEL),DIS_T(MCRD,NNODE)
                DIMENSION
ELE_DU_DEF(3*NNODE),ELE_U_DEF(3*NNODE)
                DIMENSION DTEMP(NNODE),TEMP(NNODE),DTEMPDX(3)
                DIMENSION
COORDS(MCRD,NNODE),COORDS0(MCRD,NNODE)
                DIMENSION COORDS2(MCRD,NNODE)
                DIMENSION DELTAM(3,3)
                DIMENSION DMATRIX(6,6),CMATRIX(3,3,3,3)
                DIMENSION POINTS2(IPNML,4),POINTS(IPNML,4)
                DIMENSION XI(3),XI3(3)
                DIMENSION SF2(NNODE),SF3(NNODE)
                DIMENSION DSFDX0(NNODE,MCRD)
                DIMENSION
DSFDX2(NNODE,MCRD),DSFDX3(NNODE,MCRD)
                DIMENSION DG(3,3),DGI(3,3),DG2(3,3),DGI2(3,3),DG2I(3,3)
                DIMENSION B_VOL2(NNODE,3),B_TOTAL2(6,3*NNODE)
```

```
      DIMENSION
DBAR1(3*NNODE,3*NNODE),DBAR2(3*NNODE,3*NNODE)
      DIMENSION
DBAR3(3*NNODE,3*NNODE),DBAR4(3*NNODE,3*NNODE)
      DIMENSION
DBAR5(3*NNODE,3*NNODE),DBAR6(3*NNODE,3*NNODE)
      DIMENSION
TN1(3*NNODE,3*NNODE),TN2(3*NNODE,3*NNODE)
      DIMENSION
TN3(3*NNODE,3*NNODE),TN4(3*NNODE,3*NNODE)
      DIMENSION
TN5(3*NNODE,3*NNODE),TN6(3*NNODE,3*NNODE)
      DIMENSION AKL(3*NNODE,3*NNODE)
      DIMENSION
AKNL1(3*NNODE,3*NNODE),AKNL2(3*NNODE,3*NNODE)
      DIMENSION
AKTHETAU(NNODE,3*NNODE),AKTHETAU_T(NNODE,3*NNODE)
      DIMENSION
AKUTHETA(3*NNODE,NNODE),AKUTHETA_T(3*NNODE,NNODE)
      DIMENSION SIGMA(6)
      DIMENSION SIGMA_MAT(3,3)
      DIMENSION BBAR(3,3),DG2BAR(3,3),HMAT(3,3,3,3)
      DIMENSION DISTGR(3,3),DSTRAN(6)
      DIMENSION
RHS_DIFF(NNODE),AMATRX_DIFF(NNODE,NNODE)
      DIMENSION
RHS_DIFF_T(NNODE),AMATRX_DIFF_T(NNODE,NNODE)
      DIMENSION AKTHETATHETA(NNODE,NNODE)
      DIMENSION AKTHETATHETA_T(NNODE,NNODE)
      DIMENSION FLUX(3),TEMPDX(3)
      DIMENSION
SIGMA_GAUSS(IPNML,6),SIGMA_NODE(NNODE,6)
      DIMENSION GMAT_INV(8,8)

C     ---IDENTITY MATRIX---
      DELTAM=0.D0
      DELTAM(1,1)=1.D0
      DELTAM(2,2)=1.D0
      DELTAM(3,3)=1.D0

      DCHEM_AVG=0.D0
      DO I=1,NNODE
            DCHEM_AVG=DCHEM_AVG+DTEMP(I)
      ENDDO
      DCHEM_AVG=DCHEM_AVG/DBLE(NNODE)
```

```
                CHEM0_AVG=0.D0
                DO I=1,NNODE
                        CHEM0_AVG=CHEM0_AVG+TEMP(I)
                ENDDO
                CHEM0_AVG=CHEM0_AVG/DBLE(NNODE)

            DO INODE=1,NNODE
                        DO IMCRD=1,MCRD

        DIS_T(IMCRD,INODE)=ELE_U_DEF(IMCRD+MCRD*(INODE-1))
                        ENDDO
                ENDDO

                CALL GET_POINTS (IPNML,POINTS)
                CALL GET_POINTS2(IPNML,POINTS2)

                B_VOL2=0.D0
                EL_VOL2=0.D0
                DETJAC2_AVG=0.D0

                DO IPOINT=1,IPNML
                        XI=POINTS(IPOINT,1:3)
                        WEIGHT=POINTS(IPOINT,4)
                   CALL
GRADIENT(NNODE,COORDS2,XI,DETJAC2,SF2,DSFDX2,
            &            DG2,DGI2,JELEM,DIS_T,COORDS0,DSFDX0)
                        DO I=1,NNODE
                                DO J=1,3

        B_VOL2(I,J)=B_VOL2(I,J)+DSFDX2(I,J)*WEIGHT*DETJAC2
                                ENDDO
                        ENDDO
                        EL_VOL2=EL_VOL2+WEIGHT*DETJAC2
                        DETJAC2_AVG=DETJAC2_AVG+DETJAC2
                ENDDO

                B_VOL2=B_VOL2/EL_VOL2
                DETJAC2_AVG=DETJAC2_AVG/DBLE(IPNML)

                RHS_T=0.D0
                AMATRX_T=0.D0
                RHS_DIFF_T=0.D0
                AMATRX_DIFF_T=0.D0
                AKTHETAU_T=0.D0
```

```
            AKUTHETA_T=0.D0
            SIGMA_GAUSS=0.D0
            SIGMA_NODE=0.D0
            DO IPOINT=1,IPNML !Integration loop
                  XI=POINTS(IPOINT,1:3)
                  WEIGHT=POINTS(IPOINT,4)
      C     ---Lumped matrix is used,Gaussian point value is
      C     ---replaced by nodal value---
                  XI3=POINTS2(IPOINT,1:3)
               CALL
GRADIENT(NNODE,COORDS,XI3,DETJAC,SF3,DSFDX3,
     &           DG,DGI,JELEM,DIS_T,COORDS0,DSFDX0)
               CALL
GRADIENT(NNODE,COORDS2,XI,DETJAC2,SF2,DSFDX2,
     &           DG2,DGI,JELEM,DIS_T,COORDS0,DSFDX0)
      C     ---B-BAR Matrix---
            B_TOTAL2=0.D0
                  DO I=1,6
                        DO J=1,3*NNODE
                              J_TEMP=MOD(J,3)
                              IF(MOD(J,3).EQ.0)J_TEMP=3
                              IF(I.LE.3)THEN
                                    IF(J_TEMP.EQ.I)THEN
                                          IF(MOD(J,3).NE.0)THEN

      B_TOTAL2(I,J)=(B_VOL2(J/3+1,J_TEMP)
     &                              -DSFDX2(J/3+1,J_TEMP))/3.D0
     &                              +DSFDX2(J/3+1,J_TEMP)
                                          ELSE

      B_TOTAL2(I,J)=(B_VOL2(J/3,J_TEMP)
     &                              -DSFDX2(J/3,J_TEMP))/3.D0
     &                              +DSFDX2(J/3,J_TEMP)
                                          ENDIF
                                    ELSE
                                          IF(MOD(J,3).NE.0)THEN

      B_TOTAL2(I,J)=(B_VOL2(J/3+1,J_TEMP)
     &                              -DSFDX2(J/3+1,J_TEMP))/3.D0
                                          ELSE

      B_TOTAL2(I,J)=(B_VOL2(J/3,J_TEMP)
     &                              -DSFDX2(J/3,J_TEMP))/3.D0
                                          ENDIF
                                    ENDIF
```

```
                        ENDIF
                        IF(I.EQ.4)THEN
                              IF(J_TEMP.EQ.2)THEN
                              B_TOTAL2(I,J)=DSFDX2(J/3+1,3)
                              ENDIF

                              IF(J_TEMP.EQ.3)THEN
                              B_TOTAL2(I,J)=DSFDX2(J/3,2)
                              ENDIF
                        ENDIF

                        IF(I.EQ.5)THEN
                              IF(J_TEMP.EQ.1)THEN
                              B_TOTAL2(I,J)=DSFDX2(J/3+1,3)
                              ENDIF

                              IF(J_TEMP.EQ.3)THEN
                              B_TOTAL2(I,J)=DSFDX2(J/3,1)
                              ENDIF
                        ENDIF
                        IF(I.EQ.6)THEN
                              IF(J_TEMP.EQ.1)THEN
                              B_TOTAL2(I,J)=DSFDX2(J/3+1,2)
                              ENDIF

                              IF(J_TEMP.EQ.2)THEN
                              B_TOTAL2(I,J)=DSFDX2(J/3+1,1)
                              ENDIF
                        ENDIF
                  ENDDO
            ENDDO

      DG2=DG2*(DETJAC2_AVG/DETJAC2)**(1.D0/3.D0)
      DET=DG2(1,1)*DG2(2,2)*DG2(3,3)
&-DG2(1,1)*DG2(2,3)*DG2(3,2)
&-DG2(2,1)*DG2(1,2)*DG2(3,3)
&-DG2(2,1)*DG2(1,3)*DG2(3,2)
&+DG2(3,1)*DG2(1,2)*DG2(2,3)
&-DG2(3,1)*DG2(2,2)*DG2(1,3)
      DG2I(1,1)= (DG2(2,2)*DG2(3,3)-DG2(2,3)*DG2(3,2))/DET
      DG2I(1,2)=-(DG2(1,2)*DG2(3,3)-DG2(1,3)*DG2(3,2))/DET
      DG2I(1,3)=-(DG2(1,3)*DG2(2,2)-DG2(1,2)*DG2(2,3))/DET
      DG2I(2,1)=-(DG2(2,1)*DG2(3,3)-DG2(2,3)*DG2(3,1))/DET
      DG2I(2,2)= (DG2(1,1)*DG2(3,3)-DG2(1,3)*DG2(3,1))/DET
      DG2I(2,3)=-(DG2(1,1)*DG2(2,3)-DG2(1,3)*DG2(2,1))/DET
```

```
      DG2I(3,1)=-(DG2(2,2)*DG2(3,1)-DG2(2,1)*DG2(3,2))/DET
      DG2I(3,2)=-(DG2(1,1)*DG2(3,2)-DG2(1,2)*DG2(3,1))/DET
      DG2I(3,3)= (DG2(1,1)*DG2(2,2)-DG2(1,2)*DG2(2,1))/DET
      DO I=1,3
            DO J=1,3
            DG2BAR(I,J)=DET**(-1.D0/3.D0)*DG2(I,J)
            ENDDO
      ENDDO
      BBAR(1,1)=DG2BAR(1, 1)**2.D0+DG2BAR(1,
2)**2.D0+DG2BAR(1, 3)**2.D0
      BBAR(2,2)=DG2BAR(2, 1)**2.D0+DG2BAR(2,
2)**2.D0+DG2BAR(2, 3)**2.D0
      BBAR(3,3)=DG2BAR(3, 3)**2.D0+DG2BAR(3,
1)**2.D0+DG2BAR(3, 2)**2.D0
      BBAR(1,2)=DG2BAR(1, 1)*DG2BAR(2, 1)+DG2BAR(1,
2)*DG2BAR(2, 2)
     &+DG2BAR(1, 3)*DG2BAR(2, 3)
      BBAR(1,3)=DG2BAR(1, 1)*DG2BAR(3, 1)+DG2BAR(1,
2)*DG2BAR(3, 2)
     &+DG2BAR(1, 3)*DG2BAR(3, 3)
      BBAR(2,3)=DG2BAR(2, 1)*DG2BAR(3, 1)+DG2BAR(2,
2)*DG2BAR(3, 2)
     &+DG2BAR(2, 3)*DG2BAR(3, 3).
      BBAR(2,1)=BBAR(1,2)
      BBAR(3,1)=BBAR(1,3)
      BBAR(3,2)=BBAR(2,3)
      TRBBAR=(BBAR(1,1)+BBAR(2,2)+BBAR(3,3))/3.D0

      HMAT=0.D0
      DO I=1,3
            DO J=1,3
                  DO K=1,3
                        DO L=1,3
      HMAT(I,J,K,L)=0.5D0*(BBAR(J,L)*DELTAM(I,K)+BBAR(I,K)
*DELTAM(J,L)
     &+BBAR(J,K)*DELTAM(I,L)+BBAR(I,L)*DELTAM(J,K))
                        ENDDO
                  ENDDO
            ENDDO
      ENDDO
C     ---IMPORTANT TO USE AVERAGE VALUE!----
      CHEM0=CHEM0_AVG
      DCHEM=DCHEM_AVG
C     ---CMATRIX: Tangential modulus---
      CMATRIX=0.D0
```

```
      DO I=1,3
      DO J=1,3
            DO K=1,3
            DO L=1,3
      CMATRIX(I,J,K,L)=
     &ANV*(
     &ALAMBDA0**2.D0*DET**(-1.D0/3.D0)*HMAT(I,J,K,L)
     &+1.D0/ANV*(
     &       ALAMBDA0**3.D0*DLOG((DET*ALAMBDA0**3.D0-
1.D0)
     &/DET/ALAMBDA0**3.D0)
     &-CHI/DET**2.D0/ALAMBDA0**3.D0+
     & ALAMBDA0**3.D0/(DET*ALAMBDA0**3.D0-1.D0)
     &-CHEM0*ALAMBDA0**3.D0
     &       )*DELTAM(I,J)*DELTAM(K,L)
     &                                  )
     &-DCHEM*ALAMBDA0**3.D0*DELTAM(I,J)*DELTAM(K,L)
            ENDDO
            ENDDO
      ENDDO
      ENDDO
C     ---Convert C(3*3*3*3)to D(6*6)---
      DMATRIX=0.D0
      DMATRIX(1,1)=CMATRIX(1,1,1,1)
      DMATRIX(1,2)=CMATRIX(1,1,2,2)
      DMATRIX(1,3)=CMATRIX(1,1,3,3)
      DMATRIX(1,4)=CMATRIX(1,1,2,3)
      DMATRIX(1,5)=CMATRIX(1,1,1,3)
      DMATRIX(1,6)=CMATRIX(1,1,1,2)
      DMATRIX(2,1)=CMATRIX(2,2,1,1)
      DMATRIX(2,2)=CMATRIX(2,2,2,2)
      DMATRIX(2,3)=CMATRIX(2,2,3,3)
      DMATRIX(2,4)=CMATRIX(2,2,2,3)
      DMATRIX(2,5)=CMATRIX(2,2,1,3)
      DMATRIX(2,6)=CMATRIX(2,2,1,2)
      DMATRIX(3,1)=CMATRIX(3,3,1,1)
      DMATRIX(3,2)=CMATRIX(3,3,2,2)
      DMATRIX(3,3)=CMATRIX(3,3,3,3)
      DMATRIX(3,4)=CMATRIX(3,3,2,3)
      DMATRIX(3,5)=CMATRIX(3,3,1,3)
      DMATRIX(3,6)=CMATRIX(3,3,1,2)
      DMATRIX(4,1)=CMATRIX(2,3,1,1)
      DMATRIX(4,2)=CMATRIX(2,3,2,2)
      DMATRIX(4,3)=CMATRIX(2,3,3,3)
      DMATRIX(4,4)=CMATRIX(2,3,2,3)
```

```
            DMATRIX(4,5)=CMATRIX(2,3,1,3)
            DMATRIX(4,6)=CMATRIX(2,3,1,2)
            DMATRIX(5,1)=CMATRIX(1,3,1,1)
            DMATRIX(5,2)=CMATRIX(1,3,2,2)
            DMATRIX(5,3)=CMATRIX(1,3,3,3)
            DMATRIX(5,4)=CMATRIX(1,3,2,3)
            DMATRIX(5,5)=CMATRIX(1,3,1,3)
            DMATRIX(5,6)=CMATRIX(1,3,1,2)
            DMATRIX(6,1)=CMATRIX(1,2,1,1)
            DMATRIX(6,2)=CMATRIX(1,2,2,2)
            DMATRIX(6,3)=CMATRIX(1,2,3,3)
            DMATRIX(6,4)=CMATRIX(1,2,2,3)
            DMATRIX(6,5)=CMATRIX(1,2,1,3)
            DMATRIX(6,6)=CMATRIX(1,2,1,2)
      C     ---Cauchy Stress---
            SIGMA_MAT=0.D0
            DO I=1,3
                  DO J=1,3
            SIGMA_MAT(I,J)=ANV*(
           & DET**(-1.D0/3.D0)*BBAR(I,J)
           &*ALAMBDA0**2.D0
           &+DELTAM(I,J)/ANV*(
           &ALAMBDA0**3.D0*DLOG((DET*ALAMBDA0**3.D0-
1.D0)/DET/ALAMBDA0**3.D0)
           &+1.D0/DET+CHI/DET**2.D0/ALAMBDA0**3.D0-
CHEM0*ALAMBDA0**3.D0
           &            ) )
           &-1.D0/DET*ANV*DELTAM(I,J)
           &-DELTAM(I,J)*DCHEM*ALAMBDA0**3.D0
                  ENDDO
            ENDDO

            SIGMA(1)=SIGMA_MAT(1,1)
            SIGMA(2)=SIGMA_MAT(2,2)
            SIGMA(3)=SIGMA_MAT(3,3)
            SIGMA(4)=SIGMA_MAT(2,3)
            SIGMA(5)=SIGMA_MAT(1,3)
            SIGMA(6)=SIGMA_MAT(1,2)
            DO I=1,6
                  SIGMA_GAUSS(IPOINT,I)=SIGMA(I)
            ENDDO
      C     ---AKL:B^[transpose]*D*B---
      C     ---AKNL1: -2*[sigma]*[delta_epsilon]*[d_epsilon]---
      C     ---AKNL2:[sigma]*[du/dx^[transpose]]*[delta_u/dx]---
            AKL=0.D0
```

```
      DO I=1,3*NNODE
            DO J=1,3*NNODE
                  DO K=1,6
                        DO L=1,6
      AKL(I,J)=AKL(I,J)+B_TOTAL2(K,I)*DMATRIX(K,L)*B_TOT
AL2(L,J)
                        ENDDO
                  ENDDO
            ENDDO
      ENDDO

      TN1=0.D0
      TN2=0.D0
      TN3=0.D0
      TN4=0.D0
      TN5=0.D0
      TN6=0.D0
      DO I=1,NNODE
            DO J=1,NNODE
            TN1(3*(I-1)+1,3*(J-1)+1)=DSFDX2(I,1)*DSFDX2(J,1)
            TN1(3*(I-1)+2,3*(J-1)+2)=DSFDX2(I,1)*DSFDX2(J,1)
            TN1(3*I,3*J)      =DSFDX2(I,1)*DSFDX2(J,1)
            TN2(3*(I-1)+1,3*(J-1)+1)=DSFDX2(I,2)*DSFDX2(J,2)
            TN2(3*(I-1)+2,3*(J-1)+2)=DSFDX2(I,2)*DSFDX2(J,2)
            TN2(3*I,3*J)      =DSFDX2(I,2)*DSFDX2(J,2)
            TN3(3*(I-1)+1,3*(J-1)+1)=DSFDX2(I,3)*DSFDX2(J,3)
            TN3(3*(I-1)+2,3*(J-1)+2)=DSFDX2(I,3)*DSFDX2(J,3)
            TN3(3*I,3*J)      =DSFDX2(I,3)*DSFDX2(J,3)
            TN4(3*(I-1)+1,3*(J-1)+1)=DSFDX2(I,2)*DSFDX2(J,3)
     &            +DSFDX2(I,3)*DSFDX2(J,2)
            TN4(3*(I-1)+2,3*(J-1)+2)=DSFDX2(I,2)*DSFDX2(J,3)
     &            +DSFDX2(I,3)*DSFDX2(J,2)
            TN4(3*I,3*J)      =DSFDX2(I,2)*DSFDX2(J,3)
     &            +DSFDX2(I,3)*DSFDX2(J,2)
            TN5(3*(I-1)+1,3*(J-1)+1)=DSFDX2(I,1)*DSFDX2(J,3)
     &            +DSFDX2(I,3)*DSFDX2(J,1)
            TN5(3*(I-1)+2,3*(J-1)+2)=DSFDX2(I,1)*DSFDX2(J,3)
     &            +DSFDX2(I,3)*DSFDX2(J,1)
            TN5(3*I,3*J)      =DSFDX2(I,1)*DSFDX2(J,3)
     &            +DSFDX2(I,3)*DSFDX2(J,1)
            TN6(3*(I-1)+1,3*(J-1)+1)=DSFDX2(I,1)*DSFDX2(J,2)
     &            +DSFDX2(I,2)*DSFDX2(J,1)
            TN6(3*(I-1)+2,3*(J-1)+2)=DSFDX2(I,1)*DSFDX2(J,2)
     &            +DSFDX2(I,2)*DSFDX2(J,1)
            TN6(3*I,3*J)      =DSFDX2(I,1)*DSFDX2(J,2)
```

```
&                    +DSFDX2(I,2)*DSFDX2(J,1)
            ENDDO
        ENDDO

        DBAR1=0.D0
        DBAR2=0.D0
        DBAR3=0.D0
        DBAR4=0.D0
        DBAR5=0.D0
        DBAR6=0.D0
        AKNL1=0.D0
        AKNL2=0.D0

        DO I=1,3*NNODE
            DO J=1,3*NNODE
            DBAR1(I,J)=B_TOTAL2(1,I)*B_TOTAL2(1,J)
&           +0.25D0*B_TOTAL2(6,I)*B_TOTAL2(6,J)
&       +0.25D0*B_TOTAL2(5,I)*B_TOTAL2(5,J)
            DBAR2(I,J)=0.25D0*B_TOTAL2(6,I)*B_TOTAL2(6,J)
&           +B_TOTAL2(2,I)*B_TOTAL2(2,J)
&       +0.25D0*B_TOTAL2(4,I)*B_TOTAL2(4,J)
            DBAR3(I,J)=0.25D0*B_TOTAL2(5,I)*B_TOTAL2(5,J)
&           +0.25D0*B_TOTAL2(4,I)*B_TOTAL2(4,J)
&       +B_TOTAL2(3,I)*B_TOTAL2(3,J)

DBAR4(I,J)=2.D0*(0.25D0*B_TOTAL2(6,I)*B_TOTAL2(5,J)
&           +0.25D0*B_TOTAL2(5,I)*B_TOTAL2(6,J)
&           +0.5D0*B_TOTAL2(2,I)*B_TOTAL2(4,J)
&           +0.5D0*B_TOTAL2(4,I)*B_TOTAL2(2,J)
&       +0.5D0*B_TOTAL2(4,I)*B_TOTAL2(3,J)
&       +0.5D0*B_TOTAL2(3,I)*B_TOTAL2(4,J))

DBAR5(I,J)=2.D0*(0.5D0*B_TOTAL2(1,I)*B_TOTAL2(5,J)
&           +0.5D0*B_TOTAL2(5,I)*B_TOTAL2(1,J)
&           +0.25D0*B_TOTAL2(6,I)*B_TOTAL2(4,J)
&           +0.25D0*B_TOTAL2(4,I)*B_TOTAL2(6,J)
&       +0.5D0*B_TOTAL2(5,I)*B_TOTAL2(3,J)
&       +0.5D0*B_TOTAL2(3,I)*B_TOTAL2(5,J))

DBAR6(I,J)=2.D0*(0.5D0*B_TOTAL2(1,I)*B_TOTAL2(6,J)
&           +0.5D0*B_TOTAL2(6,I)*B_TOTAL2(1,J)
&           +0.5D0*B_TOTAL2(6,I)*B_TOTAL2(2,J)
&           +0.5D0*B_TOTAL2(2,I)*B_TOTAL2(6,J)
&       +0.25D0*B_TOTAL2(5,I)*B_TOTAL2(4,J)
&       +0.25D0*B_TOTAL2(4,I)*B_TOTAL2(5,J))
```

```
                ENDDO
            ENDDO

            DO I=1,3*NNODE
                DO J=1,3*NNODE
                AKNL1(I,J)=-2.D0*SIGMA(1)*DBAR1(I,J)
     & -2.D0*SIGMA(2)*DBAR2(I,J)-2.D0*SIGMA(3)*DBAR3(I,J)
     & -SIGMA(4)*DBAR4(I,J)-SIGMA(5)*DBAR5(I,J)
     & -SIGMA(6)*DBAR6(I,J)
                AKNL2(I,J)=  SIGMA(1)*TN1(I,J)+SIGMA(2)*TN2(I,J)
     &          +SIGMA(3)*TN3(I,J)+SIGMA(4)*TN4(I,J)
     &          +SIGMA(5)*TN5(I,J)+SIGMA(6)*TN6(I,J)
                ENDDO
            ENDDO

      C     ---AKTHETAU: K_[chempoten,disp]---
      C     ---AKUTHETA: K_[disp,chempoten]---
                AKTHETAU=0.D0
                AKUTHETA=0.D0
                TEMPDX  =0.D0

                DO I=1,NNODE
                    DO J=1,3

     TEMPDX(J)=TEMPDX(J)+DSFDX2(I,J)*(DTEMP(I)+TEMP(I))
                    ENDDO
                ENDDO

                DO IP=1,NNODE
                    DO IQ=1,NNODE
                        DO I=1,3
                            DO K=1,3
                AKTHETAU(IP,3*IQ-2)=AKTHETAU(IP,3*IQ-
2)+1.D0/DTIME*SF3(IP)
     &/DET/ALAMBDA0**3.D0*DG2I(K,1)*DSFDX0(IQ,K)
     &+(DSFDX2(IP,1)*TEMPDX(1)+DSFDX2(IP,2)*TEMPDX(2)

&+DSFDX2(IP,3)*TEMPDX(3))*DD/DET/ALAMBDA0**3.D0*DG2I(K,1)
     &*DSFDX0(IQ,K)
                AKTHETAU(IP,3*IQ-1)=AKTHETAU(IP,3*IQ-
1)+1.D0/DTIME*SF3(IP)
     &/DET/ALAMBDA0**3.D0*DG2I(K,2)*DSFDX0(IQ,K)
     &+(DSFDX2(IP,1)*TEMPDX(1)+DSFDX2(IP,2)*TEMPDX(2)

&+DSFDX2(IP,3)*TEMPDX(3))*DD/DET/ALAMBDA0**3.D0*DG2I(K,2)
```

```
     &*DSFDX0(IQ,K)

     AKTHETAU(IP,3*IQ  )=AKTHETAU(IP,3*IQ  )+1.D0/DTIME*SF3(IP)
     &/DET/ALAMBDA0**3.D0*DG2I(K,3)*DSFDX0(IQ,K)
     &+(DSFDX2(IP,1)*TEMPDX(1)+DSFDX2(IP,2)*TEMPDX(2)

&+DSFDX2(IP,3)*TEMPDX(3))*DD/DET/ALAMBDA0**3.D0*DG2I(K,3)
     &*DSFDX0(IQ,K)
                                        ENDDO
                                   ENDDO
                              ENDDO
                         ENDDO
C
                         DO I=1,3*NNODE
                              DO J=1,NNODE
                         AKUTHETA(I,J)=AKUTHETA(I,J)-
     &     (B_TOTAL2(1,I)+B_TOTAL2(2,I)+B_TOTAL2(3,I))*SF2(J)
                              ENDDO
                         ENDDO

                         RHS   =0.D0
                         AMATRX=0.D0
                         DO J=1,3*NNODE
                              DO I=1,6
                              RHS(J)=RHS(J)-SIGMA(I)*B_TOTAL2(I,J)
                              ENDDO
                         ENDDO
                         DO I=1,3*NNODE
                              DO J=1,3*NNODE

     AMATRX(I,J)=(AKL(I,J)+AKNL1(I,J)+AKNL2(I,J))
                              ENDDO
                         ENDDO

                    FLUX=0.D0
                         RHS_DIFF=0.D0
                         DO I=1,3
                         FLUX(I)=-(ALAMBDA0**3.D0*DET-1.D0)/DET
     &/ALAMBDA0**3.D0*DD*TEMPDX(I)
                         ENDDO
                         DO I=1,NNODE
                              RHS_DIFF(I)=RHS_DIFF(I)
     &          -1.D0/DTIME*SF3(I)/DET/ALAMBDA0**3.D0
     &     *(DET*ALAMBDA0**3.D0-1.D0**3.D0)
     &          +DSFDX2(I,1)*FLUX(1)+DSFDX2(I,2)*FLUX(2)
```

```
     &          +DSFDX2(I,3)*FLUX(3)
                ENDDO

                AMATRX_DIFF=0.D0
                DO I=1,NNODE
                      DO J=1,NNODE
                            DO K=1,3

      AMATRX_DIFF(I,J)=AMATRX_DIFF(I,J)+DSFDX2(I,K)
        &                  *((ALAMBDA0**3.D0*DET-1.D0)*DD/DET
        &                  /ALAMBDA0**3.D0)*DSFDX2(J,K)
                               ENDDO
                         ENDDO
                ENDDO
      C       ---Sum up all integration points---

AKTHETAU_T=AKTHETAU_T+AKTHETAU*WEIGHT*DETJAC2

AKUTHETA_T=AKUTHETA_T+AKUTHETA*WEIGHT*DETJAC2
                RHS_T=RHS_T+RHS*WEIGHT*DETJAC2
                AMATRX_T=AMATRX_T+AMATRX*WEIGHT*DETJAC2
                RHS_DIFF_T=RHS_DIFF_T+RHS_DIFF*WEIGHT*DETJAC2

AMATRX_DIFF_T=AMATRX_DIFF_T+AMATRX_DIFF*WEIGHT*DETJA
C2
      C       ---Get nodal stress from Gaussian point---
              CALL GAUSS_INV(GMAT_INV)
              DO I=1,8
                    SIGMA_NODE(I,1)=SIGMA_NODE(I,1)
        &           +GMAT_INV(I,IPOINT)*SIGMA_GAUSS(IPOINT,1)
                    SIGMA_NODE(I,2)=SIGMA_NODE(I,2)
        &           +GMAT_INV(I,IPOINT)*SIGMA_GAUSS(IPOINT,2)
                    SIGMA_NODE(I,3)=SIGMA_NODE(I,3)
        &           +GMAT_INV(I,IPOINT)*SIGMA_GAUSS(IPOINT,3)
                    SIGMA_NODE(I,4)=SIGMA_NODE(I,4)
        &           +GMAT_INV(I,IPOINT)*SIGMA_GAUSS(IPOINT,4)
                    SIGMA_NODE(I,5)=SIGMA_NODE(I,5)
        &           +GMAT_INV(I,IPOINT)*SIGMA_GAUSS(IPOINT,5)
                    SIGMA_NODE(I,6)=SIGMA_NODE(I,6)
        &           +GMAT_INV(I,IPOINT)*SIGMA_GAUSS(IPOINT,6)
              ENDDO

              ENDDO ! END OF INTEGRATION LOOP
```

```
      RETURN
      END

C     ----Calculate shape function and its gradient-------
      SUBROUTINE
GRADIENT(NNODE,XYZ,XI,DETJAC,SF,DSFDX,
     &          DG,DGI,JELEM,DIS_T,XYZ0,DSFDX0)

      IMPLICIT DOUBLE PRECISION (A-H, O-Z)
      DIMENSION XYZ(3,NNODE),XI(3)
      DIMENSION
SF(NNODE),DSFDXI(NNODE,3),DSFDX(NNODE,3)
      DIMENSION FJAC(3,3),FJACI(3,3),FJAC0(3,3),FJAC0I(3,3)
      DIMENSION
DG(3,3),DGI(3,3),XYZ0(3,NNODE),DSFDX0(NNODE,3)
      DIMENSION DIS_T(3,NNODE),CC(3,3)
C     SF: Shape function(N)
      SF(1)=(1.D0-XI(1))*(1.D0+XI(2))*(1.D0+XI(3))*0.125D0
      SF(2)=(1.D0-XI(1))*(1.D0-XI(2))*(1.D0+XI(3))*0.125D0
      SF(3)=(1.D0-XI(1))*(1.D0-XI(2))*(1.D0-XI(3))*0.125D0
      SF(4)=(1.D0-XI(1))*(1.D0+XI(2))*(1.D0-XI(3))*0.125D0
      SF(5)=(1.D0+XI(1))*(1.D0+XI(2))*(1.D0+XI(3))*0.125D0
      SF(6)=(1.D0+XI(1))*(1.D0-XI(2))*(1.D0+XI(3))*0.125D0
      SF(7)=(1.D0+XI(1))*(1.D0-XI(2))*(1.D0-XI(3))*0.125D0
      SF(8)=(1.D0+XI(1))*(1.D0+XI(2))*(1.D0-XI(3))*0.125D0
C     DSFDXI: dN/d_xi or dN/d_eta or dN/d_zeta
      DSFDXI(1,1)=-(1.D0+XI(2))*(1.D0+XI(3))*0.125D0
      DSFDXI(1,2)= (1.D0-XI(1))*(1.D0+XI(3))*0.125D0
      DSFDXI(1,3)= (1.D0-XI(1))*(1.D0+XI(2))*0.125D0
      DSFDXI(2,1)=-(1.D0-XI(2))*(1.D0+XI(3))*0.125D0
      DSFDXI(2,2)=-(1.D0-XI(1))*(1.D0+XI(3))*0.125D0
      DSFDXI(2,3)= (1.D0-XI(1))*(1.D0-XI(2))*0.125D0
      DSFDXI(3,1)=-(1.D0-XI(2))*(1.D0-XI(3))*0.125D0
      DSFDXI(3,2)=-(1.D0-XI(1))*(1.D0-XI(3))*0.125D0
      DSFDXI(3,3)=-(1.D0-XI(1))*(1.D0-XI(2))*0.125D0
      DSFDXI(4,1)=-(1.D0+XI(2))*(1.D0-XI(3))*0.125D0
      DSFDXI(4,2)= (1.D0-XI(1))*(1.D0-XI(3))*0.125D0
      DSFDXI(4,3)=-(1.D0-XI(1))*(1.D0+XI(2))*0.125D0
      DSFDXI(5,1)= (1.D0+XI(2))*(1.D0+XI(3))*0.125D0
      DSFDXI(5,2)= (1.D0+XI(1))*(1.D0+XI(3))*0.125D0
      DSFDXI(5,3)= (1.D0+XI(1))*(1.D0+XI(2))*0.125D0
      DSFDXI(6,1)= (1.D0-XI(2))*(1.D0+XI(3))*0.125D0
      DSFDXI(6,2)=-(1.D0+XI(1))*(1.D0+XI(3))*0.125D0
      DSFDXI(6,3)= (1.D0+XI(1))*(1.D0-XI(2))*0.125D0
      DSFDXI(7,1)= (1.D0-XI(2))*(1.D0-XI(3))*0.125D0
```

```
                DSFDXI(7,2)=-(1.D0+XI(1))*(1.D0-XI(3))*0.125D0
                DSFDXI(7,3)=-(1.D0+XI(1))*(1.D0-XI(2))*0.125D0
                DSFDXI(8,1)= (1.D0+XI(2))*(1.D0-XI(3))*0.125D0
                DSFDXI(8,2)= (1.D0+XI(1))*(1.D0-XI(3))*0.125D0
                DSFDXI(8,3)=-(1.D0+XI(1))*(1.D0+XI(2))*0.125D0
        C     ---JACOBIAN MATRIX: dx/d_xi,etc.---
                FJAC=0.0D0
              DO I=1,3
                 DO J=1,3
                  DO K=1,NNODE
                   FJAC(I,J)=FJAC(I,J)+DSFDXI(K,J)*XYZ(I,K)
                  ENDDO
                 ENDDO
                ENDDO

                DETJAC=FJAC(1,1)*FJAC(2,2)*FJAC(3,3)-
FJAC(1,1)*FJAC(2,3)*FJAC(3,2)
             &  -
FJAC(2,1)*FJAC(1,2)*FJAC(3,3)+FJAC(2,1)*FJAC(1,3)*FJAC(3,2)
             &  +FJAC(3,1)*FJAC(1,2)*FJAC(2,3)-
FJAC(3,1)*FJAC(1,3)*FJAC(2,2)

        C     ---Inverse of Jacobian---
                FJACI(1,1)= (FJAC(2,2)*FJAC(3,3)-
FJAC(2,3)*FJAC(3,2))/DETJAC
                FJACI(1,2)=-(FJAC(1,2)*FJAC(3,3)-
FJAC(1,3)*FJAC(3,2))/DETJAC
                FJACI(1,3)=-(FJAC(1,3)*FJAC(2,2)-
FJAC(1,2)*FJAC(2,3))/DETJAC
                FJACI(2,1)=-(FJAC(2,1)*FJAC(3,3)-
FJAC(2,3)*FJAC(3,1))/DETJAC
                FJACI(2,2)= (FJAC(1,1)*FJAC(3,3)-
FJAC(1,3)*FJAC(3,1))/DETJAC
                FJACI(2,3)=-(FJAC(1,1)*FJAC(2,3)-
FJAC(1,3)*FJAC(2,1))/DETJAC
                FJACI(3,1)=-(FJAC(2,2)*FJAC(3,1)-
FJAC(2,1)*FJAC(3,2))/DETJAC
                FJACI(3,2)=-(FJAC(1,1)*FJAC(3,2)-
FJAC(1,2)*FJAC(3,1))/DETJAC
                FJACI(3,3)= (FJAC(1,1)*FJAC(2,2)-
FJAC(1,2)*FJAC(2,1))/DETJAC
        C     ---dN/dx, dN/dy,dN/dZ---
              DSFDX=0.D0
                DO I=1,NNODE
                        DO J=1,3
```

```
                        DO K=1,3

      DSFDX(I,J)=DSFDX(I,J)+FJACI(K,J)*DSFDXI(I,K)
                        ENDDO
                    ENDDO
                ENDDO
      C         ---dX/d_xi,dY/d_xi,etc.
                FJAC0=0.D0
              DO I=1,3
                  DO J=1,3
                    DO K=1,NNODE
                     FJAC0(I,J)=FJAC0(I,J)+DSFDXI(K,J)*XYZ0(I,K)
                    ENDDO
                  ENDDO
                ENDDO

                DETJAC0=FJAC0(1,1)*FJAC0(2,2)*FJAC0(3,3)
             &  -FJAC0(1,1)*FJAC0(2,3)*FJAC0(3,2)
             &  -FJAC0(2,1)*FJAC0(1,2)*FJAC0(3,3)
             &  +FJAC0(2,1)*FJAC0(1,3)*FJAC0(3,2)
             &  +FJAC0(3,1)*FJAC0(1,2)*FJAC0(2,3)
             &  -FJAC0(3,1)*FJAC0(1,3)*FJAC0(2,2)

      C     ----d_xi/dX,d_xi/dY,etc.---
                FJAC0I(1,1)= (FJAC0(2,2)*FJAC0(3,3)-
FJAC0(2,3)*FJAC0(3,2))/DETJAC0
                FJAC0I(1,2)=-(FJAC0(1,2)*FJAC0(3,3)-
FJAC0(1,3)*FJAC0(3,2))/DETJAC0
                FJAC0I(1,3)=-(FJAC0(1,3)*FJAC0(2,2)-
FJAC0(1,2)*FJAC0(2,3))/DETJAC0
                FJAC0I(2,1)=-(FJAC0(2,1)*FJAC0(3,3)-
FJAC0(2,3)*FJAC0(3,1))/DETJAC0
                FJAC0I(2,2)= (FJAC0(1,1)*FJAC0(3,3)-
FJAC0(1,3)*FJAC0(3,1))/DETJAC0
                FJAC0I(2,3)=-(FJAC0(1,1)*FJAC0(2,3)-
FJAC0(1,3)*FJAC0(2,1))/DETJAC0
                FJAC0I(3,1)=-(FJAC0(2,2)*FJAC0(3,1)-
FJAC0(2,1)*FJAC0(3,2))/DETJAC0
                FJAC0I(3,2)=-(FJAC0(1,1)*FJAC0(3,2)-
FJAC0(1,2)*FJAC0(3,1))/DETJAC0
                FJAC0I(3,3)= (FJAC0(1,1)*FJAC0(2,2)-
FJAC0(1,2)*FJAC0(2,1))/DETJAC0
      C         ---dN/dX,dN/dY,dN/dZ---
              DSFDX0=0.D0
                DO I=1,NNODE
```

```
                DO J=1,3
                    DO K=1,3

DSFDX0(I,J)=DSFDX0(I,J)+FJAC0I(K,J)*DSFDXI(I,K)
                    ENDDO
                ENDDO
            ENDDO
C           ---DG: Deformation Gradient F=dx/dX---
            DG=0.D0
            DO I=1,NNODE
               DG(1,1)=DG(1,1)+DSFDX0(I,1)*DIS_T(1,I)
                DG(1,2)=DG(1,2)+DSFDX0(I,2)*DIS_T(1,I)
                DG(1,3)=DG(1,3)+DSFDX0(I,3)*DIS_T(1,I)
                DG(2,1)=DG(2,1)+DSFDX0(I,1)*DIS_T(2,I)
                DG(2,2)=DG(2,2)+DSFDX0(I,2)*DIS_T(2,I)
                DG(2,3)=DG(2,3)+DSFDX0(I,3)*DIS_T(2,I)
                DG(3,1)=DG(3,1)+DSFDX0(I,1)*DIS_T(3,I)
                DG(3,2)=DG(3,2)+DSFDX0(I,2)*DIS_T(3,I)
                DG(3,3)=DG(3,3)+DSFDX0(I,3)*DIS_T(3,I)
            ENDDO
            DG(1,1)=1.D0+DG(1,1)
            DG(2,2)=1.D0+DG(2,2)
            DG(3,3)=1.D0+DG(3,3)
c           ---Cauchy-Born tensor: C=F^[Transpose]*F---
            CC=0.D0
            DO I=1,3
                    DO J=1,3
                        DO K=1,3
                            CC(I,J)=CC(I,J)+DG(K,I)*DG(K,J)
                        ENDDO
                    ENDDO
            ENDDO
            AI3=CC(1,1)*CC(2,2)*CC(3,3)-CC(1,1)*CC(2,3)*CC(3,2)
     &      -CC(2,1)*CC(1,2)*CC(3,3)+CC(2,1)*CC(1,3)*CC(3,2)
     &      +CC(3,1)*CC(1,2)*CC(2,3)-CC(3,1)*CC(1,3)*CC(2,2)

            DETDG=DSQRT(AI3)
C       ---Inverse of DG: H=F^[-1]---
            DGI(1,1)= (DG(2,2)*DG(3,3)-DG(2,3)*DG(3,2))/DETDG
            DGI(1,2)=-(DG(1,2)*DG(3,3)-DG(1,3)*DG(3,2))/DETDG
            DGI(1,3)=-(DG(1,3)*DG(2,2)-DG(1,2)*DG(2,3))/DETDG
            DGI(2,1)=-(DG(2,1)*DG(3,3)-DG(2,3)*DG(3,1))/DETDG
            DGI(2,2)= (DG(1,1)*DG(3,3)-DG(1,3)*DG(3,1))/DETDG
            DGI(2,3)=-(DG(1,1)*DG(2,3)-DG(1,3)*DG(2,1))/DETDG
            DGI(3,1)=-(DG(2,2)*DG(3,1)-DG(2,1)*DG(3,2))/DETDG
```

```
      DGI(3,2)=-(DG(1,1)*DG(3,2)-DG(1,2)*DG(3,1))/DETDG
      DGI(3,3)= (DG(1,1)*DG(2,2)-DG(1,2)*DG(2,1))/DETDG

      RETURN
      END

C     -------Normal gaussian point position and weight----
      SUBROUTINE GET_POINTS(IP,POINTS)
      IMPLICIT DOUBLE PRECISION (A-H, O-Z)
      DIMENSION POINTS(IP,4)
C     --POINTS(*,1:3): location
C     --POINTS(*,1:4): Weight
      AA=1.D0/DSQRT(3.D0)
      POINTS(1,1)=-AA
      POINTS(1,2)= AA
      POINTS(1,3)= AA
      POINTS(1,4)= 1.D0
      POINTS(2,1)=-AA
      POINTS(2,2)=-AA
      POINTS(2,3)= AA
      POINTS(2,4)= 1.D0
      POINTS(3,1)=-AA
      POINTS(3,2)=-AA
      POINTS(3,3)=-AA
      POINTS(3,4)= 1.D0
      POINTS(4,1)=-AA
      POINTS(4,2)= AA
      POINTS(4,3)=-AA
      POINTS(4,4)= 1.D0
      POINTS(5,1)= AA
      POINTS(5,2)= AA
      POINTS(5,3)= AA
      POINTS(5,4)= 1.D0
      POINTS(6,1)= AA
      POINTS(6,2)=-AA
      POINTS(6,3)= AA
      POINTS(6,4)= 1.D0
      POINTS(7,1)= AA
      POINTS(7,2)=-AA
      POINTS(7,3)=-AA
      POINTS(7,4)= 1.D0
      POINTS(8,1)= AA
      POINTS(8,2)= AA
      POINTS(8,3)=-AA
      POINTS(8,4)= 1.D0
```

```
      RETURN
      END
C     ------This subroutine ensures gaussian point value--
C     ------be replaced by nearlest nodal value-----------
      SUBROUTINE GET_POINTS2(IP,POINTS)
      IMPLICIT DOUBLE PRECISION (A-H, O-Z)
      DIMENSION POINTS(IP,4)
      DOUBLE PRECISION AA
C     ---Approximate to Nodal value---
      AA=1.D0
      POINTS(1,1)=-AA
      POINTS(1,2)= AA
      POINTS(1,3)= AA
      POINTS(1,4)= 1.D0
      POINTS(2,1)=-AA
      POINTS(2,2)=-AA
      POINTS(2,3)= AA
      POINTS(2,4)= 1.D0
      POINTS(3,1)=-AA
      POINTS(3,2)=-AA
      POINTS(3,3)=-AA
      POINTS(3,4)= 1.D0
      POINTS(4,1)=-AA
      POINTS(4,2)= AA
      POINTS(4,3)=-AA
      POINTS(4,4)= 1.D0
      POINTS(5,1)= AA
      POINTS(5,2)= AA
      POINTS(5,3)= AA
      POINTS(5,4)= 1.D0
      POINTS(6,1)= AA
      POINTS(6,2)=-AA
      POINTS(6,3)= AA
      POINTS(6,4)= 1.D0
      POINTS(7,1)= AA
      POINTS(7,2)=-AA
      POINTS(7,3)=-AA
      POINTS(7,4)= 1.D0
      POINTS(8,1)= AA
      POINTS(8,2)= AA
      POINTS(8,3)=-AA
      POINTS(8,4)= 1.D0

      RETURN
```

```
      END

C     ---------------------------------------
      SUBROUTINE GAUSS_INV(GMAT_INV)
      IMPLICIT DOUBLE PRECISION(A-H,O-Z)

      DIMENSION GMAT(8,8),GMAT_INV(8,8)
      DIMENSION POINTS(8,4),XI(3)

      AA=1.D0/DSQRT(3.D0)
      POINTS(1,1)=-AA
      POINTS(1,2)= AA
      POINTS(1,3)= AA
      POINTS(1,4)= 1.D0
      POINTS(2,1)=-AA
      POINTS(2,2)=-AA
      POINTS(2,3)= AA
      POINTS(2,4)= 1.D0
      POINTS(3,1)=-AA
      POINTS(3,2)=-AA
      POINTS(3,3)=-AA
      POINTS(3,4)= 1.D0
      POINTS(4,1)=-AA
      POINTS(4,2)= AA
      POINTS(4,3)=-AA
      POINTS(4,4)= 1.D0
      POINTS(5,1)= AA
      POINTS(5,2)= AA
      POINTS(5,3)= AA
      POINTS(5,4)= 1.D0
      POINTS(6,1)= AA
      POINTS(6,2)=-AA
      POINTS(6,3)= AA
      POINTS(6,4)= 1.D0
      POINTS(7,1)= AA
      POINTS(7,2)=-AA
      POINTS(7,3)=-AA
      POINTS(7,4)= 1.D0
      POINTS(8,1)= AA
      POINTS(8,2)= AA
      POINTS(8,3)=-AA
      POINTS(8,4)= 1.D0

      GMAT=0.D0
      DO I=1,8
```

```
          XI(1)=POINTS(I,1)
          XI(2)=POINTS(I,2)
          XI(3)=POINTS(I,3)
          GMAT(I,1)=(1.D0-XI(1))*(1.D0+XI(2))*(1.D0+XI(3))*0.125D0
          GMAT(I,2)=(1.D0-XI(1))*(1.D0-XI(2))*(1.D0+XI(3))*0.125D0
          GMAT(I,3)=(1.D0-XI(1))*(1.D0-XI(2))*(1.D0-XI(3))*0.125D0
          GMAT(I,4)=(1.D0-XI(1))*(1.D0+XI(2))*(1.D0-XI(3))*0.125D0
          GMAT(I,5)=(1.D0+XI(1))*(1.D0+XI(2))*(1.D0+XI(3))*0.125D0
          GMAT(I,6)=(1.D0+XI(1))*(1.D0-XI(2))*(1.D0+XI(3))*0.125D0
          GMAT(I,7)=(1.D0+XI(1))*(1.D0-XI(2))*(1.D0-XI(3))*0.125D0
          GMAT(I,8)=(1.D0+XI(1))*(1.D0+XI(2))*(1.D0-XI(3))*0.125D0
        ENDDO
C       ---Inverse of GMAT---
        CALL DLSGRR (8,8,GMAT,8,1E-8,IRANK,GMAT_INV,8)

        RETURN
        END
----------Contents within file PARS.TXT----------
64   27   48   37
----------Contents within file XYZ.TXT----------
 1, 3., 3., 3.,-2.066806650
 2, 3., 2., 3.,-2.066806650
 3, 3., 1., 3.,-2.066806650
 4, 3., 0., 3.,-2.066806650
 5, 3., 3., 2.,-2.066806650
 6, 3., 2., 2.,-2.066806650
 7, 3., 1., 2.,-2.066806650
 8, 3., 0., 2.,-2.066806650
 9, 3., 3., 1.,-2.066806650
10, 3., 2., 1.,-2.066806650
11, 3., 1., 1.,-2.066806650
12, 3., 0., 1.,-2.066806650
13, 3., 3., 0.,-2.066806650
14, 3., 2., 0.,-2.066806650
15, 3., 1., 0.,-2.066806650
16, 3., 0., 0.,-2.066806650
17, 2., 3., 3.,-2.066806650
18, 2., 2., 3.,-2.066806650
19, 2., 1., 3.,-2.066806650
20, 2., 0., 3.,-2.066806650
21, 2., 3., 2.,-2.066806650
22, 2., 2., 2.,-2.066806650
23, 2., 1., 2.,-2.066806650
24, 2., 0., 2.,-2.066806650
25, 2., 3., 1.,-2.066806650
```

26, 2., 2., 1.,-2.066806650
27, 2., 1., 1.,-2.066806650
28, 2., 0., 1.,-2.066806650
29, 2., 3., 0.,-2.066806650
30, 2., 2., 0.,-2.066806650
31, 2., 1., 0.,-2.066806650
32, 2., 0., 0.,-2.066806650
33, 1., 3., 3.,-2.066806650
34, 1., 2., 3.,-2.066806650
35, 1., 1., 3.,-2.066806650
36, 1., 0., 3.,-2.066806650
37, 1., 3., 2.,-2.066806650
38, 1., 2., 2.,-2.066806650
39, 1., 1., 2.,-2.066806650
40, 1., 0., 2.,-2.066806650
41, 1., 3., 1.,-2.066806650
42, 1., 2., 1.,-2.066806650
43, 1., 1., 1.,-2.066806650
44, 1., 0., 1.,-2.066806650
45, 1., 3., 0.,-2.066806650
46, 1., 2., 0.,-2.066806650
47, 1., 1., 0.,-2.066806650
48, 1., 0., 0.,-2.066806650
49, 0., 3., 3.,-2.066806650
50, 0., 2., 3.,-2.066806650
51, 0., 1., 3.,-2.066806650
52, 0., 0., 3.,-2.066806650
53, 0., 3., 2.,-2.066806650
54, 0., 2., 2.,-2.066806650
55, 0., 1., 2.,-2.066806650
56, 0., 0., 2.,-2.066806650
57, 0., 3., 1.,-2.066806650
58, 0., 2., 1.,-2.066806650
59, 0., 1., 1.,-2.066806650
60, 0., 0., 1.,-2.066806650
61, 0., 3., 0.,-2.066806650
62, 0., 2., 0.,-2.066806650
63, 0., 1., 0.,-2.066806650
64, 0., 0., 0.,-2.066806650
----------Contents within file ELEMENT.TXT----------
1, 17, 18, 22, 21, 1, 2, 6, 5
2, 18, 19, 23, 22, 2, 3, 7, 6
3, 19, 20, 24, 23, 3, 4, 8, 7
4, 21, 22, 26, 25, 5, 6, 10, 9
5, 22, 23, 27, 26, 6, 7, 11, 10

6, 23, 24, 28, 27, 7, 8, 12, 11
7, 25, 26, 30, 29, 9, 10, 14, 13
8, 26, 27, 31, 30, 10, 11, 15, 14
9, 27, 28, 32, 31, 11, 12, 16, 15
10, 33, 34, 38, 37, 17, 18, 22, 21
11, 34, 35, 39, 38, 18, 19, 23, 22
12, 35, 36, 40, 39, 19, 20, 24, 23
13, 37, 38, 42, 41, 21, 22, 26, 25
14, 38, 39, 43, 42, 22, 23, 27, 26
15, 39, 40, 44, 43, 23, 24, 28, 27
16, 41, 42, 46, 45, 25, 26, 30, 29
17, 42, 43, 47, 46, 26, 27, 31, 30
18, 43, 44, 48, 47, 27, 28, 32, 31
19, 49, 50, 54, 53, 33, 34, 38, 37
20, 50, 51, 55, 54, 34, 35, 39, 38
21, 51, 52, 56, 55, 35, 36, 40, 39
22, 53, 54, 58, 57, 37, 38, 42, 41
23, 54, 55, 59, 58, 38, 39, 43, 42
24, 55, 56, 60, 59, 39, 40, 44, 43
25, 57, 58, 62, 61, 41, 42, 46, 45
26, 58, 59, 63, 62, 42, 43, 47, 46
27, 59, 60, 64, 63, 43, 44, 48, 47
----------Contents within file BOUNDARY.TXT----------
4,2,0.0
8,2,0.0
12,2,0.0
13,3,0.0
14,3,0.0
15,3,0.0
16,2,0.0
16,3,0.0
20,2,0.0
24,2,0.0
28,2,0.0
29,3,0.0
30,3,0.0
31,3,0.0
32,2,0.0
32,3,0.0
36,2,0.0
40,2,0.0
44,2,0.0
45,3,0.0
46,3,0.0
47,3,0.0

48,2,0.0
48,3,0.0
49,1,0.0
50,1,0.0
51,1,0.0
52,1,0.0
52,2,0.0
53,1,0.0
54,1,0.0
55,1,0.0
56,1,0.0
56,2,0.0
57,1,0.0
58,1,0.0
59,1,0.0
60,1,0.0
60,2,0.0
61,1,0.0
61,3,0.0
62,1,0.0
62,3,0.0
63,1,0.0
63,3,0.0
64,1,0.0
64,2,0.0
64,3,0.0
1,2.066806650
2,2.066806650
3,2.066806650
4,2.066806650
5,2.066806650
6,2.066806650
7,2.066806650
8,2.066806650
9,2.066806650
10,2.066806650
11,2.066806650
12,2.066806650
13,2.066806650
14,2.066806650
15,2.066806650
16,2.066806650
17,2.066806650
18,2.066806650
19,2.066806650

20,2.066806650
21,2.066806650
25,2.066806650
29,2.066806650
33,2.066806650
34,2.066806650
35,2.066806650
36,2.066806650
37,2.066806650
41,2.066806650
45,2.066806650
49,2.066806650
50,2.066806650
51,2.066806650
52,2.066806650
53,2.066806650
57,2.066806650
61,2.066806650
----------After run, output within Message.txt----------
NITERATION= 1
DEF_MAX= 1.000000000000000E-008
DIFF_MAX= 1.34454935388183
NITERATION= 2
DEF_MAX= 5.700785991953337E-002
DIFF_MAX= 3.929062641978638E-004
NITERATION= 3
DEF_MAX= 6.881834166439282E-002
DIFF_MAX= 2.146335049417928E-003
NITERATION= 4
DEF_MAX= 7.289915722088940E-002
DIFF_MAX= 8.907029093520921E-003
NITERATION= 5
DEF_MAX= 6.061136080388950E-002
DIFF_MAX= 3.042996199181101E-002
NITERATION= 6
DEF_MAX= 3.672698334132694E-002
DIFF_MAX= 9.023256077435543E-002
NITERATION= 7
DEF_MAX= 3.457737792395722E-002
DIFF_MAX= 0.146142877512428
NITERATION= 8
DEF_MAX= 4.168708381825438E-002
DIFF_MAX= 6.618580311989061E-002
NITERATION= 9
DEF_MAX= 3.580546407053177E-002

DIFF_MAX= 0.123667923664602
NITERATION= 10
DEF_MAX= 3.895712788978343E-002
DIFF_MAX= 6.558145386133224E-002
NITERATION= 11
DEF_MAX= 3.859201725015116E-002
DIFF_MAX= 0.121486359222665
NITERATION= 12
DEF_MAX= 3.491222162558437E-002
DIFF_MAX= 6.857497408053131E-002
NITERATION= 13
DEF_MAX= 4.573790092790622E-002
DIFF_MAX= 0.156643915749655
NITERATION= 14
DEF_MAX= 3.338172211949230E-002
DIFF_MAX= 6.977512270783176E-002
NITERATION= 15
DEF_MAX= 6.052508138531003E-002
DIFF_MAX= 0.213912223031153
NITERATION= 16
DEF_MAX= 4.183281674576045E-002
DIFF_MAX= 6.951118824104617E-002
NITERATION= 17
DEF_MAX= 6.991832688652218E-002
DIFF_MAX= 0.283568179341242
NITERATION= 18
DEF_MAX= 4.752993776580022E-002
DIFF_MAX= 5.323158357892497E-002
NITERATION= 19
DEF_MAX= 7.823595020782698E-002
DIFF_MAX= 0.511299089101092
NITERATION= 20
DEF_MAX= 5.384947011627144E-002
DIFF_MAX= 1.157657990934700E-002
NITERATION= 21
DEF_MAX= 2.445617065251353E-002
DIFF_MAX= 0.131938275488519
NITERATION= 22
DEF_MAX= 1.606573282730855E-002
DIFF_MAX= 0.112782142247387
NITERATION= 23
DEF_MAX= 2.837500428988920E-002
DIFF_MAX= 0.258754151547199
NITERATION= 24
DEF_MAX= 1.293487858019075E-002

DIFF_MAX= 1.355315574637489E-002
NITERATION= 25
DEF_MAX= 1.067901630650200E-002
DIFF_MAX= 3.713771131218958E-002
NITERATION= 26
DEF_MAX= 2.603970026547386E-003
DIFF_MAX= 6.660145411439699E-003
NITERATION= 27
DEF_MAX= 1.177731744255397E-003
DIFF_MAX= 2.692214005169753E-003
NITERATION= 28
DEF_MAX= 8.401790022447415E-004
DIFF_MAX= 8.494018663051152E-004
NITERATION= 29
DEF_MAX= 2.627129856315273E-004
DIFF_MAX= 1.831343461315394E-004
NITERATION= 30
DEF_MAX= 1.063054824373539E-004
DIFF_MAX= 3.662881408500746E-005
NITERATION= 31
DEF_MAX= 4.454764287846009E-005
DIFF_MAX= 2.103362269162045E-005
NITERATION= 32
DEF_MAX= 2.631919053788328E-005
DIFF_MAX= 1.169264941345573E-005
NITERATION= 33
DEF_MAX= 1.131124180930603E-005
DIFF_MAX= 3.006716813504506E-006
NITERATION= 34
DEF_MAX= 5.044656430966398E-006
DIFF_MAX= 1.835038055722425E-006